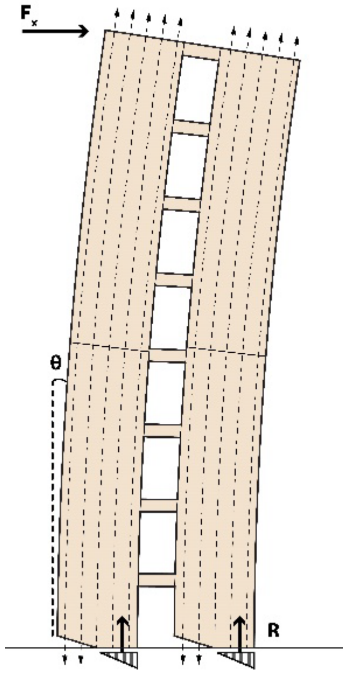

A Post-tensioned Cross-Laminated Timber core for buildings

By

T. Znabei

A post-tensioned Cross-Laminated Timber core

By

T. Znabei

in partial fulfilment of the requirements for the degree of

Master of Science
in Civil Engineering

at the Delft University of Technology,
to be defended publicly on September 7, 2020 at 12:15 PM.

Thesis Committee:	Prof.dr.ir. J.W.G. van de Kuilen, TU Delft
	Dr.ir. G.J.P. Ravenshorst, TU Delft
	Dr.ir. M.A.N. Hendriks, TU Delft
	Ir. S. Ren, Arup
	Ir. R.W.A Verhaegh, Arup

An electronic version of this thesis is available at http://repository.tudelft.nl/

Preface

This thesis was written in conclusion of my studies in Civil Engineering, master track Structural Engineering, with specialization in Structural mechanics at Delft University of Technology and in collaboration with Arup.

I started my studies at the faculty of Architecture, where I have learned how a well-designed environment enhances quality of life. It is also there that I began to understand the impact of structures on the environment and the major need for the construction industry to adopt environmentally friendly materials. This thesis combines my interest in mechanics, architecture and sustainability.

Writing the thesis has been a personal challenge. I am most content working in a team and with short deadlines, which is nearly the opposite of a writing a Master Thesis. The Covid-19 pandemic and the lock-down did not make things easier. I am happy to finally be able to present to you this thesis.

I have been lucky to have my thesis supervisors and colleagues at Arup who were supportive and available along the way, no less during the pandemic. I would like to thank Shibo Ren for supporting me in my search for a topic and for teaching me a lot on modelling. I also would like to thank Rob Verhaegh for bringing much appreciated knowledge and endless enthusiasm for timber structures. He has spent more time reading and critically reviewing my thesis than I could have wished for. Both have been my patient mentors during the process. Thanks also to my supervisors at TU Delft. Max Hendriks helped me a lot with DIANA modelling by providing concise answers to any questions I had, generally within a day. Jan-Willem van de Kuilen and Geert Ravenshorst I thank for the progress meetings we had.

I am grateful for my mom who has taught me perseverance and how to be flexible in life. As a single mom with two kids, she has given up a lot to one day see me graduate. Thank you, Mom. My friends and my sister had genuine interest in how I was doing with my thesis, though I want to thank them especially for all the times they did not ask about it and took my mind off it. I am lucky to have my boyfriend, Yannick, who helped me in the first months of my thesis when I had a tough time. He moved with me to Amsterdam, where we worked together from home during the pandemic. He was always there to talk to me, to motivate me and to make me laugh.

T. Znabei

Amsterdam, 30 July 2020

Summary

This master thesis is on post-tensioning cross-laminated timber stability cores for multiple story buildings. When designing a CLT core, significantly larger core sections will be needed than when designing a stabilizing core in concrete. This is for one part due to the limited stiffness of the CLT compared to concrete. For another part it is due to the limited stiffness of connectors in CLT. Sliding and uplift can occur in connections in CLT loaded in tension and shear respectively. The CLT panels behave like rigid bodies, with most of the displacement occurring at the connections. In addition, cooperation between flange and web may be limited, depending on the stiffness of the corner connection and the occurrence of shear lag. Post-tensioning is suggested as a solution to diminish uplift and sliding in the connectors. In this way, with the same core section, a taller building may be realized compared to the non-post-tensioned case. In the thesis also the long-term effects on the prestress level is assessed, as estimating these effects is important for the safety of the system.

This thesis adds to the body of knowledge on post-tensioned CLT structures. Firstly, previous studies on post-tensioned CLT focus on individual shear walls and on seismic design situations. This thesis explores how beneficial post-tensioning is from the perspective of serviceability limit state governed design. Furthermore, though post-tensioning as a prestressing method has been applied often in concrete structures, prestressing of CLT is a novel research subject. Especially the estimation of long-term force loss is a topic that still requires research. This thesis provides the designer with a straightforward calculation method (using python) for estimation of prestress force loss in the long-term.

The research was carried out with a literature study and a case-study. The literature research comprised of studies on structural design with CLT loaded in-plane; the effective flange of a CLT core; stiffness of connections in CLT; prestressing of CLT; a design approach for post-tensioning; time dependent losses in post-tensioned CLT. The case study was based on a fictitious floorplan including a "minimal core", and at expressing the benefit of post-tensioning in terms of height gain.

The degree to which the flange and the web cooperate showed highly dependent on the connection between flange and web and the core height. In the case study, the effective flange width showed to depend highly on the height of the core and the stiffness of the connection between flange and web.

In the case-study, without post-tensioning, approximately half of the displacements could be attributed to the connections. With post-tensioning, the uplift and sliding displacements in the horizontal joints was eliminated. Consequently, the attainable height was significantly increased: from 5 storeys in the un-post-tensioned case, to 8 storeys in the post-tensioned case. Long-term effects on the prestress loss were considerable. In the case-study, approximately 40% loss of post-tension force in the lifetime of the building was predicted and included in the design. Largest cause of force loss was due to changes of moisture content during construction. The remaining lateral displacements after post-tensioning were due to bending and shear.

Post-tensioning of CLT cores is a powerful method for reducing lateral displacements in cases where uplift and sliding are dominant contributors to the lateral displacements. This is especially the case in light-weight buildings. Uplift and sliding displacements can be eliminated altogether with post-tensioning. The designer should realize that post-tensioning does not increase the bending and shear stiffness of the core. The thesis also concludes that with the post-tensioning of CLT walls, the compressive strength of the CLT in the so-called "compression-toe" might be exceeded. It is an important check in design. Furthermore, depending on the decision to re-tighten the rods at some point or not, the post-tension force loss should be calculated and included in finding the right prestress level. For this estimation of the moisture level of the CLT proved to be an important but difficult step. It is likely that the 40% force loss in the case-study is on the conservative side, since a large change in moisture content has been assumed. In practice, the moisture content can be measured on site. This can help verify the assumptions on the moisture content used in force loss calculations. This can help in assuring the structure is safe in the long-term.

Keywords: CLT, core, lateral displacements, uplift, sliding, effective-flange, shear lag, prestress, post-tensioning, prestress loss.

Contents

1 Introduction

1.1 Research Motivation

1.1.1 Responsibility of the engineer towards the environment

There is a wide-spread consensus that the built environment is responsible for a large part of the global greenhouse gas emissions. It is estimated that the building industry is responsible for 35% of global greenhouse gas emissions [1]. The built environment is one of the focus points of the Dutch Climate Agreement which provides binding emission targets specific to industries [2].

Though the Climate Agreement focusses mostly on emission related with the use-phase of buildings, there is also a significant emission related with the "embodied carbon" in buildings. According to "Meten is Weten", a report by CE Delft, the construction industry in the Netherlands was responsible for 9.5 Mton CO_2 equivalent, which is about 5% of the total emissions of the Netherlands in the same year. This includes materials, transport, construction and demolition activities and construction- and demolition waste [3].

To lower these emissions, a big change is needed in the construction industry. It is up to the current and next generation of engineers to also limit the embodied carbon of buildings. Timber is a renewable, biodegradable and recyclable material. The use timber as a construction material contributes to mitigating climate change [4] [5]. If forests are sustainably managed and trees removed from forests are turned into timber products, structures made from that CLT can provide additional long-term carbon storage [6]. Research into CLT as a material for construction will help the transition of the industry into the use of sustainable materials.

1.1.2 Cross-Laminated Timber as an inspiring material

CLT is a relatively new and sustainable material that is suitable for application in tall buildings, mainly due to the possibility to produce CLT in large sizes. CLT is fit for use in both gravity and lateral load resisting systems.

As CLT is a new material, more research on the material and structural behaviour is necessary. The European Cooperation of Science and Technology has acknowledged CLT as a promising material. Many engineers collaborate in the COST research program to bridge the gap between scientific results and information needed for design by the engineer. [7]. With the thesis, there is an opportunity to help in bridging this gap by providing insight in how to design a CLT stability system for multiple storey buildings.

1.2 Problem definition

A minimum core size in a building is generally needed for reasons other than structural. Stairs, elevators and technical space is generally placed in a core. This core can also be utilized for providing stability to the building when it is loaded by lateral loads. In the Netherlands, the main lateral load is wind load. In this type of stability system, the columns carry gravity load only (Figure 1). The core then carries all lateral load. The wind load hits the façade and is transferred from façade to the floors. The floors will transfer then transfer lateral load to the core (Figure 2). However, to date, no research into applying CLT to a core that provides stability is available. Often concrete cores are used to provide stability for CLT buildings. There are advantages to using a concrete core. There is a lot of experience designing stability systems with concrete which makes it a reliable option. Furthermore, concrete cores are stiffer and have a higher capacity [8].

There are however important reasons to favour a CLT core over a concrete core. Firstly, a CLT core would result in less embodied carbon, causing less impact on the environment. Furthermore, a CLT core could result in less differential shortening. There are also advantages for construction. Avoiding mixing of materials will increase speed of construction and is more convenient for planning construction activities [8].

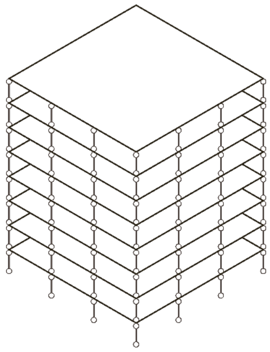

Figure 1 Hinged columns for gravity load only, source: author

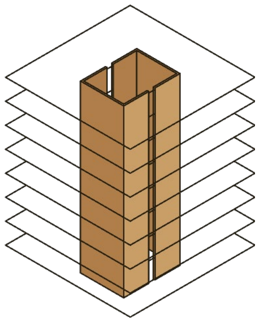

Figure 2 Wind load transferred by the floors to the core, source: author

There are challenges when it comes to designing a CLT core for building stability. Although CLT is stiffer than other timber products, it is still much less stiff than concrete or steel. In addition, connections in timber have a limited stiffness, therefore large displacements can occur in the connections. These displacements are dependent on the stiffness of the connectors. Data on the stiffness of connectors is not always available.

When regarding the displacement in the connections, a challenge is the so called "rocking" or "uplift" that can occur in timber structures. Resulting tensile forces from wind load in CLT buildings are transferred to the foundation with hold-down connectors. In other locations tensile plate connectors may be used for tensile force transfer. Due to the limited stiffness of these connections, gaps form at the location of connections. It can be expected that the gaps contribute a lot to the total lateral displacement of the building.

Another challenge in designing CLT cores is the lack of knowledge on how the different walls in the core cooperate. Firstly, there is a possibility for the occurrence of shear lag. This causes in-plane deformation of the flange. This means that the normal stresses are not linear over the height of the core section, lowering the stiffness of the core. Furthermore, the connections between the different perpendicular core walls (or flange-web connection) most likely negatively influence the bending stiffness of the core. Currently, designers have no guidelines on how much perpendicular CLT walls cooperate.

Post-tensioning might be a solution for some of the challenges associated with a non-post-tensioned CLT core. Post-tensioning can make it possible to lower tensile stresses at the base of the core or eliminate them altogether. This is expected to decrease the total lateral displacements of the building compared to applying no post-tensioning. Furthermore, hold-downs or plate connectors for tensile force transfer may be avoided as the rods or tendons used for prestressing can transfer tensile forces to the foundation.

However, prestressing CLT comes with its own challenges. Post-tensioning is a common method in concrete structures but has not often been applied to timber structures. The ability to maintain the stress level in the rods in the long term is crucial for the function and safety of the system and cannot be neglected in the design of a post-tensioned CLT structure. Especially prediction of long-term behaviour of post-tensioned CLT requires research. An additional challenge is that post-tensioning increases the risk of exceeding the compressive stress in the CLT.

1.3 Objective

1.3.1 Research Questions

In section 1.2, post-tensioning has been introduced as a method that might decrease the lateral displacements in a building. The main objective of the thesis is to analyse how effective post-tensioning is when applied to a CLT core. This also requires understanding of how large lateral displacements are in un-post-tensioned CLT cores. The stiffness of an un-post-tensioned core should be compared with that of a post-tensioned core.

Bending stiffness of the core depends on the occurrence of shear lag and the cooperation between the flange and the web. This cooperation can be expressed in an "effective flange width". One objective in the thesis is to find an estimation of the effective flange width of CLT cores.

It has also been stated that the post-tension force is expected to decrease in time. The thesis aims at providing a method for quantifying the most important post-tension losses and including the calculation of these losses in the design process.

Main Research Question

How effective is post-tensioning a CLT core for reducing lateral displacements of a building?

Sub Research Questions

What is the effective flange width for bending in a CLT core?
How do long-term effects influence the prestress force and how should the prestress losses be quantified?

1.3.2 Methodology

Several methods are used throughout the thesis to be able to answer the research questions in paragraph 1.3.1.

- Literature Research

The first part of the literature research focusses on CLT as a structural material (Chapter 2) and structural design with CLT (Chapter 3). Since no literature on the structural behaviour of cores in CLT is found, the structural behaviour of CLT shear walls is discussed instead in section 3.6. Chapter 4 focusses on the connectors often used in CLT structures, as the connections are expected to play a large role in lateral displacement in un-post-tensioned cores. Chapter 5 aims in providing knowledge on how different CLT walls cooperate. This knowledge is beneficial for determining the bending stiffness of CLT cores.
Chapter 6 focusses on the particularities of applying post-tensioning to CLT. This chapter also discusses previous (research projects) that include post-tensioned CLT shear walls. Chapter 7 goes further into depth on the long-term prestress losses that were introduced in chapter 6. In this chapter a python model developed for this thesis is introduced that provides designers with a way of estimating long-term prestress losses. Lastly, in chapter 8, insight is given in the design process of a post-tensioned CLT core. A design scheme is introduced that shows how the prestress losses discussed in chapter 8 should be included in the design.

- Case Study

  A quantitative answer to the main research question of this thesis can only be given in relation to a specific design context. No real-life project is available for the case that utilizes exclusively a post-tensioned core for its stability design. Therefore, a fictitious building is introduced for the case study in Chapter 9. The core included in the floorplan of the building can be regarded a "minimal core", such as explained in section 1.2. Two situations are analysed for the stability design: (1) a non-post-tensioned core and (2) a post-tensioned core. These two situations are compared, and the benefit of post-tensioning is expressed in terms of gain of achievable height. From this case-study, more general conclusions will be drawn on post-tensioned CLT cores.
- Numerical Modelling

  Due to the complexity of the problem (3D structure + nonlinear effects from the connections and/or prestressing rod), it is cumbersome to evaluate the displacements of the core by hand. Therefore, in the Case-Study (Chapter 9), the lateral displacements of a post-tensioned core and a non-post-tensioned core are analysed with the help of a Finite Element Model. The finite element program used is DIANA FEA. Attention points for modelling post-tensioned CLT in DIANA are discussed in section 9.3.

1.3.3 Scope

To be able to answer the research questions in the time frame of the thesis, several simplifications and assumptions proved necessary. This paragraph provides an overview of the assumptions that have been made for the research.

- The lateral load resisting system studied is a single CLT core. Prestressing could also be applied to other lateral load resisting systems, such as shear walls distributed throughout the building, or outrigger systems. Such other load resisting systems are not studied in this thesis.
- A single core is assumed to be placed in the centre of the building. The core is not studied for torsional loading.
- The building solely relies on the core for resisting of lateral loads. Columns are hinged and other structural elements do not add to the stiffness for lateral loading.
- The gravity load resisting system is not included in the analysis. In case assumptions for the gravity load resisting system are needed (e.g. for loads on the core), these are made based on estimation and reference projects.
- The stiffness of timber floors and their diaphragm behaviour is an interesting study on its own. Multiple research papers on the topic can be found [9]. In the current thesis the floors are regarded rigid.
- The core is analysed for wind load as the only lateral load. Wind load is the most important lateral load in the Netherlands. In other regions of the world, earthquake loading might be applicable.

2 Cross Laminated Timber

In Chapter 1, Cross-Laminated Timber has been underlined as a promising material for application in structures of buildings. The current chapter will introduce the material CLT. Structural design with CLT will be discussed in Chapter 3.

2.1 Description and Advantages

Cross-Laminated Timber (CLT) is a relatively new timber product composed of crosswise glued timber lamellas (see Figure 3 and Figure 4). It is made up of uneven numbers of layers, most common number of layers being 3, 5 and 7. For the base material, different types of softwoods are possible, such as: spruce, fine, fir, pine, larch or Douglas fir. Recently, CLT is also produced with hard woods, for special applications. In practice, almost exclusively Spruce C24 is used.

CLT has become an important and celebrated product in the industry. The development of CLT started in the 1990's and has increased since (See Figure 5). According to the Economic and Social Council of the United Nations, the use of CLT will continue to grow globally. The council reports a global CLT market of $603 million in 2017, and a projection of $1.6 billion in 2024. The European region is the product leader, responsible for 60% of the CLT production [10]. The reason for becoming such a celebrated product is that CLT opens new possibilities for construction of tall buildings. CLT has significant advantages over solid timber for use in structures:

- A CLT plate behaves in diaphragm action, meaning it can bear loads in two directions.
- Due to the cross-lamination, CLT is less susceptible to deformations caused by moisture level changes.
- The cross-lamination makes that CLT shows less variation in mechanical properties.
- Lower quality wood can be used in CLT to produce products that have similar properties than that of a high-quality solid wood.
- Large dimensions are possible.

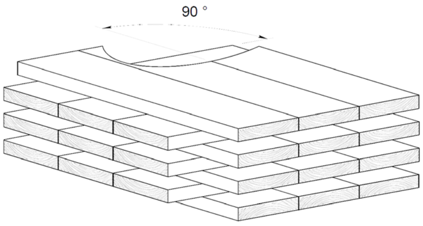

Figure 3 Principle of a CLT plate [11]

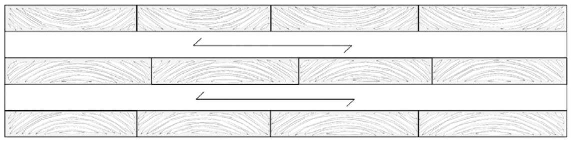

Figure 4 Principle of a five-layer CLT panel [11]

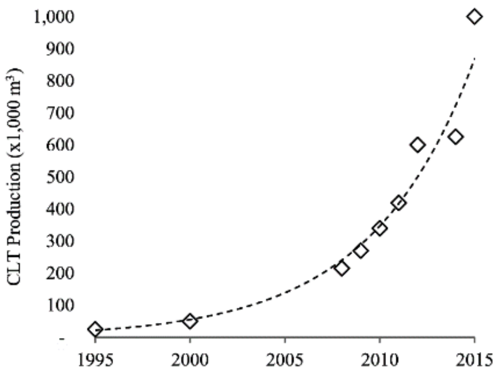

Figure 5 Increase in Production of CLT [12]

2.2 Dimensions

Figure 6 shows examples of different CLT panel build-up that are available on the market. CLT is generally produced with 3 or 5 layers but can also be produced with more layers if desired. As an example, Derix produces CLT panels with 3, 5, 7, 9 and 11 layers [13]. The thickness of the boards of which the CLT is produced can also vary. Common sizes are 20, 30 and 40 mm of board thickness [13]. Different board thickness may be combined in a single panel. The CLT panels are produced with the outer layers of the CLT panel either perpendicular (L) or parallel to the CLT panel construction width (Q), which is illustrated in Figure 7.

Different CLT panel types may have a different ratio of longitudinal and perpendicular boards. In the most basic case (a panel with three layers, all equal thickness), one third of the thickness runs in one direction, while two thirds of the thickness run in the other direction. CLT panels can also be produced with a very dominant direction. To give an example, panels are produced with build-up *[mm] 40-20-40-20-40*. These panels have 75% of the thickness running parallel to the outer layers, and 25% perpendicular to the outer layers.

An advantage of CLT is that it can be produced in large sizes. The size is only limited by the production process (see section 2.3) and vary for different producers. As an example, the maximum dimensions as by Derix are shown in Figure 8 [13].

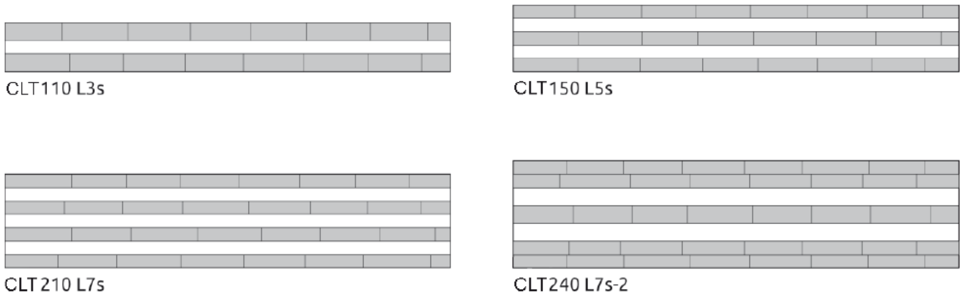

Figure 6 Examples of CLT panel build-up with their designation [14]

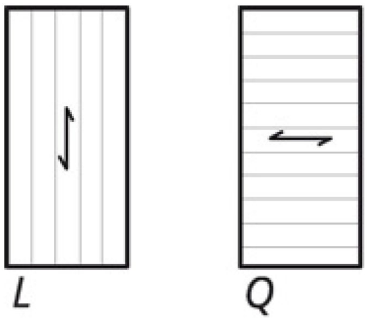

Figure 7 Outer layers perpendicular (L) or parallel (Q) to the construction width [14]

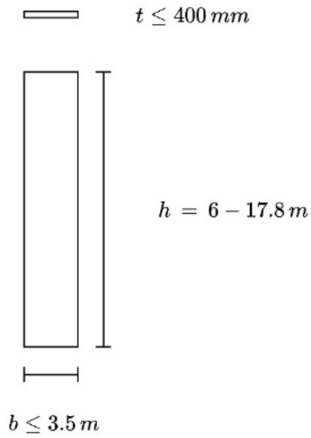

Figure 8 Maximum dimensions of CLT plates produced by Derix [13], source: author

2.3 Production Process

The production sequence for CLT panels is shown in Figure 9. The process is very similar to the production process of glued-laminated timber, which has been on the market for longer than CLT. The production process of the CLT can be adjusted according to the specific needs of the client. This includes non-standard sizes, different internal geometry, moisture content restrictions, custom cut-outs (see Figure 11) and different surface qualities.

CLT is produced in a CLT production line, where large equipment is used. The production process takes much space. The central machine in the production process of CLT is the press, which is used in the third step of Figure 9. CLT panels are pressed in a controlled climate with a hydraulic press, such as the press by Ledinek shown in Figure 10. The size of the available press determines the maximum dimensions of the CLT. The press also determines for a large part the quality of the CLT.

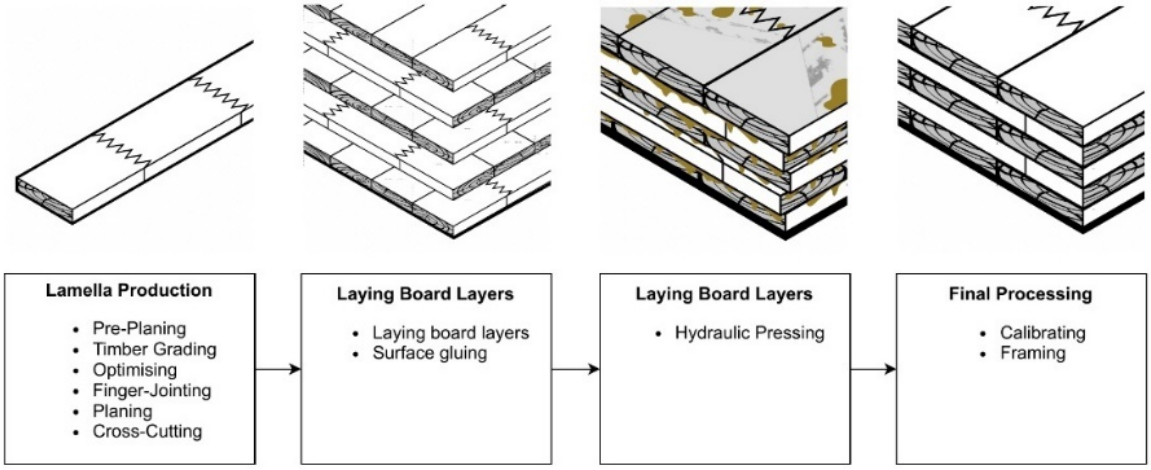

Figure 9 The production process of a CLT plate (adapted from [15])

Figure 10 "X-Press" CLT press by Ledinek [16]

Figure 11 CLT panels with custom shape including cut outs for windows and doors [17]

2.4 Conclusion

CLT is a relatively new timber product but is becoming a more and more common construction material. It has clear advantages for use in construction in comparison with sawn wood, which include the possibility for large sizes and the ability of the panel to carry loads in two directions (diaphragm action). Panels can be produced in large sizes, under different moisture level restrictions and with custom cut-outs for openings among other project specific demands. CLT is identified as a promising material for use in structures for tall buildings.

3 Structural design with CLT

In Chapter 2, Cross-Laminated Timber had been introduced as a promising material for application in building structures. In the current chapter, the most important topics for structural design with CLT are highlighted. Research on structural design with CLT was especially important for the thesis because CLT is a relatively new product and methods for structural design of CLT are still in development.

3.1 Norms

At present, CLT is not included in the Eurocode on design on timber structures (EN1995). The quality of CLT products is instead regulated through European Technical Approvals (ETA's). ETA's are provided by the supplier and in relation to the CLT product.

Since CLT is a new product compared to other structural materials, research on structural application of CLT is still in development and scientific research on CLT as a structural material is increasing. The European Cooperation of Science and Technology has started Action FP1402, which aims at bridging the gap between scientific research results and specific information needed by engineers for design. The documents under this action provide the engineer with valuable knowledge for design of CLT structures [18] and have been of value for the present thesis.

Different practical guides are also available for design. It is the responsibility of the designer to choose sources that can be considered reliable. An example of a comprehensive guideline for structural design with CLT is "Cross-Laminated Timber Structural Design" by Proholz [14]. This guide provides information on structural design with CLT based on the limit state design philosophy from EN1995 [14] .

3.2 Mechanical properties of the base material

CLT is produced almost exclusively from Spruce of strength class C24. The properties of the CLT plate can be derived from the properties of the base material (the material of the lamellas). Values for the mechanical properties timber for different strength classes are provided in NEN-EN338 [19]. Find the density and stiffness of C24 lamellas in Table 1 and Table 2 respectively. The design strength for bending, compression and tension of C24 timber can be found in Table 3. The in-plane shear stiffness of a CLT plate is a special topic and is treated more in depth in Appendix A. For the shear strength reference is made to Proholz [14] (See Table 4).

Table 1 Density of the C24 lamellas [19]

Density of the C24 timber according to EN 338[1]		
Characteristic minimum value of bulk density	ρ_k	$350\,\frac{kg}{m^3}$
Mean bulk density	ρ_{mean}	$420\,\frac{kg}{m^3}$

[1] note that for load assumptions, $\gamma = 5.5\ kN/m3$ is assumed like suggested in Proholz [14], this is an overestimation.

Table 2 Stiffness of the C24 lamellas [19]

Stiffness of the C24 timber according to EN338		$[\boldsymbol{N/mm^2}]$
Modulus of elasticity In the fibre direction	$E_{0,mean}$	11000
	$E_{0.05}$	7400
Modulus of elasticity	$E_{90,mean}$	370
Shear modulus In the fibre direction	$G_{0,mean}$	690

Table 3 Strength of C24 lamellas [19]

Design strength[1] of C24 timber $k_{mod} = 0.8$ and $\gamma_m = 1.25$ assumed Characteristic values are according to EN338		$[\boldsymbol{\frac{N}{mm^2}}]$
Flexural strength	$f_{m,d}$	15.30
Tensile strength	$f_{t,0,d}$	9.28
Compressive strength in direction of the fibre	$f_{c,0,d}$	13.40

Lateral compressive strength	$f_{c,90,d}$	1.60

[1] See 3.5.1.

Table 4 Design shear strength of the CLT panel according to Proholz [14]

Design shear strength of a CLT panel according to Proholz		$[\frac{N}{mm^2}]$
Shear strength of the plate (Mechanism 1)	$f_{V,S,d}$	3.20
Torsional strength of the glued joints (mechanism 2)	$f_{V,T,d}$	1.60
Shear Strength (mechanism 3)	$f_{V,d}$	1.60
Rolling shear strength	$f_{V,R,d}$	0.7

3.3 Cross-Sectional Values

When there is a dominant direction of loading of CLT panels, the CLT panel can be analysed using a strip approach. Using strip approach, for the limit state verifications for the ULS and SLS verifications (3.4 and 3.5, respectively), certain cross-sectional values are required. These are explained in this section.

Dependent on the loading and the type of verification, CLT plates can be analysed based on the net (3.3.2) or the effective section (3.3.3). When to apply the different approaches is illustrated in Table 5. In general, verifications can be made on the net-section. An exception is the SLS verification of CLT plates loaded out-of-plane.

When no clear dominant direction of loading can be identified, the CLT wall should be analysed like a plate. Orthotropic plate theory for plates loaded in-plane is discussed in 3.3.4. For plate theory for plates loaded out of plane, the Proholz guide can be consulted [14].

Table 5 application of net- and effective section to different verifications in the "strip-method"

Type of loading		Verification	
		ULS	SLS
In-plane loading	Axial load	Net-Section	Net-Section
	In-plane Bending	Net-Section	Net-Section
Out-of-plane loading		Net-Section	Effective section

3.3.1 "0" and "90" direction

As CLT is an orthotropic material, designations are required for the different directions in the CLT plate (Figure 12). The direction parallel to the boards in the outer layer of the CLT is called the "0"-direction. Perpendicular to this direction is the auxiliary direction, denoted the "90"-direction. For both the effective section and the net section, it is assumed that the modulus of elasticity of the boards transverse to the fibre is equal to 0 ($E_{90} = 0$), as the ratio $\frac{E_{0,mean}}{E_{90},mea} \approx 30$ for Spruce C24 (Table 2, Page 11).

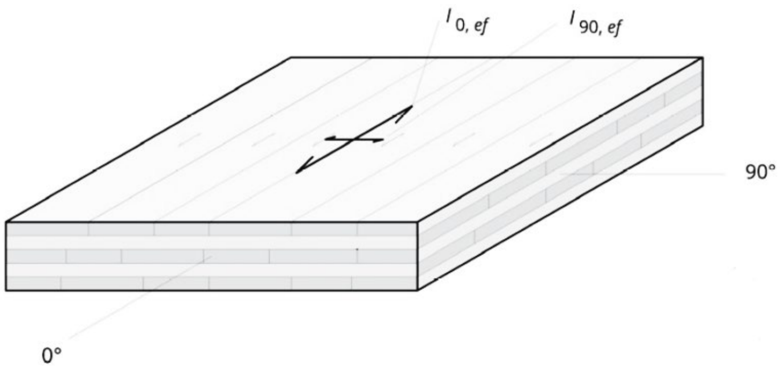

Figure 12 "0" and "90" direction of the CLT plate [14]

3.3.2 The Net Section

The determination of the net section A_{net} (Eq. 1) is shown in Figure 13. For bending in the out of plane direction, the It is shown for the main direction of the CLT (direction "0"). The net section in the "90"-direction may be determined similarly. Note that though the bending stresses are assumed only in the net-section, the shear stresses are assumed to develop over the full section, as is shown for the graph for shear stress τ, most right in Figure 13.

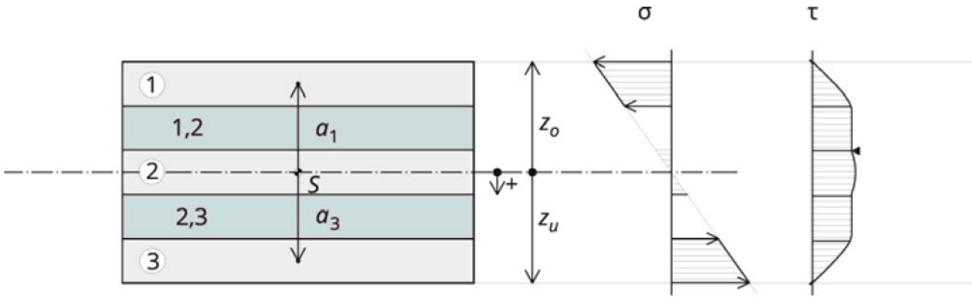

Figure 13 Net-Section for the "0" direction of the CLT, symmetrical section [14]

$$A_{0,net} = \sum_{i=0}^{n} b \cdot d_i \tag{1}$$

$$I_{0,net} = \sum_{i=1}^{n} \frac{b \cdot d_i^3}{12} + \sum_{i=1}^{n} b \cdot d_i \cdot a_i^2 \tag{2}$$

3.3.3 The Effective Section

In CLT panels loaded out-of-plane, rolling shear deformation leads to an increase of displacements (see Figure 14). Variation of normal and shear stresses over the height of the CLT plate is displayed in Figure 15. The increase in displacement can be reflected by assigning an effective stiffness to the panel. Multiple methods exist for determining the effective section, such as the gamma method and the shear analogy method [14]. The rest of this paragraph explains the gamma method, which is included in Eurocode 5.

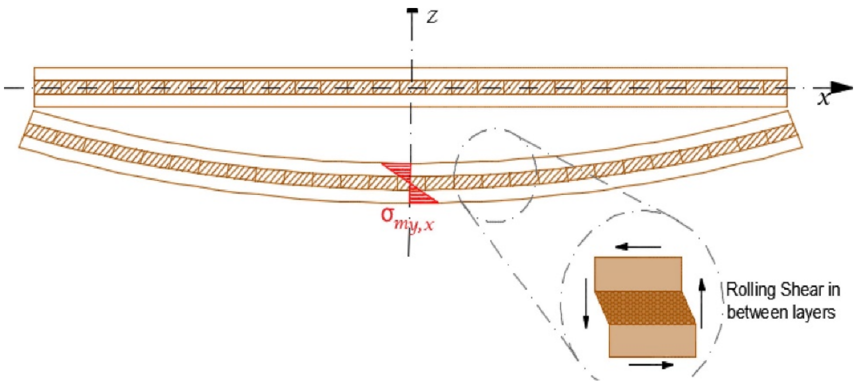

Figure 14 rolling shear deformation for a CLT plate loaded out-of-plane [20]

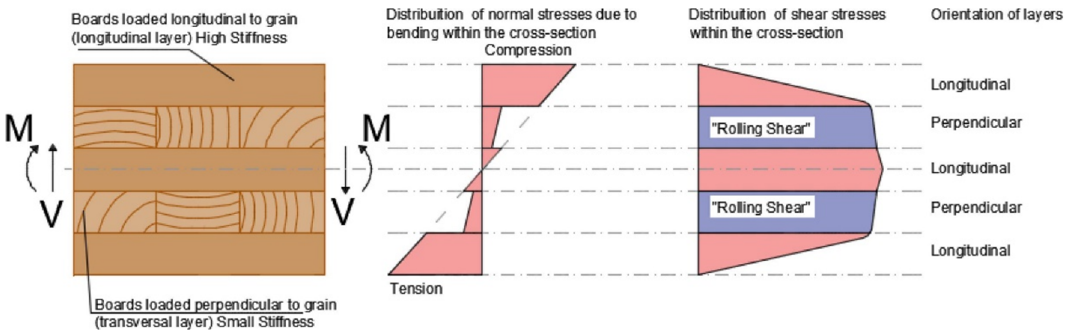

Figure 15 Strip method, stresses and strains [20]

For bending out of plane, the most common method applied in Europe is the Gamma method. In the Gamma method, the shear deformation is considered in an equivalent bending stiffness. The method relies on reducing the Steiner components of each layer with a factor γ. Using this effective stiffness, the element can be regarded to be an Euler-Bernoulli beam element when performing analysis [21]. The gamma method is valid for a CLT plate of up to 3 longitudinal ("0") layers. For CLT plates with more than 3 longitudinal layers (e.g. with 7 or 9 layers in total), the extended Gamma method can be used. This method involves solving of a system of equations (See Appendix B).

Equations for the effective stiffness of CLT plates are given in the CLT guide by Proholz [14]. Proholz' equations are based on equations in EN11995-1-1 for flexibly connected beams. The procedure for finding the effective stiffness is shown in equations 3-9. Corresponding distances are shown in Figure 16. The reference lengths in the gamma equations should be taken as in Table 6.

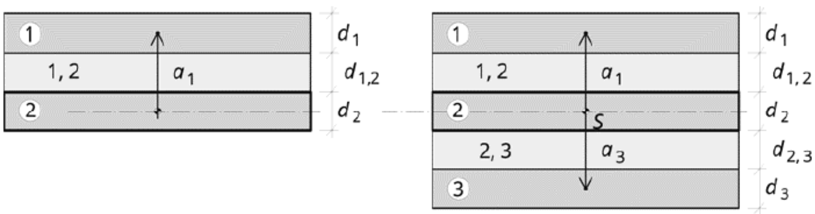

Figure 16 Distances for the gamma method for CLT with 2 longitudinal layers (left) and three longitudinal layers (right) [14]

$$\gamma_1 = \frac{1}{1 + \frac{\pi^2 \cdot E_1 \cdot A_1}{l_{ref}^2} \cdot \frac{d_{1,2}}{b \cdot G_{R,12}}} \left[\frac{1}{m}\right] \tag{3}$$

$$\gamma_2 = 1.0 \left[\frac{1}{m}\right] \tag{4}$$

$$\gamma_3 = \frac{1}{1 + \frac{\pi^2 \cdot E_3 \cdot A_3}{l_{ref}^2} \cdot \frac{d_{2,3}}{b \cdot G_{R,23}}} \left[\frac{1}{m}\right] \tag{5}$$

$$a_2 = \frac{\gamma_1 \cdot \frac{E_1}{E_c} \cdot b \cdot d_1 \cdot \left(\frac{d_1}{2} + d_{1,2} + \frac{d_2}{2}\right) - \gamma_3 \cdot \frac{E_3}{E_c} \cdot b \cdot d_3 \cdot (\frac{d_2}{2} + d_{2,3} + \frac{d_3}{2})}{\sum_{i=1}^{3} \gamma_i \cdot \frac{E_i}{E_c} \cdot b \cdot d_i} \tag{6}$$

$$a_1 = \left(\frac{d_1}{2} + d_{1,2} + \frac{d_2}{2}\right) - a_2 \tag{7}$$

$$a_3 = \left(\frac{d_2}{2} + d_{2,3} + \frac{d_3}{2}\right) + a_2 \tag{8}$$

$$I_{0,eff} = \sum_{i=0}^{3} \frac{E_i}{E_c} \cdot \frac{b \cdot d_i^3}{12} + \sum_{i=0}^{3} \gamma_i \cdot \frac{E_i}{E_c} \cdot b \cdot d_i \cdot a_i^2 \tag{9}$$

Table 6 Reference length for determination of the effective stiffness [14]

Reference length for calculation of $I_{0,eff}$	
Type of element	l_{ref}
Single-Span girders	l
Continuous girders	$\frac{4}{5} \cdot l_{min}$
Cantilevers	$2 \cdot l$
Buckling members	l_{ki}

3.3.4 Orthotropic plate for in-plane loading

When there is not a distinct dominant direction of loading, the CLT plate must be analysed using plate theory instead of the strip method. In this paragraph, this is explained for in-plane loading.

A CLT plate can be viewed as a membrane element (Figure 17). When the CLT plate is predominantly loaded in plane, it can be assumed that the normal stresses n_{xx} and n_{yy} only are present in the layers of the CLT that run parallel to the direction of the normal stresses (A_{net}) (See 3.3.2). Shear stresses are assumed to be developing along the full section A_{gross}.

Equation shows the stiffness matrix for a membrane element of CLT, as according to Proholz [14]. In the stiffness matrix the non-diagonal terms are often assumed equal to zero [14]. Stiffnesses $K_{1,2}$ and $K_{2,1}$ are the terms related to transverse expansion of the plate. The poisons ratio is often assumed equal to zero. This implies degrees of freedom of the plate are uncoupled. In this way, it is possible to perform hand-calculations on the displacements and stresses of the CLT plates. The entries in the stiffness matrix can also be computed by the CLTdesigner software, which can be downloaded from their website [22].

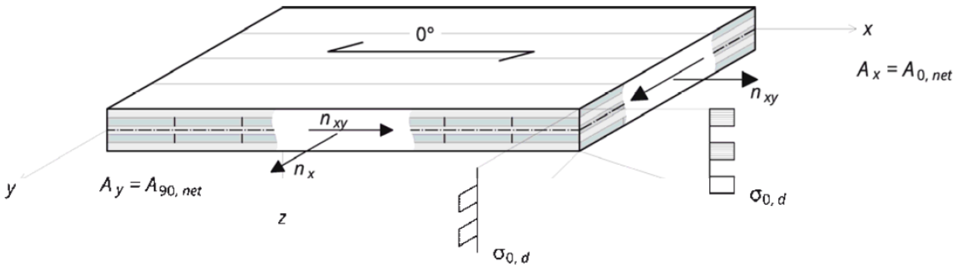

Figure 17 Internal forces and designations for orthotropic CLT plates [14]

$$\begin{bmatrix} n_{xx} \\ n_{yy} \\ n_{xy} \end{bmatrix} = K_{plate} \cdot \begin{bmatrix} \frac{\delta u_x}{\delta x} \\ \frac{\delta u_y}{\delta y} \\ \frac{\delta u_x}{\delta y} - \frac{\delta u_y}{\delta x} \end{bmatrix} \tag{10}$$

$$K_{plate} = \begin{bmatrix} E_{0,mean} \cdot A_{0,net} & 0 & 0 \\ 0 & E_{0,mean} \cdot A_{90,net} & 0 \\ 0 & 0 & G_{S,mean} \cdot A_{gross} \end{bmatrix} \tag{11}$$

3.4 Serviceability Limit State verifications

Serviceability limit state verifications (SLS) are made under characteristic values of the loads and resistances. The in-plane bending stiffness is based on the net-section approach. The in-plane shear stiffness of CLT plates is a complicated topic, since this characteristic depends on the internal geometry of the CLT.

3.4.1 Stiffness of the CLT plate for in-plane shear

The in-plane shear stiffness depends on the build-up of the CLT and on whether the interfaces are glued. Bogensberger et al. [23] proposed equations for the in-plane shear stiffness and -strength of CLT plates that relate the shear stiffness of the plate to the board c, board thickness and shear stiffness of the bulk material. A simplified approximation is that the in-plane stiffness of the CLT panel is about $\frac{3}{4}$ times the in-plane shear stiffness of the bulk material. However, CLT suppliers often report lower shear stiffnesses of their plates. More information on in-plane shear of CLT plates can be found in Appendix A.

$$G_{S,mean} = \frac{1}{1 + 6 \cdot \alpha_{FE} \cdot \left(\frac{d_{mean}}{a}\right)^2} \cdot G_{mean} \approx 0.75 \cdot G_{mean}$$

$$\alpha_{FE} = 0.32 \cdot \left(\frac{d_{mean}}{a}\right)^{-0.77} \tag{12}$$

[23]

Where:

$G_{S,mean}$	In-plane shear stiffness of the CLT-plate loaded
d_{mean}	Average board thickness in the cross-section
a	Board width (150 mm is recommended)

3.4.2 Stiffness of the CLT plate for in-plane bending

When performing hand-calculations on CLT elements loaded in-plane, the net-section approach should be used. Only layers perpendicular to the direction of loading are included in the verification.

3.4.3 Deformation factors

The Eurocode approach for considering long-term effects on the deformation is to increase the displacements by including a deformation factor k_{def}. The k_{def} values for CLT found in literature are comparable with k_{def} for plywood in EN1995-1-1 (Table 7). Schickhofer [24] mentions that CLT with number of layers smaller or equal to 7 are more sensitive to long-term load than CLT with more than 7 layers. Table 7 shows the deformation factors k_{def} for plywood and cross-laminated timber.

$$u_{fin} = u_{t=0} \cdot (1 + k_{\mathrm{def}}) \tag{13}$$

Table 7 k_{def} factors for CLT

	k_{def}	
Service Class	1	2
Cross Laminated Timber $n_{layers} > 7$ (prEN 16351)	0.80	1.00
Cross Laminated Timber $n_{layers} \leq 7$ (prEN 16351)	0.85	1.10

Plywood according (EN 1995-1-1:2009)	0.80	1.00

3.5 Ultimate Limit State verifications

3.5.1 Design resistance

Verifications in the ultimate limit state (ULS) are made under design value of the loads and resistances. The design value of the resistance of a CLT plate is determined with Eq. 14. The modification factor k_{mod} is a factor that considers the load duration and moisture effects on the compressive resistance of the timber. The factor k_{mod} is to depends on the timber product, the service class and the load duration. For determining the k_{mod} factor, the representative load duration should be determined. No k_{mod} factors for CLT are provided by the Eurocode yet. Research by Shickhofer [24] showed that the behaviour of CLT under moisture is comparable to Glued Laminated Timber. Schickhofer therefore suggests the k_{mod} factors listed in Table 8. These are equal to the modification factors in Eurocode 5 for glulam in Service Class 1 and Service Class 2 [25]. Because CLT is not intended for use in Service Class 3 conditions, no k_{mod} values for Service Class 3 are provided.

When multiple loads are present, the load with the shortest load duration should be used for calculation of k_{mod} [26]. For several loads that are relevant to the thesis, their load duration is given in Table 7.

The material factor γ_m accounts for the variability of the material. Because of the lamination, the variability of the CLT plate is smaller than the variability in the base material for the CLT. Therefore, a smaller γ_m may be used compared to solid wood. Schickhofer suggests the CLT to be classified as glulam [24].

$$R_d = k_{mod} \cdot \frac{R_k}{\gamma_m} \tag{14}$$

[25]

$$\gamma_{m,CLT} = 1.25 \tag{15}$$

[24]

Table 8 k_{mod} factors for CLT [24]

Service class	Load duration				
	Permanent	Long	Medium	Short	Very short
1	0.60	0.70	0.80	0.90	1.10
2	0.60	0.70	0.80	0.90	1.10

Table 9 Load durations corresponding with different load types

Load	Load duration
Wind load	Short-term
Self-weight	Permanent
Prestress	Permanent
Imposed load	Medium-term

3.5.2 Verification of CLT loaded in-plane

The verifications of CLT loaded in-plane are made on the net-section. As an example, the verification method for CLT loaded in compression in the parallel direction (Figure 18) and in-plane bending (Figure 19) are shown in equations 16 and 17 . For other load situations in plane, and for all verifications for out-of-plane loading, reference is made to Proholz [14].

In the approach shown, the normal stresses are assumed to be linear over the height of the CLT panel. With decreasing ratio of $\frac{l}{h}$, the linear stress assumption becomes less valid. In that case the CLT plate should not be analysed with beam analogy [14].

Compression in direction 0

$$\sigma_{c,0,d} \leq f_{c,0,d}$$

$$\frac{N_{0,d}}{A_{0,net}} \leq k_{mod} \cdot \frac{f_{c,0,k}}{\gamma_m} \tag{16}$$

$$A_{net} = b \cdot d_{0,net}$$

[14]

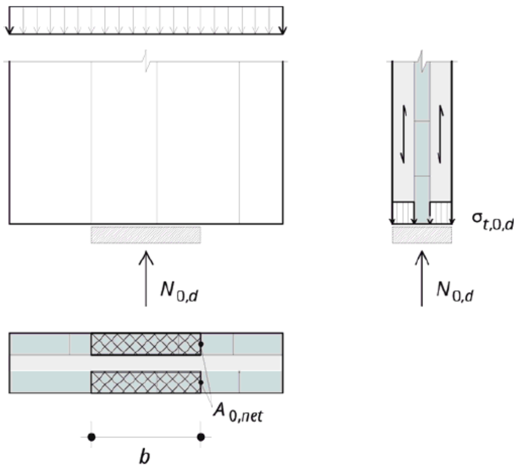

Figure 18 CLT plate loaded in-plane compression direction 0 [14]

In-plane bending

$$\sigma_{m,z,d} \leq f_{m,d}$$
$$\frac{M_{z,d}}{W_{z,0,net}} \leq k_{mod} \cdot \frac{f_{m,k}}{\gamma_m} \tag{17}$$
$$W_{z,0,net} = \frac{\sum d_0 \cdot h^2}{6}$$

[14]

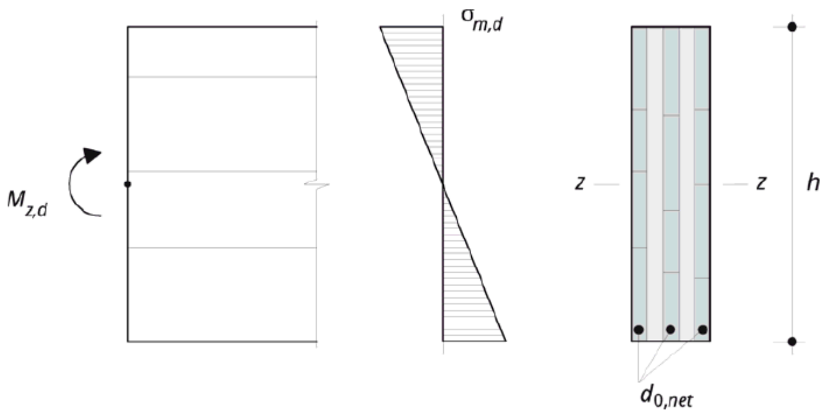

Figure 19 CLT plate in-plane bending [14]

3.5.3 Buckling

When a slender CLT wall is loaded by an in-plane compressive force, the stability of this wall needs to be checked. See Figure 20 for a CLT wall buckling from the element plane. A verification method according to Proholz [14] are given in Eq. 18 - 23. This verification is done in line with the Eurocode method for verification of buckling of columns. In this verification the critical buckling load only accounts for longitudinal stiffness (EI_{eff}). Other methods also include shear deformations by finding the critical buckling load according to the Timoshenko Beam Theory (e.g. in [27]). Note that the influence of the influence of **rolling** shear in the 90-direction is included in by taking the **effective** stiffness $I_{y,0,ef}$. Imperfections are included with factor β_c.

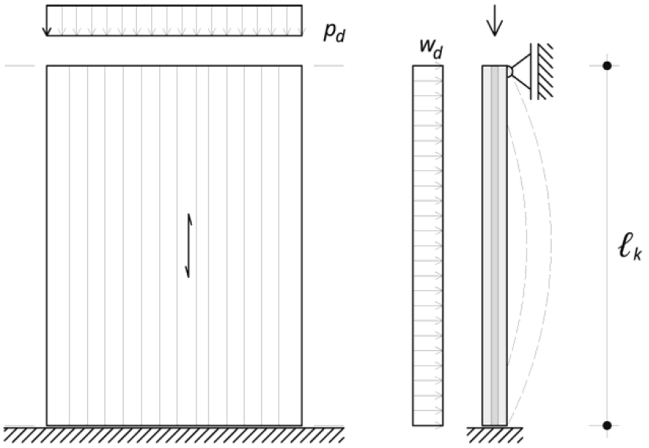

Figure 20 CLT wall buckling from the element plane (Adapted from [14])

$$\frac{\sigma_{c,0,d}}{k_{c,y} \cdot f_{c,0,d}} \pm \frac{\sigma_{m,d}}{f_{m,d}} \leq 1 \tag{18}$$

$$\frac{\frac{N_d}{A_{net}}}{k_{c,y} \cdot f_{c,0,d}} + \frac{\frac{M_d}{W_{net}}}{f_{m,d}} \leq 1 \tag{19}$$

$$i_{y,0,ef} = \sqrt{\frac{I_{y,0,ef}}{A_{0,net}}} \tag{20}$$

$$\lambda_y = \frac{l_{ki}}{i_{y,0,ef}} \tag{21}$$

Where:

$k_{c,y}$	Buckling coefficient
k_y	Buckling coefficient
β_c	Coefficient of imperfection
$\lambda_{rel,y}$	Relative degree of slenderness for lateral buckling

$$k_{c,y} = \frac{1}{k_y + \sqrt{k_y^2 - \lambda_{rel,y}^2}} \tag{22}$$

$$k_y = 0.5\left(1 + \beta_c\left(\lambda_{rel,y} - 0.3\right) + \lambda_{rel,y}^2\right)$$

$$\beta_c = 0.1 \text{ for CLT}$$

$$\lambda_{rel,y} = \frac{\lambda_y}{\pi}\sqrt{\frac{f_{c,0,k}}{E_{0,05}}} \tag{23}$$

3.6 Lateral displacement analysis of CLT shear walls

No literature on the displacement behaviour of CLT cores has been found in literature. Due to three-dimensional nature of the problem, it is expected that lateral displacement analysis of a CLT core is not suitable for calculation by hand. However, lateral displacement of single CLT shear walls has been studied before and is fit for analytical analysis. Therefore, it is discussed in this paragraph. A CLT core is essentially several CLT shear walls that are interconnected.

The lateral displacement in a CLT shear wall can be analysed by hand. Four displacement modes can be distinguished, of which two are related to the CLT panel and two are related to the connections. These displacement modes are shown in Figure 21 for CLT shear walls that are stacked vertically. The same displacement modes hold for single walls. When a CLT shear wall is loaded in the lateral direction, the panel itself experiences in plane bending and in plane shear. This causes a deformation of the panels (denoted u_{EI} and u_{GA}). At the location of the foundation, a couple forms. On the compressive side, the CLT panel takes the compression force. The tensile force is generally transferred by a hold down. Shear force at the base of the wall is normally transferred to the foundation by means of shear angles. The uplift causes a displacement u_{ϕ} and the sliding causes a displacement u_s. The sum of these four contributions is to the total lateral displacement.

Abeysekera et al. [28] concluded that the stiffness of the shear wall can be regarded as a series of springs (Figure 22). The different springs represent the stiffness each displacement mode. An equivalent stiffness can be computed (see eq. 25). In the following paragraphs, the lateral displacements for each displacement mode are derived. For alternative methods for finding the stiffness of CLT shear walls, see Appendix C.

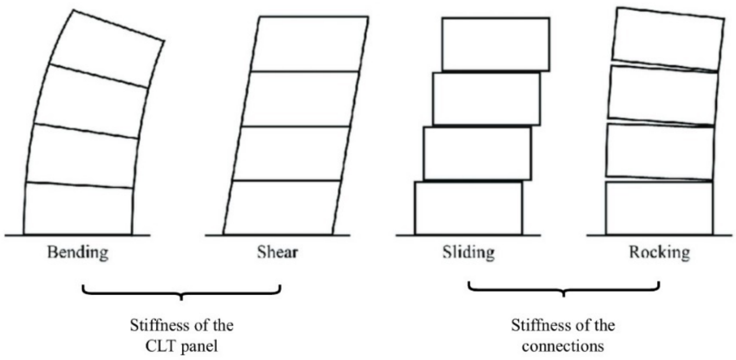

Figure 21 Displacement modes in CLT shear walls (Adapted from [29])

$$u_{TOTAL} = u_{EI} + u_{GA} + u_{\phi} + u_s \tag{24}$$

[28]

$$k_{eq} = \frac{1}{\frac{1}{k_{bending}} + \frac{1}{k_{shear}} + \frac{1}{k_{uplift}} + \frac{1}{k_{sliding}}} \tag{25}$$

[28]

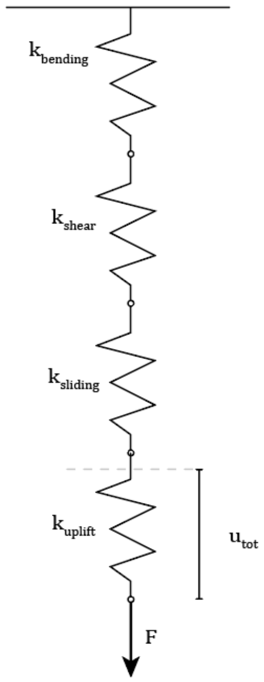

Figure 22 CLT shear wall as a spring in series

3.6.1 Lateral displacements related to the CLT plate

Bending and shear deformations of the CLT plate result in lateral displacements. These can be calculated with Timoshenko beam theory.

$$u_{bending} = \frac{F \cdot h^3}{3E_{mean}I_{net,0}} \tag{26}$$

$$I_{net,0} = \frac{1}{12} d_{0,net} b^3$$

$$u_{shear} = \frac{F \cdot h}{GA_s} \tag{27}$$

$$GA_s = 0.74 \cdot G_{mean} \cdot \left(b \cdot d_{gross}\right)$$

Table 10 Bending and Shear displacement of a CLT shear wall, source: author

<table>
<tr><th>Bending</th><th>Shear</th></tr>
<tr><td>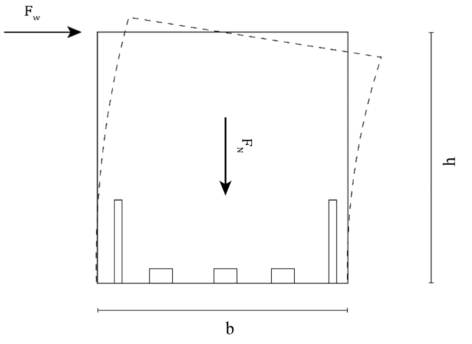</td><td>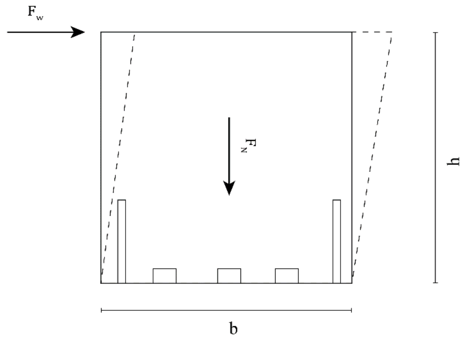</td></tr>
</table>

3.6.2 Lateral displacements due to sliding

Sliding of the CLT wall is shown in Figure 23. It is generally prevented by shear angles that connect the wall with the foundation, and by friction between the wall and the floor. The lateral displacement of the wall due to sliding only is given in equation 28. The static friction force depends on the friction coefficient μ and the downwards vertical force on the wall F_N. $K_{bracket}$ is the linear stiffness of the angle bracket and n is the number of shear brackets. If the result is a negative number, the sliding displacement is set to 0. μ_F is the static friction coefficient and depends on the type of interface.

In some load cases the friction between the shear wall and the floorplate may not be guaranteed. In this case it is better to not reduce the sliding displacement for the friction [30]. In that case, it is assumed that all force is transferred through the shear angles.

$$w_{cs} = \frac{F_w - \mu_F \cdot F_N}{n \cdot K_{bracket}} \tag{28}$$

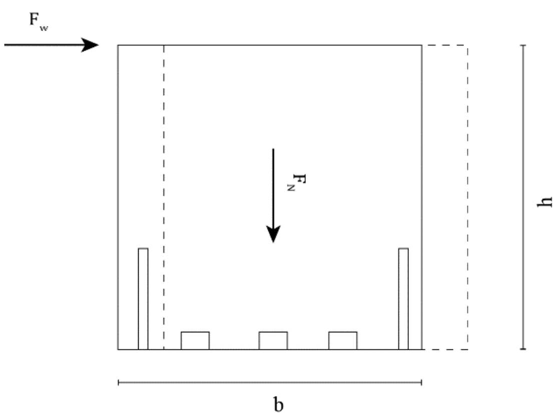

Figure 23 Displacement of a CLT shear wall due to sliding, source: author

Table 11 friction coefficients of timber to timber and timber to concrete [31]

Material	μ_F
Timber and timber	0.4
Rough concrete and timber	0.7

3.6.3 Lateral displacements due to uplift

Uplift of a CLT wall is depicted in Figure 24. This is counteracted by the hold-downs that transfer the tension force. This model assumes that the shear angles do not prevent uplift. For finding the displacement due to uplift, a rigid body rotation can be assumed. The elongation of the hold-down can be found with Eq. 30. In this equation k_{tierod} is the stiffness of the connection for tensile force in N/mm. Eq. 31 serves for finding the rigid body rotation of the wall. The lateral displacement at the top of the wall due to this rotation is found with eq. 32.

$$F_{tierod} = F_w \cdot \frac{h}{b} - \frac{F_N}{2} \tag{29}$$

$$\Delta_{tierod} = \frac{F_w \cdot h}{b \cdot k_{tierod}} - \frac{F_N}{2 \cdot k_{tierod}} \tag{30}$$

$$\theta = \frac{\Delta_{tierod}}{b} \tag{31}$$

$$u_{cu} = \frac{F_w \cdot h^2}{b^2 \cdot k_{tierod}} - \frac{F_N \cdot h}{2 \cdot b \cdot k_{tierod}} \tag{32}$$

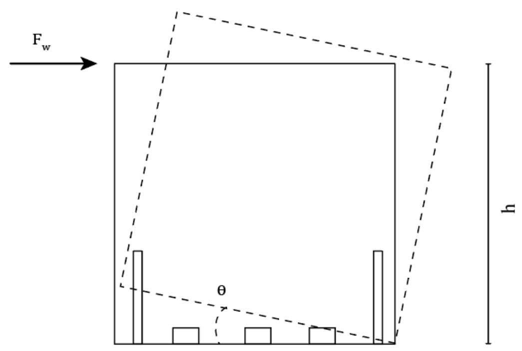

Figure 24 Displacement of a CLT shear wall due to uplift, source: author

3.7 Conclusion

CLT is an orthotropic material that is stiff and strong for loading in-plane. It can carry loads in two directions through diaphragm action. Although CLT is not included in the Eurocode or Dutch

National Annex, multiple guidelines exist for structural design with CLT. Furthermore, the quality of CLT is regulated by European Technical Approvements, which are provided by the supplier.

The mechanical properties of a CLT panel can be attributed to those of the base material. Because of the orthotropic nature of the CLT panel, there are extra points of attention when performing SLS and ULS verifications. The direction of the layers should be included in the verification. Dependent on the verification and the direction of loading, the checks are performed on the "net-section" or the "effective-section". The in-plane shear stiffness of a CLT panel is a complicated topic and is still a subject of study. The stiffness is dependent on the internal geometry of the CLT. For the thesis, the in-plane shear stiffness will be assumed as $\frac{3}{4}$ times the shear stiffness of the base material.

Another important aspect of structural design with CLT is long-term behaviour of the structure. The influence of creep and moisture can be included in SLS verifications by increasing deformations with factor k_{def} and in ULS verifications by adjusting resistances with factor k_{mod}. Values for both k_{def} and k_{mod} are provided based on research by Schikhofer [24]. Including the long-term influences is important for post-tensioned systems as the long-term behaviour of the CLT will influence the prestress level.

Although no research on displacement behaviour of CLT cores is known to the author, CLT shear walls and their behaviour has been the subject of multiple studies. Lateral displacement of a CLT shear wall is a superposition of lateral displacement related to the CLT panel (bending and shear) and to the connections (sliding and rocking). The lateral displacement of a single CLT wall can be found with the analytical equations provided in this chapter. For assessing the lateral displacement related to the connections, the stiffness of connectors in CLT is needed. This will be discussed in Chapter 4.

4 Connections in CLT walls

In Chapter 3, it is shown that for CLT structures, the displacement behaviour is not only dependent on the structural characteristics of the CLT plate but also on the connections (see 3.6 on Lateral displacement analysis of CLT shear walls). The connections in CLT plates have relatively low stiffness properties compared with the stiffness of the plate itself. Therefore, they must be included in the analysis.

In addition, the benefit of post-tensioning depends on the stiffness of the connections. If the CLT core is post-tensioned, the displacements related to the connections are most likely decreased. The displacements related to CLT panel itself are likely not decreased. Thus, the effectiveness of the post-tensioning relies on the role that the connections play in the overall lateral displacements. To answer the main research question of the thesis, a reasonable estimation of the stiffness is therefore required.

Designers usually rely on tests for the stiffness properties of CLT connectors. For some connections, stiffness values from tests are available in ETA's. Unfortunately, this is not always the case. The stiffnesses provided in this chapter are from Rothoblaas seismic testing and tests by Graz University (STS). When test data is not available, interpretations have been made from other Rothoblaas tests.

In this chapter, the stiffness and strength properties of regular connectors is discussed. Recently, different types of special connectors are available on the market for special applications. These connections are considered outside the scope of the thesis. The connectors considered here are Shear Angles (SA), Hold-Downs (HD), and Self-Tapping Screws (STS), which are products that are currently on the market.

4.1 Self-tapping Screws

A common method of connecting multiple CLT walls is with multiple Self-Tapping Screws (STS) in a row. The STS can be used to connect two walls in plane, or to connect perpendicular walls. STS are available on the market in large lengths of up to 600 mm. Often, they are applied under an angle of $90°$ or $45°$. Some possible connection designs for STS connecting two CLT plates in-plane are shown in Figure 25.

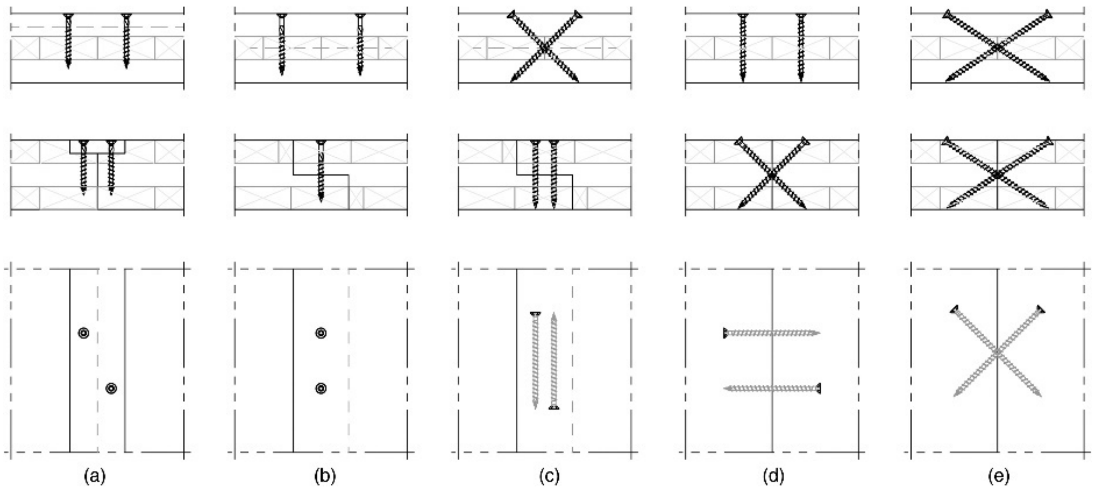

Figure 25 Connection designs for connecting two CLT plates in-plane with STS [32]

4.1.1 Stiffness and strength

The stiffness and strength of the self-tapping screws (STS) depends on the direction of loading. Tests performed by the University of Graz give an indication of the stiffness and strength of STS under an angle of $45°$ and $90°$ for lateral load and axial load. Test configurations were like in Figure 26. It is likely that the screw diameter and screw length have an influence on the stiffness. However, the diameter and length of the screws tested are not provided in the test paper.

The results of the tests are summarized in Table 12. Note that in this table, results of the tests on STS under $90°$ angle are given for a single screw, while results for STS under $45°$ are given for STS-pairs. This corresponds with the test configurations shown in Figure 26. The results of the tests show that for lateral loading, there is a clear benefit of placing the screws under an angle of $45°$. The stiffness of a single screw under $90°$ under lateral loading is only $0.5\ kN/mm$. Placing the screw under $45°$ instead increases the stiffness to $\approx 10\ kN/mm$.

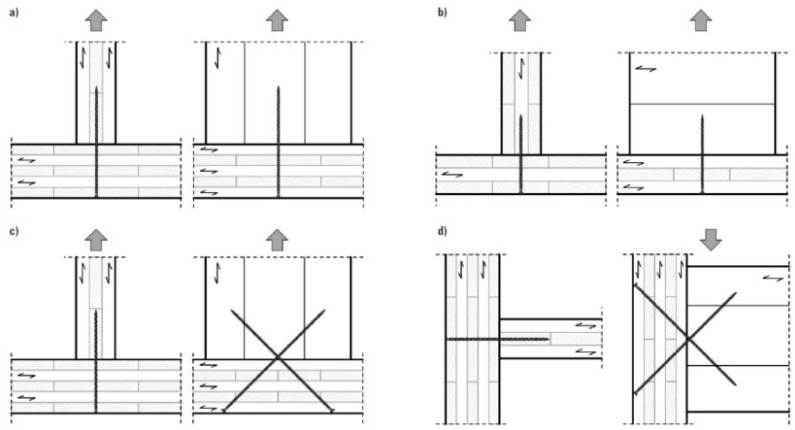

Figure 26 STS test configurations [33]

Table 12 Test results stiffness and strength of STS connections [33]

Angle	Loading	F_{max} [kN]	K_{ser} [kN/mm]
90°	Axial	20.8	17.5
90°	Lateral	10.3	0.5
45°	Axial	33.6	16.6
45°	Lateral	30.0	19.9

4.2 Hold-downs

Hold-downs are often used to transfer tensile forces from shear walls to the foundation. Hold-downs of different sizes are available on the market. In Figure 28a common hold-down for CLT structures by Rothoblaas is shown.

4.2.1 Stiffness

Rothoblaas performed tests on hold-downs in different configurations and nailing patterns. The WHT620 connection (see Figure 27) connecting CLT to a steel beam was tested in a lab. Rothoblaas' test configuration for this test is displayed in Figure 28. An overview of all tests on Rothoblaas' hold-downs is shown in Appendix D.

The stiffness of the hold-down may be increased by for instance changing to a larger hold-down to allow for more screws or changing the length of the screws.

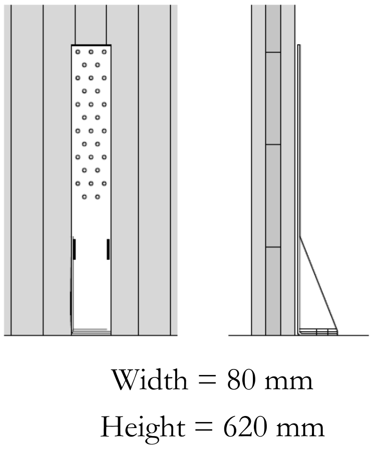

Figure 27 front and side view of hold-down WHT620 by Rothoblaas [34]

Figure 28 Rothoblaas test of WHT620 hold-down [34]

Table 13 Rothoblaas' test results for the stiffness of WHT620 connectors [35]

Connection type	Fastening	Nails / screws	Stiffness $K_{ser,1}$ $[\frac{N}{mm}]$
WHT620 CLT on Steel beam	Total Fastening 52/55 With washer	Nails Ø4 × 60	10310

4.2.2 Strength

Rothoblaas' ETA provides guidelines for finding the strength of hold-downs in line with a Eurocode approach. The resistance of the HD is the minimum of: (1) the resistance in the CLT, (2) the steel cross-section and (3) the embedding in the concrete (Eq. 33) [34]. The characteristic values of the resistances for the Rothoblaas WHT620 hold-down is presented in Figure 29. For the complete calculation design resistance of the WHT62- hold-downs, see Appendix E.

$$R_{d,HD} = \min \begin{cases} \dfrac{R_{1,k,timber} \cdot k_{mod}}{\gamma_m} \\ \dfrac{R_{1,k,steel}}{\gamma_{steel}} \\ \dfrac{R_{1,k,cls}}{\gamma_{cls}} \end{cases} \tag{33}$$

WHT620

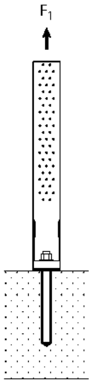

CHARACTERISTIC VALUES

	$R_{1,k}$ TIMBER				$R_{1,k}$ STEEL			$R_{1,k}$ UNCRACKED CONCRETE			$R_{1,k}$ CRACKED CONCRETE		
configuration	fasteners holes Ø5			$R_{1,k\ timber}$	washer	$R_{1,k\ steel}$		anchor VINYLPRO	$R_{1,k\ cls}$		anchor EPOPLUS	$R_{1,k\ cls}$	
	type	**Ø x L** [mm]	n_v [pcs]	[kN]		[kN]	γ_{steel}	**Ø x L** [mm]	[kN]	γ_{cls}	**Ø x L** [mm]	[kN]	γ_{cls}
• total fixing • washer WHTBS70L • M24 anchor	nails LBA	Ø4,0 x 40	55	**86,4**	WHTBS70L	**85,2**	γ_{m2}	M24 x 270	**148,98**	1,8	M24 x 270	**70,57**	2,1
		Ø4,0 x 60	55	**106,2**							M24 x 330 [(1)]	**90,93**	2,1
	screws LBS	Ø5,0 x 40	55	**86,4**									
		Ø5,0 x 50	55	**106,2**									
• partial fixing • washer WHTBS70L • M24 anchor	nails LBA	Ø4,0 x 40	33	**51,8**	WHTBS70L	**85,2**	γ_{m2}	M24 x 270	**148,98**	1,8	M24 x 270	**70,57**	2,1
		Ø4,0 x 60	33	**63,7**							M24 x 330 [(1)]	**90,93**	2,1
	screws LBS	Ø5,0 x 40	33	**51,8**									
		Ø5,0 x 50	33	**63,7**									
• total fixing • washer WHTBS70 • M20 anchor	nails LBA	Ø4,0 x 40	55	**86,4**	WHTBS70	**85,2**	γ_{m2}	M20 x 240	**114,35**	1,8	M20 x 240	**57,17**	2,1
		Ø4,0 x 60	55	**106,2**									
	screws LBS	Ø5,0 x 40	55	**86,4**									
		Ø5,0 x 50	55	**106,2**									
• partial fixing • washer WHTBS70 • M20 anchor	nails LBA	Ø4,0 x 40	33	**51,8**	WHTBS70	**85,2**	γ_{m2}	M20 x 240	**114,35**	1,8	M20 x 240	**57,17**	2,1
		Ø4,0 x 60	33	**63,7**									
	screws LBS	Ø5,0 x 40	33	**51,8**									
		Ø5,0 x 50	33	**63,7**									

[(1)] Length obtainable from MGS threaded bars (to be cut to measure)

Figure 29 Resistance of Rothoblaas' WHT620 hold-down [34]

4.3 Shear angle

Shear angles are used for connecting CLT walls to the floor. They are used specifically for transferring shear forces to concrete or CLT floors. SA's resist sliding of CLT walls. As an example, Rothoblaas' shear angle TCN240 is discussed in this section. Find the geometry of the connector in Figure 30.

4.3.1 Stiffness

For the stiffness of SA's, Rothoblaas has performed tests on SA connecting CLT to CLT and CLT to Concrete. The test configuration is shown in Figure 31. Table 14 lists the test results for the stiffness of Rothoblaas' TCN240 connector. This is a connector that is meant for connecting a CLT wall to a concrete floor. Results indicate that though these connectors are primarily used for transfer of shear force, they also have significant tensile stiffness.

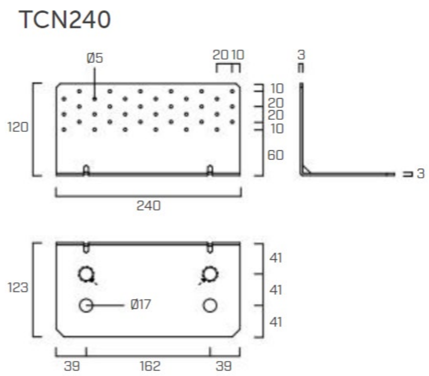

Figure 30 Geometry of TCN240 connector [36]

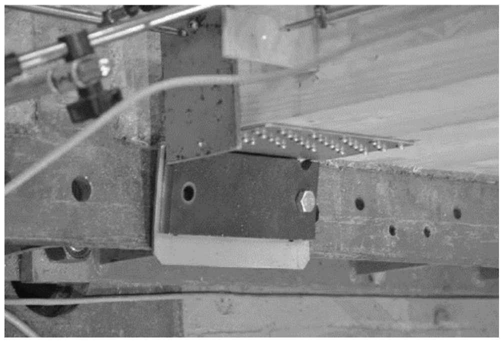

Figure 31 Test on TCN240 connection to failure [35]

Table 14 Rothoblaas' test results for the stiffness of TCN240 connectors [35]

Connection type	Fastening	Nails/Screws	Stiffness lateral $K_{ser,2/3}$ $[\frac{N}{mm}]$	Stiffness tensile K_{ser1} $[\frac{N}{mm}]$
TCN240 Without washer	14 screws in CLT 2 anchors in concrete	Nails Ø8 × 80	8200	5500

4.3.2 Strength

The strength of the shear angle is, is the minimum of the embedding strength in the concrete and in the timber and can be determined by determined by Eq. 34 [36]. The characteristic values for the embedding strength are shown in Figure 32.

$$R_{d,HD} = \min \begin{cases} \dfrac{R_{2/3,k,timber} \cdot k_{mod}}{\gamma_m} \\ \dfrac{R_{2/3,k,cls}}{\gamma_{cls}} \end{cases} \tag{34}$$

TITAN TCN240

TIMBER STRENGTH $R_{2/3}$

configuration on timber	type	hole fixing Ø5 Ø x L [mm]	hole fixing Ø5 n_V [pcs]	CHARACTERISTIC VALUES $R_{2/3,k\ timber}$ [kN]
nails	LBA	Ø4,0 x 60	36	**30,3**
screws	LBS	Ø5,0 x 50	36	**36,3**

CONCRETE STRENGTH $R_{2/3}$

configuration for type of concrete	type of anchor (3)	hole fixing Ø13 Ø x L [mm]	hole fixing Ø13 n_H [pcs]	hole fixing Ø13 steel class	CHARACTERISTIC VALUES $R_{2/3,k\ cls}$ IN (1) [kN]	CHARACTERISTIC VALUES $R_{2/3,k\ cls}$ OUT (2) [kN]	CHARACTERISTIC VALUES γ_{cls}
• uncracked concrete • screw anchor	SKR	16 x 130	2	-	**76,9**	**56,9**	1,5
• uncracked concrete • mechanical anchor	AB1	M16 x 138	2	-	**59,5**	**44,0**	1,5
• uncracked concrete • chemical anchor	VINYLPRO	M16 x 160	2	5.8	**52,7**	**39,0**	1,25
• cracked concrete • chemical anchor	EPOPLUS	M16 x 160	2	5.8	**52,7**	**39,0**	1,25

Figure 32 Resistance of Rothoblaas' TCN240 Shear Angle [36]

4.4 Conclusion

Multiple types of connections are used in CLT walls. Hold-downs are often used for transfer of tensile forces to the foundation. Shear angles are used for transfer of shear forces, though they also have significant tensile stiffness. Self-Tapping Screws are used for connections between two walls in-plane or between two perpendicular walls. Due to their limited stiffness, connections in CLT influence the structural behaviour of CLT walls significantly.

Though strength values of connectors are provided in accompanying ETA's, stiffness values are not always available. The designer relies on tests results, which are limited. In this chapter, an indication has been given for the stiffness of SA, HD and STS based on different test reports.

The stiffness of the connections also dictates how much connected walls cooperate in carrying load. This is explained in the following chapter (Chapter 5). Because of the connections in CLT walls, non-linearities are introduced which make analysis of CLT structures by hand a cumbersome task. For structures that include multiple walls, it is recommended to use a finite element model to assess the behaviour . In FEM models of CLT walls, extra attention should be paid to the modelling of connections.

5 Effective flange width

Figure 21 on page 23 showed the four displacement modes that apply to CLT shear walls. Similarly, the lateral displacement of the core can be regarded the sum of bending, shear, sliding and uplift displacements. This chapter focusses on the bending displacement of a CLT core.

The displacements of the core can be analysed by using beam analogy, by regarding the core as a cantilever beam. The stiffness of the core for bending can be calculated by assuming that plane sections remain plane. This assumption may not be valid in the case of the core, which will be explained in 5.1. The first reason is the shear lag effect, which will be elaborated in 5.2. The second reason is the connection between the different core walls. This is analysed in 5.3. The chapter proposes the "effective-width" method. Finding an appropriate effective width would benefit the designer, as it would make it possible to make quick hand calculations on the bending displacements of a CLT core.

5.1 Plane sections do not remain plane

A CLT core consists of several connected walls. In hand-calculation, the bending stiffness of the core can be assumed under the Bernoulli Hypothesis. This implies that plane sections remain plane after loading. This assumption is not applicable to a CLT core because of two reasons:

- There is a possibility for shear lag. This makes that the normal stresses in the flange are not constant over the width of the flange. This effect is discussed in 5.2.
- It is known that when the two walls are connected semi-rigidly, such as with the STS connectors, there will be a discontinuity in the strains between the flange and the web. This is explained in 5.2.3.

Both shear lag and the semi-rigid corner decrease the stiffness of the core. This reduction can be expressed by an "effective flange width". By assuming only, the effective flange width in the section of the core, the stiffness of the core can be calculated with Bernoulli beam theory.

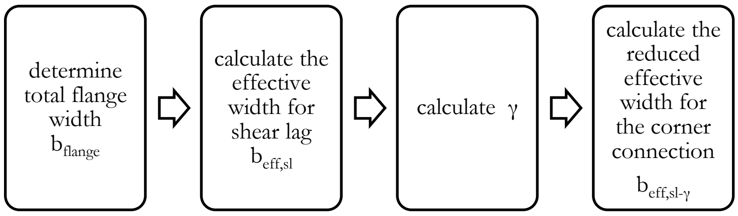

$$b_{eff,flange} = \gamma \cdot b_{flange,shear-lag} \quad (35)$$

γ	$b_{flange,sl}$
- accounts for semi-rigid connection between web and flange - calculated based on $b_{flange,sl}$	- accounts for non-linear normal stress along flange width - calculated based on assumption of rigid connection between web and flange

5.2 Effective width for shear lag

5.2.1 The shear lag effect

In a cross-section such as presented in Figure 33, the web and the flanges are connected in a way that relative displacements cannot occur at the connection. Therefore, at this connection point, the normal strain in the web is equal to that in the flange. Because of shear flow between the web and the flange, the flange plate deforms. In that way the in-plane displacements of the flanges farther away from the connection to the web, lag compared to the longitudinal displacements of flange at the connection with the web. This causes a non-linear normal stress along the flange width. This phenomenon is called shear lag. A common approach for handling shear lag is by only taking into account an "effective flange width" and assuming a constant normal stress over the width of this flange, as shown in Figure 34. In the following paragraphs, the magnitude of this effective width will be discussed.

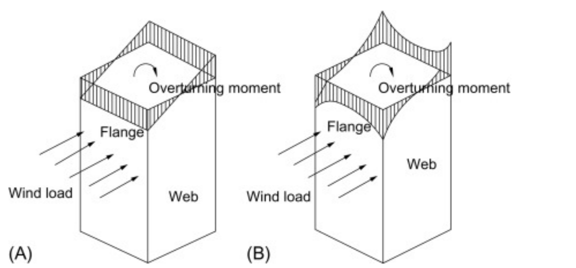

Figure 33 longitudinal stresses with: no shear lag (A), shear lag (B) [37]

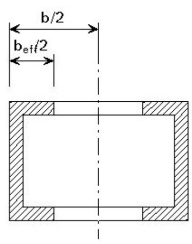

Figure 34 Effective flange width of a core [38]

5.2.2 *Effective width method applied to timber beams*

No research on the effective width of timber cores is available. In the Eurocode on timber structures (EN1995-1-1), the effective width method is mentioned in relation to timber beams. The Eurocode approach is shown in Figure 35. A timber core is not similar in ratio compared to a timber beam. Furthermore, a core, contrary to a beam, is generally not only subject to axial forces due to bending but also due to axial load. Therefore, the effective width equations for timber beams cannot be applied to a timber core one-to-one. Still, the effective width equations for timber beams will be discussed.

Currently, EN1995-1-1 includes information on the flange width reduction for shear lag is for thin flanged timber beams made of plywood, OSB or particleboard. For thin flanged beams, the maximum effective flange width is given for the simply supported case. The maximum effective width for shear lag is expressed as a ratio of the span of the beam (l) and depends on the material of the flange. In case the regarded structure is a cantilever, the span l can be taken as twice the cantilevering length.

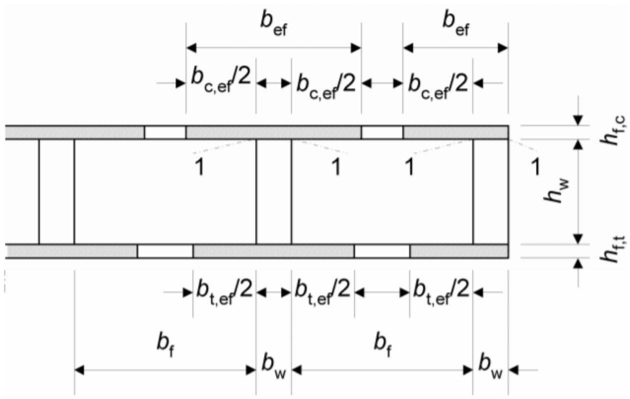

Figure 35 Effective flange width thin flanged timber beam [26]

Table 15 Maximum effective flange width Eurocode [26]

Flange Material	Shear lag
Plywood, with grain direction in the outer plies: -Parallel to the webs -Perpendicular to the webs	 $0.1 \cdot l$ $0.1 \cdot l$
OSB	$0.15 \cdot l$
Particleboard or fibreboard with random fibre orientation	$0.2 \cdot l$

5.2.3 *Effective width method applied to concrete cores*

No research has been found that focusses on effective width of timber cores. Therefore, equations for the effective width of concrete cores are discussed in this paragraph.

Equations for the effective flange width of reinforced concrete cores have been proposed by Ray (Eq. 36&37) [39]. The equations are adopted from equations for cantilever beams with a uniformly distributed load in the British Standard (BS 5400: Part 5) [40]. Definitions for the effective width can be found in Figure 36.

$$b_{e1} = 0.85 \cdot \psi \cdot b_1 \tag{36}$$

$$b_{e2} = \psi b_2 \tag{37}$$

Table 16 Effective width factors (ψ) from BS5400: Part 5 [40], H_n = height of the core

b/H_n	ψ
0	1
0.05	0.82
0.1	0.68
0.2	0.52
0.4	0.35

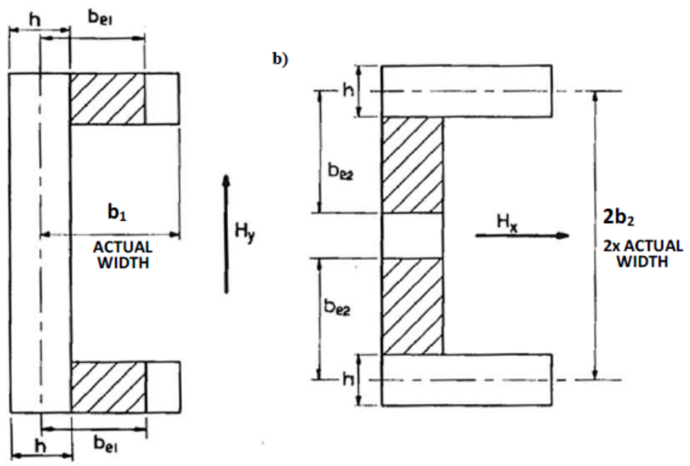

Figure 36 Effective width (b_{e1} and b_{e2}) for a C-shaped wall as proposed by Ray [39]

Hoult [41] states that the effective-width equations for cantilever beams do not accurately reflect the behaviour of C-shaped reinforced concrete cores. For C-shaped cores, Hoult proposes equation 38 for the effective width. Parameters α and β depend on the parameters in Table 17. According to Hoult, the height of the core does not have a significant influence. Dependent on the parameters in Table 17, $0.64 \leq \alpha \leq 0.87$ and $-3.6 \leq \beta \leq 1.0$. This means that excluding the effect of the axial load, 64%-87% of the flange can be regarded effective. For more information about how to determine the factors α and β, reference is made to Appendix D.

$$b_{eff} = \alpha b(1 + \beta ALR) \tag{38}$$

[41]

Where:

b_{eff}	Effective width
b	Total width of the flange
ALR	Axial load ratio (ratio between the axial load and the axial capacity)
α, β	Effective width coefficients (see Appendix D)

Table 17 Parameters of influence on the effective width by Hoult [41]

Parameters of influence on the effective width of C-Shaped concrete cores by Hoult [41]
Load direction (see Appendix D)
Flange/web in tension or compression
Performance level (yield or ULS)
Distributed or concentrated reinforcement

5.3 Semi-rigid connection between flange and web

When the flange and the web are connected semi-rigidly, relative displacements will occur between the flange and the web of the core. Because of these relative displacements, the Bernoulli hypothesis that the strain is linear over the height of the section does not fulfil.

For the stiffness of the core, two limits can be distinguished: (1) all walls cooperate perfectly and (2) all walls are completely disconnected. For a thin walled square section, the displacements in situation (2) are four times larger than in (1). The derivation for this analysis is provided in Appendix G.

To find a realistic stiffness between the two limits, the gamma method for mechanically connected beams may be used. This method is shown in Figure 37. This method is valid for cross-sections with up to three different parts connected with fasteners. The γ-expresses the degree of cooperation of the different parts in the cross-section. It takes on a value between 0 and 1. This number denotes the value by which the Steiner parts need to be reduced in the stiffness calculation.

1. $\gamma = 1$ The bending stiffness is the stiffness of the section with rigid joints (Steiner parts are fully included).
2. $\gamma = 0$ The bending stiffness is the stiffness of a section with unconnected parts (no Steiner parts are included).

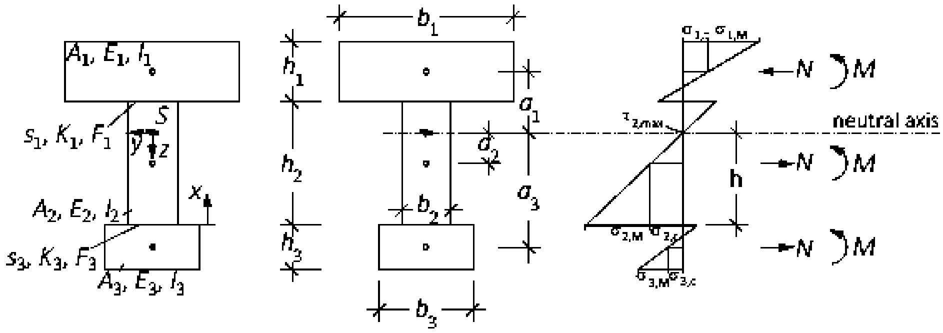

3. *Figure 37 Stresses assumed not linear over height of the section [26]*

$$(EI)_{eff} = \sum_{i-1}^{3} (E_i \cdot I_i + \gamma_i \cdot E_i \cdot A_i \cdot a_i^2) \tag{39}$$

[26]

An expression for the γ-factor was provided by Möhler (Eq. 40 & 41) [26]. Strictly speaking, the expression for γ is only valid for simply supported beams with a sinusoidal load. The method can, however, be used to beams with uniformly distributed loading, as differences in the results are small. With inputting an appropriate length l equal to twice the cantilever-beam-length, the expression for γ can also be used for cantilever beams. The γ-method does not consider the out of plane shear deformation, thus works best for beams with a high span, such that the out of plane shear deformations a are negligible compared to the bending deformations.

$$\gamma_i = \frac{1}{1 + \frac{\pi^2 \cdot E_i \cdot A_i \cdot s_i}{K_i \cdot l^2}} \text{ for i =1 and i=3} \tag{40}$$

$$\gamma_2 = 1 \tag{41}$$

Where:

E_i	Modulus of elasticity
A_i	Cross-sectional area
I_i	Second moment of area
s_i	Fastener spacing in joint between individual components
k_i	Slip modulus of the fasteners
l	Member length
h_i	Depth of individual component

5.4 Conclusion

Both the shear lag effect and semi-rigid corner connection of the core decrease the stiffness of the CLT core. An approach has been proposed for calculating the effective width of the core, which includes first calculating the effective width for shear lag, and secondly calculating the influence of the corner connection with factor γ. The bending stiffness of the core can be determined while including only the part of the flange that is considered effective.

No equations for the effective width due to shear lag for a timber core is available in literature. Effective width analysis of C-shaped concrete cores showed a cooperation of the core of 64-87 %, as found by Hoult [41] . Similar research into effective flange width of timber cores could provide the designer with practical knowledge for stability design using CLT. No studies are available that go into depth on the cooperation between different walls in a timber core, dependent on the connections between perpendicular walls. To still make an estimation of the cooperation, one can make use of the theory of mechanically connected timber beams. The theories discussed in this chapter will be applied to the case-study (9.4 Effective flange width analysis), in an attempt to further the bending stiffness of a CLT core and assess the approach suggested in the current chapter.

6 Unbonded post-tensioned CLT

This chapter focusses on the theory behind post-tensioning of CLT. In section 6.1, the state of the art with regards to prestressed CLT structures is discussed. In section 6.2, the stiffness of a CLT wall prestressed with a single prestress rod is explained. In section 6.3, needed information on the post-tension rods for design is provided. Post-tensioned CLT will experience prestress force loss over time. The different causes of prestress loss are explained in section 6.4. Some topics on the introduction of the prestressing force can be found in section 6.5.

6.1 State of the art

As far as the author's knowledge goes, no post-tensioned CLT cores have been built to this date. Also, no research projects specifically on post-tensioning a CLT core has been found.

There are, however, some realized projects and research projects on post-tensioned CLT shear walls. Most of these focus on post-tensioned CLT shear walls for earthquake design. An example of a realized building with post-tensioning is the three storey NMIT arts & media building in New-Zealand [42]. In Figure 38, the self-centering rocking walls of the NMIT building are shown. The projects focus on minimizing post-earthquake damage by the recentering effect of CLT rocking walls and on energy dissipation.

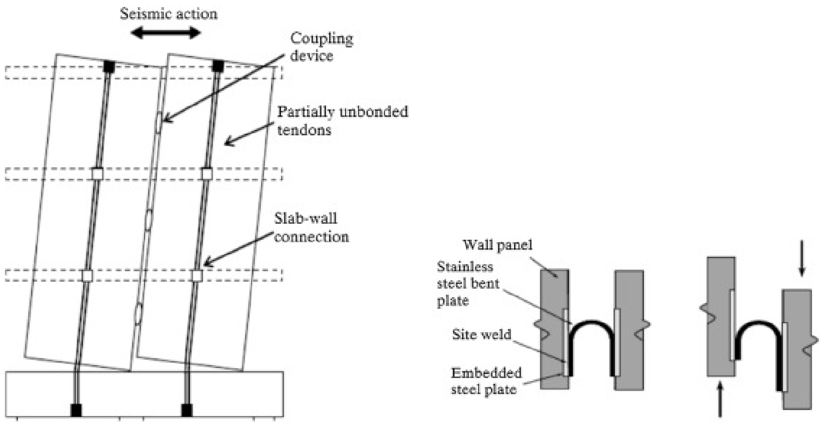

Figure 38 Rocking CLT walls (left) and steel plates as coupling device for energy dissipation (right) [42]

Figure 39 South Façade Limnologen [43]

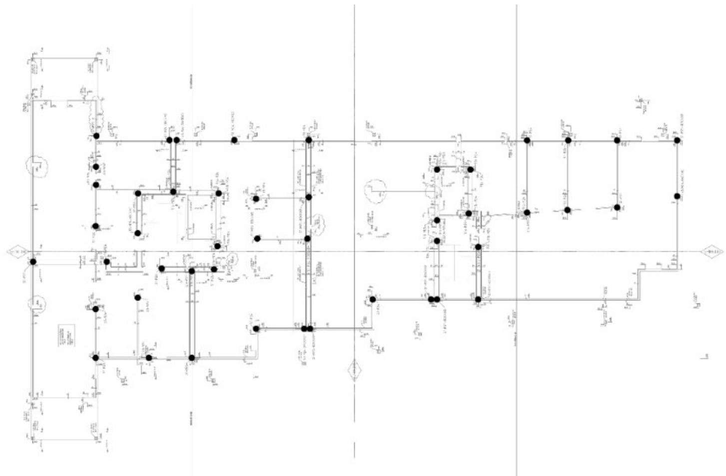

Figure 40 Floor plan level 3 Limnologen building, post-tension rods marked with black dots, adapted from [44]

Lateral displacement of CLT shear walls has been studied by Akbas et al for earthquake design [28]. He has introduced a load displacement graph of a CLT shear wall prestressed with a single tendon, displayed in Figure 41. Several "limit states" have been identified, that reflect certain points along the load displacement graph. In this thesis, the focus is on SLS governing design. Uplift will be small and the CLT will be designed to stay within the elastic range. Therefore, for this thesis, only the first three limit states from his paper are relevant. The relevant limit states for SLS level loading are shown in Figure 42. These limit states are:

a) DEC: the decompression limit. A this point, the stress in the CLT wall on the tensile side is 0. The wall is just at the limit of starting to tilt. At this point, there is not yet any uplift.
b) ELL:The effective linear limit. The steel stress is (almost) equal to the initial post-tension force. Equilibrium can be found between the stress in the CLT and the lateral force F without increase of the prestressing steel stress. From this point on, an iterative procedure is needed to find the right prestressing steel stress increase. That makes this the linear limit.
c) YCLT: yielding of the CLT. The CLT has reached the elastic strain and the lateral displacement has increased significantly.

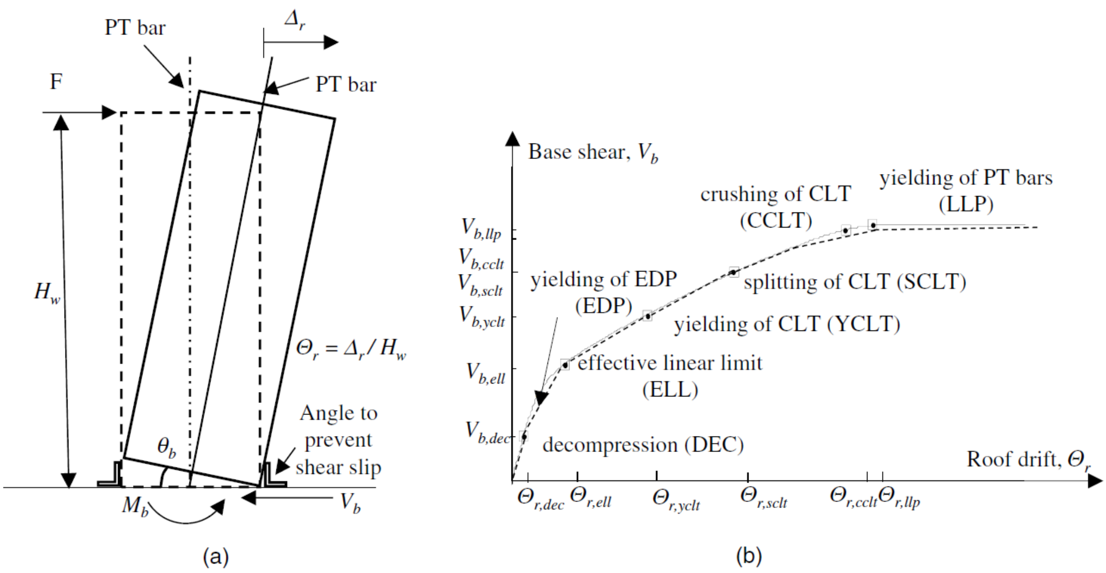

Figure 41 (a) Rocking behaviour of SC-CLT wall under lateral load; (b) base shear-roof drift behaviour of SC-CLT walls under lateral load with limit states [45]

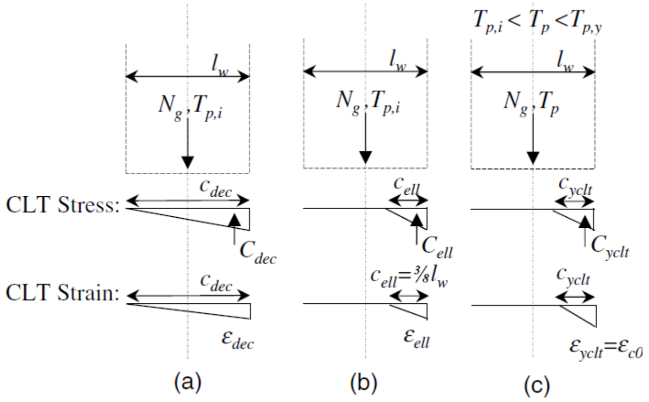

Figure 42 Limit states below yield limit of the CLT by Akbas et al. [45]

Limited literature is available on the design of post-tensioned shear walls for SLS level loading. In research by Xia and van de Kuilen [46], the lateral behaviour of a post-tensioned CLT walls is explored. With a finite element model, the lateral displacement of a 40-storey timber building stabilized with four concrete outriggers in combination with post-tensioned CLT walls is explored. A conclusion of this paper was that in the studied case, post-tensioning the CLT walls reduces the displacements with 30% [46].

The only realized post-tensioned CLT building designed for SLS governing design is the Limnologen building in Växjö, Sweden. The project is shown in

Figure 39 and Figure 40. In this project, post-tensioned CLT shear walls distributed throughout the building are used for stability and resistance against uplift. This project was part of an elaborate research project, in which the development of the prestress force over time was measured. More information on this project is stated in Appendix H on page 125.

The theory behind long term effects of post-tensioned CLT are not analysed in most of the above-mentioned projects. The time dependent deformations are mentioned as a topic for further study in the research by Xia [46]. Time dependent deformations are discussed in depth by Nguyen [47]. His research on the stiffness of CLT panels will be discussed in 6.2. His work on long-term prestress loss is a foundation for the analysis in Chapter 7.

6.2 Axial stiffness of the post-tensioned CLT plate

For a post-tensioned CLT wall, like is depicted in Figure 43 , the stiffness of the system depends on the stiffness of the CLT panel and the stiffness of the tension rod. The meaning of the variables in Figure 43 is listed in Table 18. When prestressing the CLT wall, the cable is elongated. Under the post-tension force the panel is in turn compressed. The stiffness of the cable depends on the rested cable length L_{c0}. Nguyen solved both the stiffness of the CLT wall and cable and derived the rested cable length. The stiffness of cable and CLT panel may be expressed as in Table 19. The derivation of effective cable length L_{co} can be found in Appendix I.

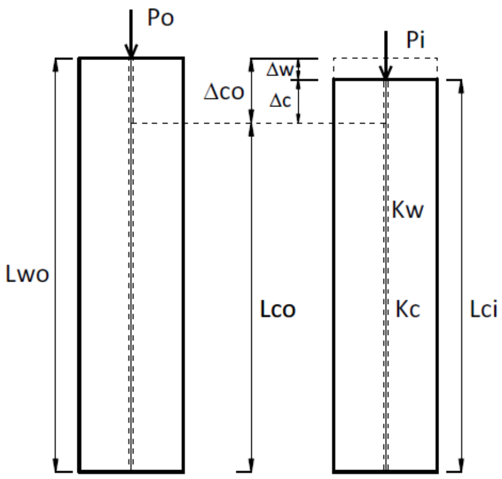

Figure 43 Equilibrium of the CLT plate and prestressing rod [47]

Table 18 Variables in Figure 43

L_{wo}	Initial length of the CLT plate
P_0	Initial prestressing force
Δw	Deflection of the CLT plate under force P_0
Δc	Elongation of the cable under the effect of P_0
K_w	Stiffness of the CLT plate
K_c	Stiffness of the tension rod

L_{co}	Rested cable length
P_i	New cable force

Table 19 Stiffness of CLT plate and prestressing rod [47]

Stiffness CLT wall	$K_w = \frac{E_w A_w}{L_{w0}}$
Stiffness Cable	$K_c = \frac{E_c A_c}{L_{c0}}$

6.3 Prestressing steel

In this thesis, it is assumed the prestressing is done with bars such as the bar in Figure 44. If large bar lengths are required, coupling may be done with coupling elements (see Figure 45). Common sizes and corresponding maximum prestress forces are shown in Table 20.

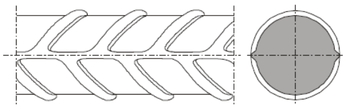

Figure 44 Ribbed prestressing bars [48]

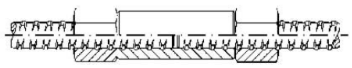

Figure 45 Coupling element by Diwidag [49]

Table 20 Common diameters of prestressing rods, their area and maximum force

Diameter $[mm]$	25	26.5	32	36	40	50
Area $[mm^2]$	491	552	804	1018	1257	1963
Maximum prestress force $[kN]$	380	427	621	787	972	1517

Figure 46 shows the stress strain relation of often used prestressing- and reinforcing steel types. Y1030H prestressing steel is characterized by a relatively low ultimate stress level and a somewhat larger yield plateau compared to cold-worked prestressing steel types (Y1670, Y1770, Y1860). The cold-worked steel types are applied to prestressing *tendons*. The behaviour of the prestressing steel can be simplified to a bilinear diagram which is useful for design (see Figure 47). The material factor (γ_s)for prestressing is equal to 1.1 in line with EN1992-1-1 [50]. Find the corresponding values for significant points in the bilinear diagram in Table 21.

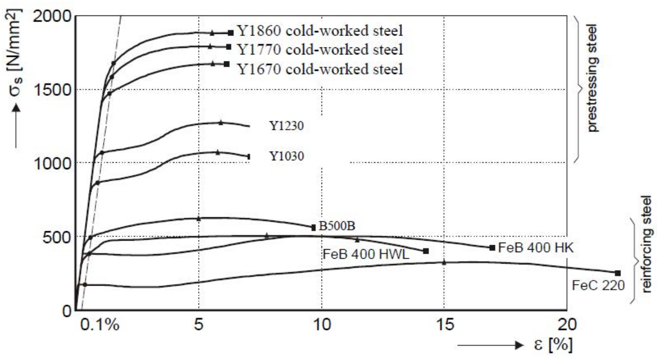

Figure 46 Stress-strain diagram prestressing steel [48]

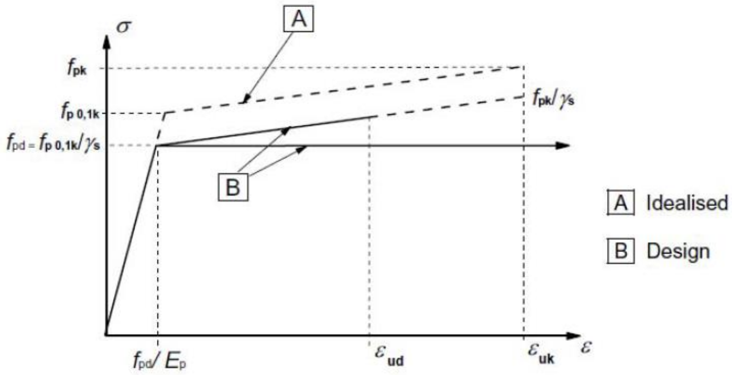

Figure 47 Bilinear stress strain relationship [48]

Table 21 Material properties Y1030H

Characteristic of Y1030H prestressing steel		
Tensile Strength	$f_{pk}\ [MPa]$	1030
	$\frac{f_{pk}}{\gamma_s}\ [MPa]$	936
Fracture strain	ϵ_{uk} [‰]	35
0.1% proof stress	$f_{p0,1k}\ [MPa]$	927
Maximum tensile stress during prestressing	$\sigma_{p_{max}}\ [MPa]$	773
Slope discontinuity in the σ-ϵ diagram (ULS)	$f_{pd}\ [MPa]$	843
Modulus of elasticity .	$E_p\ [GPa]$	205
Design fracture strain	$\epsilon_{ud} = 0.9 \cdot \epsilon_{uk}$ [‰]	31.5

6.4 Prestress Losses

There are several reasons for prestress losses in the lifetime of the post-tensioned structure. Distinction can be made between time-dependent losses, and losses that occur directly at application of the prestress force. An overview of what is presumed to be the most important prestress losses are shown in Figure 48. The time dependent losses have significant influence on the effectiveness of the post-tensioning. Since time dependent losses of post-tensioned CLT structures are a comprehensive topic, a separate chapter is dedicated to the subject (Chapter 8). The immediate losses are expected to have a far smaller influence. More information on immediate prestress losses can be found in Appendix J and Appendix K.

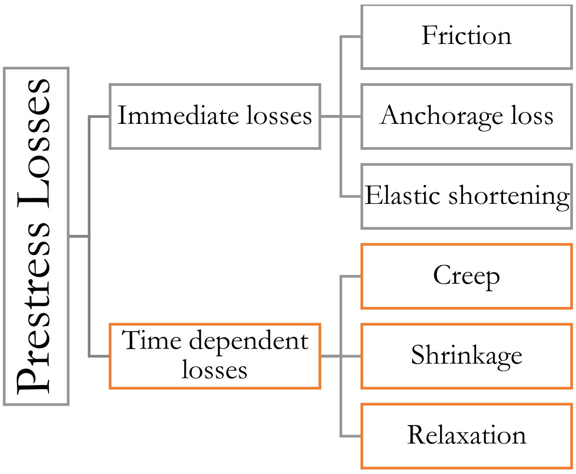

Figure 48 Most important prestress losses in CLT structures, source: author

6.5 Anchorage and splitting force

Common methods of attaching the bar to the anchor plate in concrete structures is by means of a wedge or a simple nut. Similar methods could be used for anchoring the bars to CLT. In the limnologen project, the anchorage was designed with an anchor plate and a simple nut (Figure 49). Bearing stresses should be studied to make sure the maximum compressive stress is not exceeded at the location of the anchor.

Figure 49 Anchorage of the PT bars at highest point in the Limnologen Project [51]

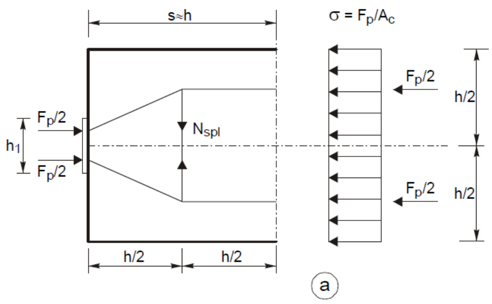

Figure 50 splitting force calculations in Concrete Structures, similar method may be applicable in CLT structures [48]

The locally introduced anchor force needs to be spread to the overall section. This makes causes tensile stresses close to the anchor, perpendicular to the prestress element axis. In prestressed concrete structures, these forces are called “splitting forces”. Analysis of the splitting forces can be done by hand or with a finite element model. A strut and tie model to analyse splitting force is shown in Figure 50. Because CLT does have some tensile capacity, it is likely that the CLT can take up the splitting forces. The orthogonal lay-up of the CLT is likely to have an influence on the spreading of the compressive force. Further study is recommended on this subject.

6.6 Conclusion

Prestressing of CLT is still an experimental subject. Not many prestressed CLT buildings have been realized, and research projects on the topic are scarce. Most projects focus on ULS governed design, specifically on self-centering in the event of an earthquake. This thesis focusses on serviceability limit state governed design. Nevertheless, the research projects on self-centering prestressed CLT shear walls were of value for understanding the mechanics of a post-tensioned CLT wall. For an example of post-tensioning applied in CLT shear walls for reduction of serviceability limit state governed design, reference can be made to the Limnologen Project in Sweden.

For the design of the prestressing, one can use bars or tendons. The material behaviour can be simplified with a bi-linear stress diagram, as in EN1992-1-1. Because there is no bond between the steel and the CLT, the system relies solely on the anchorage. Therefore, reliable design of the anchorage is important. Around the anchor, perpendicular tensile stresses may arise. For this further research is suggested.

In this chapter, the combined stiffness of prestressed CLT walls has been found successfully. This stiffness is needed for the calculation of prestress force losses. The prestress force losses are important when designing post-tensioned structures. Distinction can be made between immediate losses and long-term losses. The long-term losses are expected to be of high influence and require in depth analysis. Therefore Chapter 8 is devoted to the topic of long-term losses.

7 Time dependent prestress losses

Estimating the prestress losses is an important step in the design of a post-tensioned core, but it is presumably the most challenging step in the design process. Creep, Shrinkage are expected to be the most dominant prestress losses and are discussed in 7.1 and 7.2. A method of quantifying the relatively small prestress loss related to relaxation of the prestressing steel can be found in Appendix K. In, a Python model will be introduced for calculating the long-term prestresses losses.

Important prestress losses of post-tensioned CLT

- **Creep of the CLT panel (8.1)**
- **Shrinkage of the CLT panel (8.2)**
- **Relaxation of the steel rod**

Multiple factors make the estimation of prestress losses a complex task. First, dimensional changes of CLT due to shrinkage, and stiffness changes due to creep need to be related to a stress loss in the steel. This is a non-linear problem and asks for an extra look into the derivations in section 6.2 on the stiffness of a CLT panel. Secondly, it must be researched how CLT reacts to long-term loading. Creep of CLT is an extremely complex topic and is a subject of ongoing research. Thirdly, the creep and shrinkage of CLT depends on external factors that are hard to predict, such as weather conditions.

7.1 Creep of the CLT plate

When CLT is sustained under a constant load, deformations in the CLT increase with time. This effect is called creep. The creep deformation depends for a large part on the stress level in the CLT. Post-tensioning increases axial load and therefore creep deformations. Compared to other timber products, CLT is more susceptible to creep because it is cross-laminated and due to the gluing of the layers [47].

For timber structures, three creep phases can be distinguished (see Figure 51). Nguyen [47] mentions that in axially pressed CLT structures, the long term compressive stress in the CLT is low compared to the peak failure stress, and the tertiary creep phase can be excluded from analysis. The creep of CLT can be split into two different types: Mechano-sorptive (MS) creep and (VE) Visco-elastic creep. MS creep depends mostly on changes of the relatively humidity of the ambient air. VE creep depends mostly on load duration, type of load and temperature.

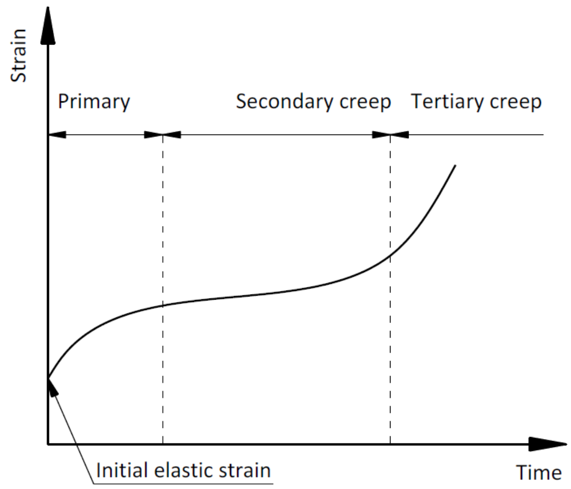

Figure 51 Creep curve characterization [47]

7.1.1 Simplified approach

Since creep of CLT is an extremely complex topic, some simplification was required to answer the research questions in the timeframe of the thesis:

- Only the end-creep is regarded. Creep behaviour of CLT is a very complicated topic. There is no consensus on a creep curve for CLT, and a possible curve would likely also depend on the internal geometry and the thickness of the CLT plate the creep development in time (the creep curve) is considered outside the scope of the thesis.
- Creep is regarded in the thesis by using a creep-factor, which represents total additional displacements due to creep. This is the deformation factor k_{def}, as discussed in 3.4.3. This implies that creep deformations are 80% to 100% of the instantaneous displacement, which is significant.

7.2 Shrinkage of the CLT plate

Moisture control of mass timber buildings is highly important since timber experiences large dimensional changes due to change of moisture content. In the case of this thesis, shrinkage becomes especially important because of the associated pretension loss.

For an estimation of the shrinkage of a CLT structure two things are important: (1) the relation between changes in moisture content (MC) and dimensional changes of the CLT panel. And (2) estimation of changes in MC during the lifetime of the building. The MC of the CLT panel depends on the ambient Relative Humidity (RH), but also on the time the CLT is exposed to that RH, as it takes time for moisture to propagate through the CLT.

7.2.1 Relation between MC and dimensional changes of the CLT

When the MC of wood changes, the timber swells or shrinks. This swelling or shrinking is not the same in all directions. The cross-lamination of CLT highly decreases the swelling and shrinkage compared to a piece of wood. The shrinkage coefficient depends on the orientation of the layers, as wood shrinks much less parallel to grain compared with the other directions (See Table 22). In literature, values in a large range are found (between 0.016 and 0.023, see Table 23).

Table 22 Shrinkage coefficient of spruce [52]

Material: Pine and Spruce	% dimensional change for a 1% change in moisture content
Parallel to grain	0.01 – 0.02
In radial direction	0.19
In tangential direction	0.36
Average across the grain	0.24

Table 23 Shrinkage coefficient of CLT

Source	Percentage dimensional change for a 1% change in moisture content
Swedish Wood CLT handbook [53]	$0.016 - 0.023$
Schickhofer [24]	$0.02 - 0.04$

7.2.2 Changes in MC during the lifetime of the building

The moisture content ω of a material is defined as in Eq. 42. The general change of moisture content from production to use-conditions in the CLT core can be assumed to be as follows. For manufacturing for CLT, a target MC of $12\% \pm 2\,\%$. This is to ensure that the CLT is bonded properly and to minimize the development of internal stresses between pieces due to differential shrinkage. If manufacture, stored and transported properly, the CLT can be assumed to arrive at the construction site at 12% MC. Dependent on the weather conditions, and the protection on site, the MC of the CLT can increase during construction. Once the building envelope is in place, the CLT will dry slowly to make equilibrium with the relative humidity of the indoor climate. In the use stage of the building, the CLT will experience a yearly cycle of swelling and shrinkage due to the changing indoor climate (winter vs summer).

$$\omega = \frac{m_\omega - m_0}{m_0} \tag{42}$$

Where:

m_ω	Weight of the material corresponding to moisture content ω
m_0	Weight of the dry material

7.2.3 Moisture level changes during construction

The largest change in moisture content will most likely take place in the construction phase. This moisture change is due to initial drying of the CLT. CLT should be protected against long-term wetting in construction. However, CLT can be used in Service Class 2, which means that the CLT should be able to take some wetting for a short period of time during construction. Prediction of the swelling/shrinkage of CLT in construction remains complex, as many factors influencing the MC of the CLT in construction are complicated to predict:

- Moisture content of CLT at manufacturing
- Conditions and duration of transport
- Conditions and duration of storing of the plates on-site
- Presence and quality of protective film on the CLT
- Weather protective measures at the site
- Conditions during construction and duration of exposure to weather

As an example of the moisture content during construction, the MC measurements of the Limnologen project (Appendix H) are discussed. In this project, measures were taken to limit the moisture content of the CLT during construction. Upon manufacturing, the panels have an MC of about 12%. The CLT is covered with protective film, and walls are transported in an open truck with a tarpaulin cover. When the CLT arrives at the site, the MC is measured to be about 14-15%. During mounting, the CLT is protected from the weather by protective roofing. Even with this protective roofing, the mounting level was occasionally subject to rain. Before finishing the walls, another MC check has been performed, and MC levels of 12-14% were measured. Incidentally, when the protective film came loose, MC of 16-17% was measured [54]. An important note on the measurement results is that these measurements were not made in the heart of the CLT panel. The MC was measured with pins close to the surface of CLT. The centre of the panel may be much dryer than the top layer of the CLT.

7.2.4 Annual fluctuation in moisture level

The moisture content of the CLT is influenced by the seasonal change if RH. In the Netherlands, in the summer, the moisture level in the outside air is higher than in winter. The indoor air follows the cycle. Additionally, the indoor air is even more dry in the winter due to heating. Next to this annual cycle, peaks in RH occur due to activities that increase the moisture in the air. Examples are cooking, showering and a party with many people in a room. These activities are of relatively short duration (compared to the annual cycle of change in RH). They are not likely to influence the moisture content in the CLT much, since timber adapts to moisture slowly.

No measurements have been found on the annual cycle of RH indoors, but one can make assumptions based on the service classes. It can be assumed that Service Class 1 is comparable with use in indoor conditions. The maximum RH levels of Service Class 1 correspond with an equilibrium moisture content of the CLT of about 12%. The CLT can reach higher moisture content during construction phase.

7.2.5 Shrinkage assumptions

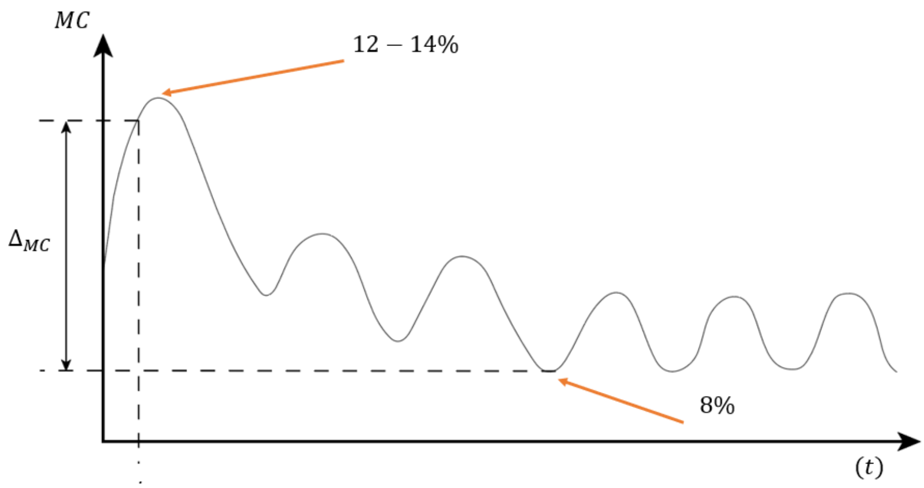

Figure 52 Assumption on Δ_{MC}, source: author

To be able to estimate the prestress loss due to shrinkage, some assumptions needed to be made on the shrinkage behaviour. These are listed below.

- A single difference in moisture content is applied to the structure. Different construction elements will have different shrinkage behaviour based on their exposure to moisture. This is not included in the analysis.
- The prestress losses are made based on a MC difference Δ_{MC}, which is illustrated in Figure 52. This value is based on moisture content at the end of construction. The worst-case scenario is initially assumed, meaning the structure is retightened at the moisture peak. Based on measurements in the Limnologen project, a maximum MC of 12%-14% is assumed at the end of construction. With an expected moisture content of 8% for the indoor climate in winter, this results in $\Delta_{MC,max} = 4 - 6\%$. This is most likely an overestimation, as it is based on measurements in the outer layer of the CLT.

7.3 *Python model for calculation of the long-term losses*

For the purpose of this research, a python model has been developed for estimation of long-term prestress force loss in prestressed CLT structures. This model is based on Nguyen's equations on the stiffness of a CLT plate, as was introduced in Section 6.2.

Nguyen has researched a method for calculation of prestress force loss due to creep by including a time dependent stiffness $E_w(t)$ in the equilibrium equations. For the python model, 2 adjustments are made to the Nguyen approach and the equations in section 6.2:

(1) Instead of a time dependent elastic modulus ($E_w(t)$), only an end-elastic modulus is included. In this way inputting of the creep curve is avoided. The stiffness of the CLT panel is determined by Eq. 43.

(2) In the Nguyen model, shrinkage is not included. To include the shrinkage in the analysis, a constant is added to the displacement of the panel (Eq. 44).

$$K_w = \frac{k_{def} \cdot E_w A_w}{L_{w0}} \tag{43}$$

$$\Delta_w = \frac{P_0 + N}{K_w} + \Delta_{w,s} \tag{44}$$

Where:

L_{w0}	Is the initial length of the CLT plate
P_0	Initial post-tension force
A_w	Section of the CLT panel (only layers parallel to the direction of the loading are included)
E_w	Elastic modulus of the CLT parallel to the fibre
$\Delta_{w,s}$	Shrinkage of the CLT panel

7.3.1 *Functions*

Because the calculation of prestress force loss includes some non-linear calculations, a Python code is written to calculate the creep, shrinkage and relaxation force loss, based on the equations. Input for the python model is shown in Figure 53. The code provides two functions `Force_after_Losses(`P_0`)` and `Force_before_Losses(`P_∞`)`. The first returns the remaining prestress after losses. The second calculates what initial prestress is required to have a certain to remain a certain prestressing force after losses. See Appendix M for the full code.

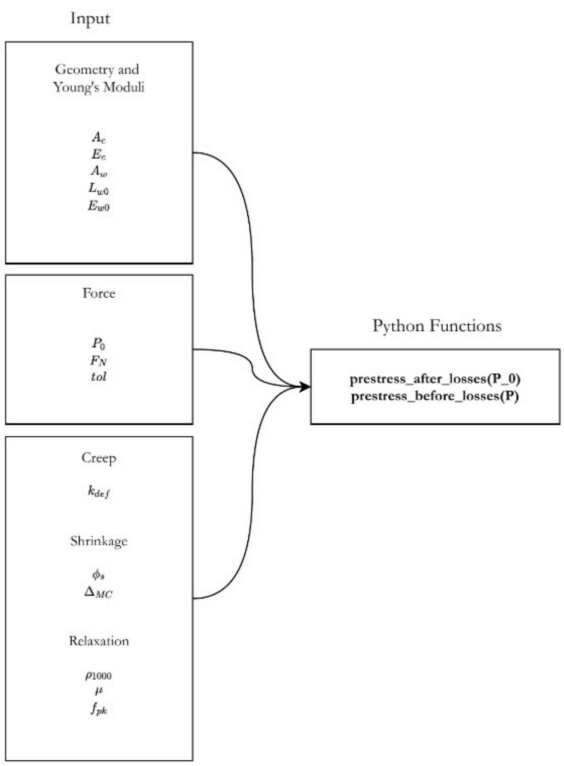

Figure 53 Input to functions of the python code, source: author

7.4 Conclusion

The most important prestress losses in CLT structures are creep, shrinkage and relaxation. In the chapter the intricacies of estimating the creep and shrinkage behaviour of CLT structures are emphasized. There are many influencing factors on the shrinkage and creep. Some assumptions have been introduced regarding creep and shrinkage. It has been shown that one can assume creep deformations by including a k_{def} factor (0.8-1.0), and a moisture content change of 4-6% can be assumed for the outer layers of CLT together with a shrinkage coefficient of 0.02 – 0.04. The designer must be cautious making these types of assumptions as creep and shrinkage remain factors that are hard to estimate.

Several topics on the creep and shrinkage behaviour can be suggested for further topic, as they would improve estimation of long-term force loss due to long-term loading and moisture:

- Propagation of MC in CLT plates.
- Change of MC of CLT plates in construction phase
- A creep curve for CLT plates for axial loading dependent on panel lay-up and moisture conditions.

For design of prestressed concrete cores, the designer should decide how to deal with the long-term prestress force losses in the design. What place the estimation of prestress force losses take in the design process of a CLT core is discussed in Chapter 8.

8 Method for design of the prestressing

For the purpose of this research, an approach is developed for the prestress design of a CLT core. This approach is explained in this chapter. This chapter aims to show how the long-term prestress losses discussed in Chapter 7 should be integrated in the design steps.

8.1 Prestress design strategy

Two limits for the prestressing force can be distinguished. This is shown in Figure 54. The prestressing of the core should be designed in such a way that the lateral displacements of the building are less than the allowable lateral displacement. Since prestressing diminishes uplift and sliding, it may seem sensible to apply a high post-tension force. However, the compressive resistance of the CLT provides an upper limit to the prestress.

It may be the case that with a certain core design, the minimum prestress needed to satisfy the deformation requirements already leads to an exceedance of the compressive resistance of the CLT. In other words, the lower limit is above the upper limit. In that case the stability design needs to be adjusted. Examples of adjustments are, among other things: a larger core, thicker CLT panels, better design of openings, stiffer connection between flange and web.

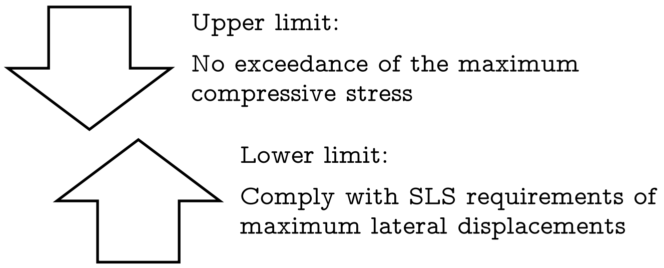

Figure 54 Upper- and Lower limit to the post-tension force, source: author

For this thesis, a design scheme has been developed that shows the steps that are required for design of a CLT core. The steps are depicted in Figure 55. The second step in the process is the estimation of the prestress loss, which can be done with the help of the python model that has been developed for the thesis (see section 7.3).

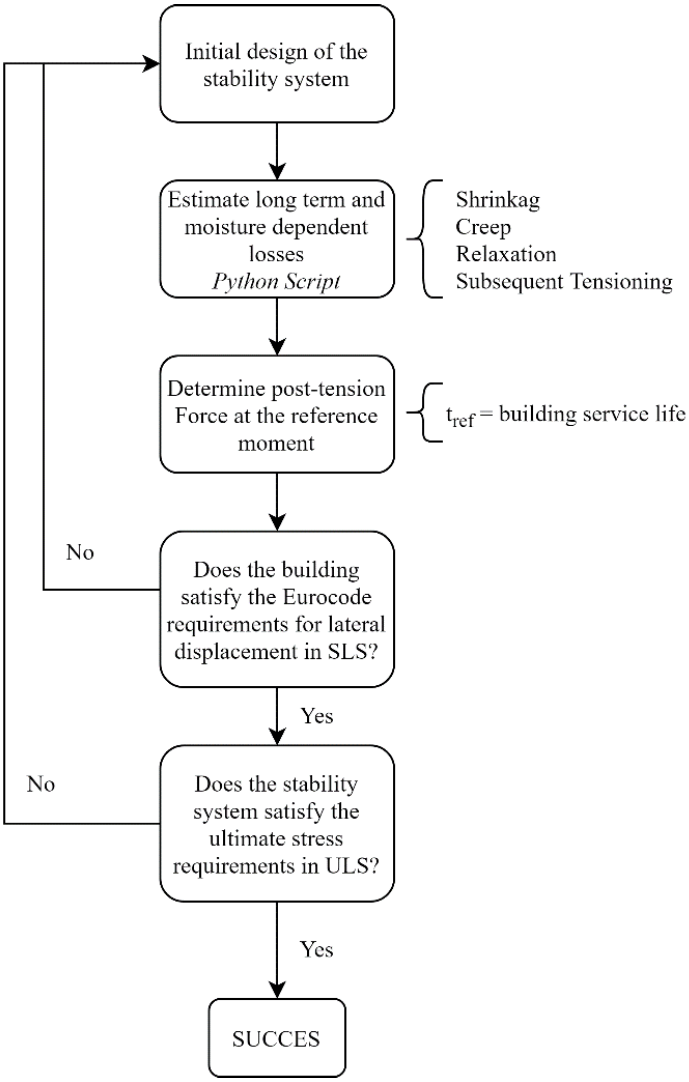

Figure 55 Design strategy, source: author

An important note on the estimation of prestress force losses is that the designer should set a time target for the post-tensioning. It is possible to design the core in such a way that re-tightening is possible without too much effort. The post-tension may also be designed in a way that no re-tightening is needed during the lifetime of the building. The time for which the prestressed system is designed to function without having to re-apply the tension is denoted t_{ref} in this thesis (see Figure 56).

This reference moment t_{ref} relates in the following way to the design scheme in Figure 55. The SLS check should be performed for time t_{ref}, meaning after the time dependent losses on the prestressing have taken place. In that case post-tension forces are smallest, leading to the largest displacements. Contrary, the ULS check should be done assuming time t_0. This moment denotes the moment of applying the prestress. No losses have taken place, the highest compressive stress is present.

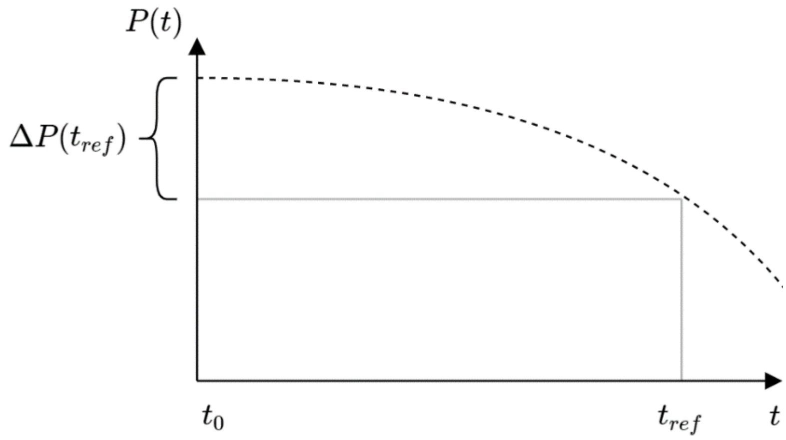

Figure 56 Prestress force vs time, source: author

8.2 Dimensioning of the prestressing steel

There are Eurocode guidelines to the dimensioning of prestressing steel. In this thesis it is assumed that the post-tensioning will be done with bars. The bars should be designed in a way that their stress will never exceed the maximum steel stress. For example, the designer can decide to initially design the prestressing steel bars such that their stress due to prestressing does not exceed $0.7 \cdot f_{pk}$.

The steel stress should be checked in both SLS and ULS combinations, as there might be an increase of prestressing steel stress causing yielding of the steel. Beyond the first branch in the bi-linear steel diagram, large deformations occur (Reduced E in the second branch). It must also be checked if in ULS, the maximum steel stress is not exceeded.

8.3 Conclusion

Several important topics for the design of the post-tensioning of CLT cores has been discussed in this chapter. The post-tension force that can be applied to the core proved limited by a lower and upper limit. The lower limit relates to the maximum lateral displacements of the building and the upper limit relates to the compressive resistance of the CLT. A reference time for the post-tension loss is introduced (t_{ref}). The reference time for the prestress losses will be the moment of re-tightening or the lifetime of the building (if no re-tightening will take place). If the post-tension losses are too high, the designer may decide to apply retightening at some point.

In the chapter, a design scheme was introduced that provides a guideline on how to design the prestressing of a CLT core. Especially, it has been explained how the post-tension force loss calculation (see Chapter 7) relates to the design process. In the following chapter (Chapter 9), the proposed design method will be tested on a case-study.

9 Case study

In this chapter, the benefit of post-tensioning a CLT core for reduction of lateral displacements of a building is analysed through a case study. When writing this thesis, no timber building stabilized with a CLT core is known to the author. Therefore, a fictitious project is introduced for the case-This project includes a floorplan and minimal core size as is explained in 9.1. The lateral displacements will depend on the assumed wind-load and floor load. Loads and load combinations are discussed in 9.2. For the case-study, a finite element model was made in DIANA. The modelling approach is discussed in 9.3. In Chapter 5 , the effective width method for shear lag and a section with connectors was discussed. In section 9.4, it is explored if this method can be used for finding the bending stiffness of the core. The Case-study also shows how high we can build using a minimal core size. Two situations are explored: no post-tensioning (9.5) vs post-tensioning (9.6). In the end, a conclusion will be made about the benefit of post-tensioning by comparing the un-post-tensioned and the post-tensioned core (9.7).

In this chapter, the limits for the lateral displacements are set to 1/1000 times the height of the building. This is based on the Eurocode demand of maximum 1/500 times the height of the building as maximum lateral displacement. The rotation of the foundation is considered beyond the scope of this thesis. The assumption is made that half of the displacements will be due to rotation in the foundation, leaving 1/1000 times the height of the building as the maximum lateral displacement for the building excluding the foundation.

9.1 Minimum core size

In different building structure and core designs, the core will benefit from post-tensioning to a different degree. It can be expected that there are a lot of factors that influence the benefit, such as the slenderness of the building, the slenderness of the core, design of the connections, among other things. Therefore, a quantitative answer to the research can only be formulated in relation to a certain building and core design.

A core in a building is not solely a structural element. In a residential building, a certain minimal core size is needed for reasons other than structural. Space is needed for circulation (stairs, lifts) and for MEP (ducts). The core size needed for these reasons is a "minimal core size". This core size depends, among other things, on the size of the floor plan, the use of the building and the height of the building. This chapter will explore how high we can build, limiting the core size to this minimal core.

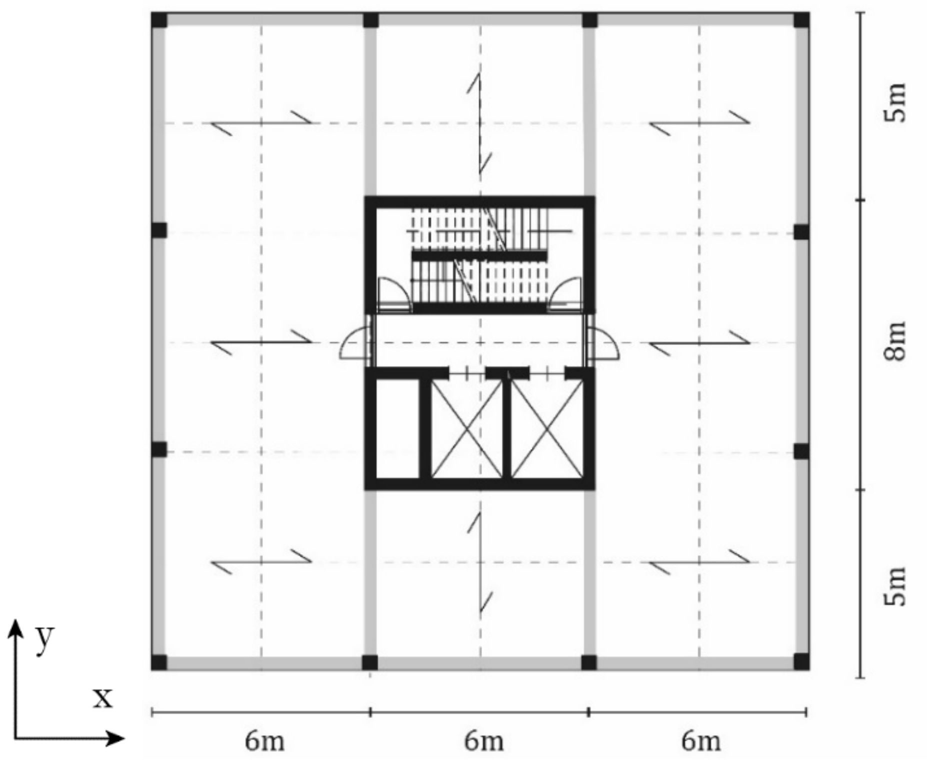

Figure 57 Case study floor plan, source: author

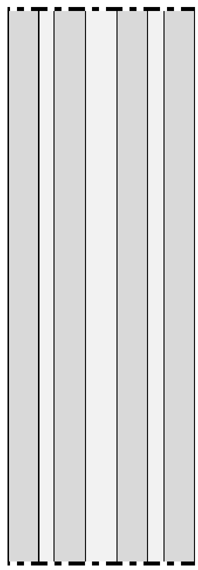
Figure 58 CLT plate, source: author

The case study has been done for a floorplan with a minimal core size for a medium high residential building. The chosen floorplan for the case study is depicted in Figure 57 . The minimal core includes stairs, two elevators and space for ducts. For the case study only the walls at the perimeter of the core are regarded structural. In the floorplan, it is also shown which direction the floors span. This is important for the case study as it determines the vertical load in the core. CLT plate. Initially 7-layer CLT plates with a thickness of 240 mm are applied (build-up 40-20-40-40-40-20-40, see Figure 58.For this CLT plate, $2/3$ of the area is of boards spanning in the stiff direction, and $1/3$ of the area is of boards spanning in the less-stiff direction.

9.2 Loads

9.2.1 Wind load

The most important lateral load on buildings in the Netherlands is the wind load. In other regions of the world, earthquake loading might need to be included as a lateral load. The wind loads are determined according to EN 1991-1-4. The wind load largely depends on the height of the building, which is a variable in this case-study. For a calculation of the wind load for different building heights, see Appendix N. In Figure 59 results are expressed in terms of base moment.

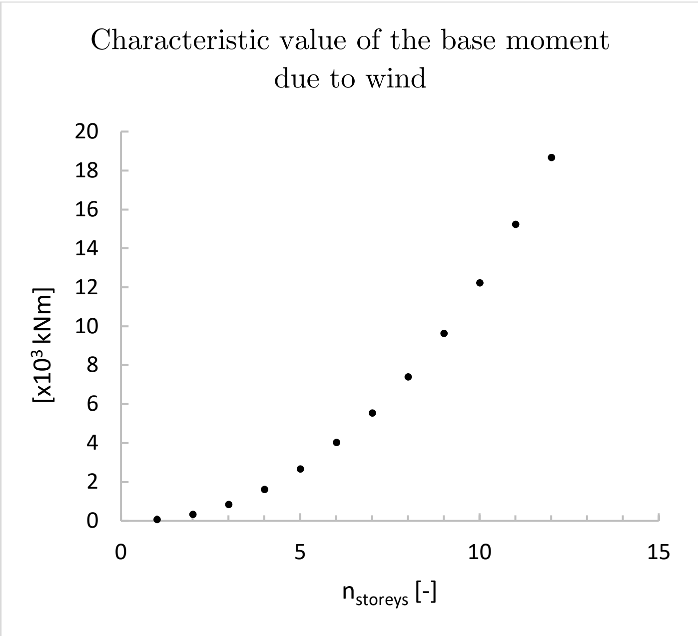

Figure 59 Case-study building base moment due to wind load, source: author

9.2.2 Floor loads

A large permanent floor load will decrease the uplift force in the core, thus decreasing lateral displacements due to uplift. To that respect, for the analysis, the assumed weight of the floors is important. The floors are assumed to be $240\ mm$ thick, which is a reasonable thickness for a floor with span of $6\ m$. The thickness is chosen in line with Derix pre-analysis dimensioning tables. In buildings with CLT floors, material needs to be added to improve vibration and acoustic performance. The build-up of the floor is adjusted from Dataholz floor *gdmtxn01-00* (see Figure 60). The build-up of this floor and corresponding weights are stated in Table 24 (See also Appendix O) [55]. Total permanent floor load has been assumed to be $2.2\ kN/m^2$, which makes it a relatively light floor. If higher acoustic performance is required in the building, another (heavier) floor may be chosen. The imposed floor load applied is equal to $2.0kN/m2$.

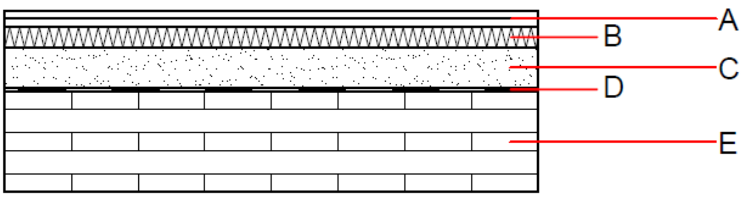

Figure 60 gdmtxn floor build-up by Dataholz [55]

Table 24 Permanent load of the floor (adjusted from [55])

		Thickness [mm]	Density [kN/m3]	Characteristic load $[kN/m^2]$
A	Cement screed	25	90	0.225
B	Impact sound absorbing subflooring	30	0.16	0.005
C	Elastic bonded fill	60	15.0	0.9
D	Trickling protection	-	-	-
E	CLT floor	240		1.08
	Total characteristic permanent load			**2.2**

Table 25 Imposed load floor

	Characteristic load $[kN/m^2]$
Characteristic value imposed load	2.0

9.2.3 Load combinations

All actions on the structure that can occur simultaneously should be combined for the design of the structure. Table 26 and Table 27 only include the load combinations that proved governing in this case study. They have been formulated in line with the Dutch national annex to EN1990. Consequence class 2 has been assumed. Because it is not likely that the maximum values of the variable loads occur simultaneously, combination factors are applied, see Table 28. In the last rows of the tables, the factors to be applied on each characteristic load are shown. In the thesis, all roofs have been treated like floors.

Table 26 SLS load combinations

	Type	Formula	G + Floor	Prestress	Floor load Imposed	Wind load
			Permanent	Permanent	Variable	Variable
SLS-1	Characteristic	$G+P+\psi_0 \cdot Q_{floor}+W$	1		0.4	1
SLS-2	Quasi-Permanent	$G+P+\psi_2 \cdot Q_{floor}$	1	1	0.3	0

Table 27 ULS load combinations

Combination	Formula	Self weight	Prestress	Floor load Imposed	Wind load
		Permanent	Permanent	Variable	Variable
ULS-1	$1.2G+P+\psi_0 \cdot Q_{floor}+1.5W$	1.2	1.0	–	1.5
ULS-2	$0.9G+\psi_0 \cdot Q_{floor}+1.5W$	0.9	1.0	–	1.5
ULS-3	$1.2G+P+1.5 \cdot Q_{floor}$	1.2	1.0	1.5	–

Table 28 ψ-factors applied

Load	ψ_0	ψ_1	ψ_2
Category A: Domestic residential areas	0.4	0.5	0.3
Wind load on buildings	0	0.2	0

9.3 *Finite Element Modelling*

The finite element models made for this thesis are made with DIANA FEA. In this paragraph, the most important topics regarding the modelling of a CLT core in DIANA are discussed. This chapter deals with both the modelling of an un post-tensioned core and a post-tensioned core.

9.3.1 *Element discretization*

2D shell elements for the CLT plate

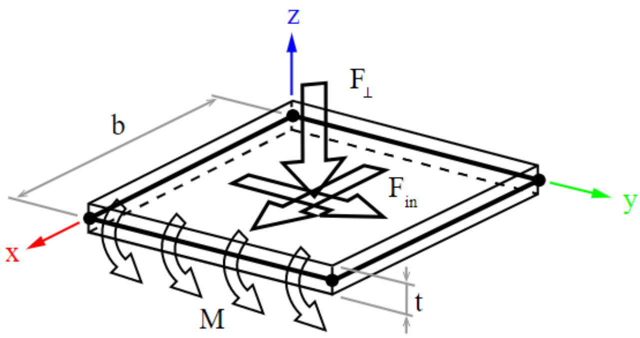

Figure 61 DIANA shell elements characteristics [56]

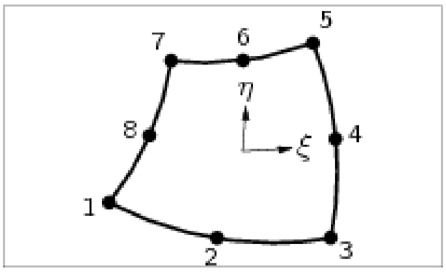

Figure 62 DIANA CQ40F Quadrilateral shell element [56]

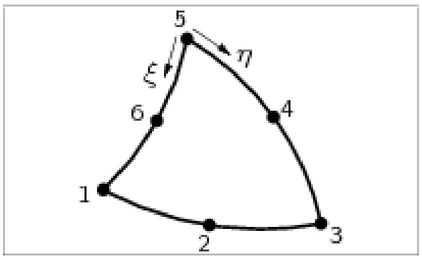

Figure 63 DIANA CT36F triangle shell element [56]

The elements shown in Figure 61, Figure 62 and Figure 63 have been used for the modelling of the CLT plates. These elements can be used for situations in which the CLT plates is loaded in-plane and out-of-plane. Special attention is required for the material model applied to these elements. DIANA does provide an option to manually input an orthotropic thickness. In that case a non-orthotopic material model may be used. In the analysis in this thesis, a different approach has been adopted. A non-orthotopic thickness has been applied. Then the material is chosen as orthotopic, and the stiffness in each direction is dependent on the net section of the CLT in that direction. Shell elements have also been used for modelling of the steel anchors.

Table 29 Stiffness of the shell elements

thickness of the CLT panel	t_{CLT}	$240\ mm$
Net-thickness in the x direction	$t_{CLT,0}$	$160\ mm$
Net-thickness in the y direction	$t_{CLT,90}$	$80\ mm$
Young's modulus of the base material C24 parallel to the grain	$E_{C24,0}$	$11000 \frac{N}{mm^2}$
Stiffness applied to the shell elements in the DIANA model	E_x	$\frac{160}{240} \cdot 11000 = 7333 \frac{N}{mm^2}$
	E_y	$\frac{80}{240} \cdot 11000 = 3667 \frac{N}{mm^2}$
Shear stiffness	G_{xy}	$518 \frac{N}{mm^2}$

Enhanced truss elements for the prestress rods and lintels

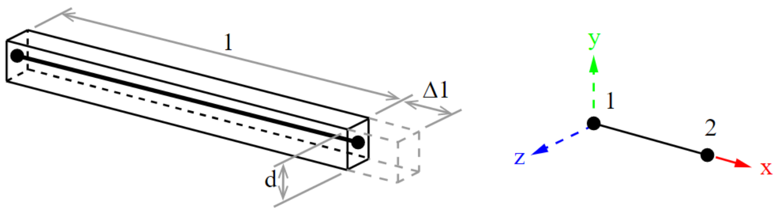

(a) characteristics (b) axes

Figure 64 DIANA Truss element characteristics [56]

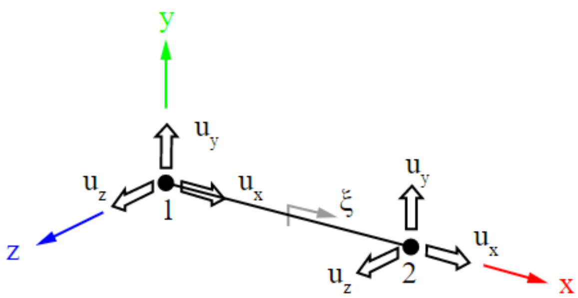

Figure 65 DIANA L6TRU enhanced truss element [56]

Enhanced truss elements (shown in Figure 64 and Figure 65) have been used for modelling the lintels and the prestress rods. The elements have 2 nodes and 6 degrees of freedom per element. The stiffness of the truss elements for the lintels are determined similar the CLT plates . The stiffness is based on the net section, depending on the orientation of the CLT panel used for the lintel. The lintels transfer no bending moment.

The prestress rods have also been modelled with enhanced truss elements. As these trusses only take the tensile loads. The material model is modelled as uni-axial nonlinear, with a very low stiffness in compression and a stiffness of $E = 205000\ N/mm^2$ in tension. In DIANA, it must be inputted that the post-tension rods are not connected to the mesh of the CLT plates. This is done through a "no-contact-connection".

Interface elements

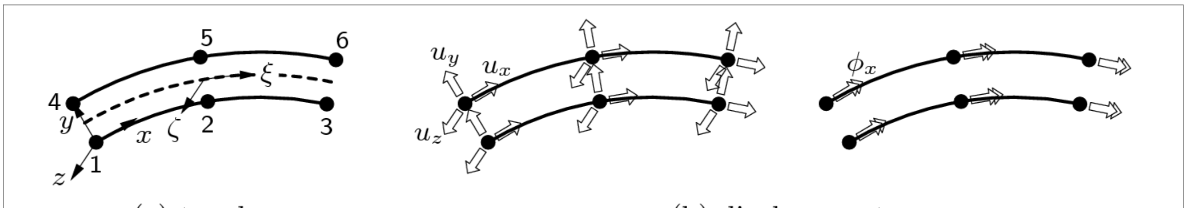

Figure 66 DIANA CL24I interface element [56]

Interface elements (shown in Figure 66) have been used in the model for different connections in the core, namely:

- Contact interfaces between different CLT plates. In this case a compression-only material is applied.
- Contact between the CLT walls and the concrete ground floor. The same compression-only material is applied.
- STS connection connecting perpendicular CLT plates. The stiffness applied relates to the stiffness of the

The shell interface elements have 4 degrees of freedom in each node. Displacements in 3 directions and one rotation degree of freedom, which makes the interface elements compatible with curved shell elements. The thickness of the line to line interface elements are set to the total thickness of the CLT plate (i.e. 240 mm).

The material model for the interface elements depends on the application. For the compression only contact, a no tension constant shear material model is used with high stiffness applied in compression (based on a 10 mm layer of CLT). For the connection between two perpendicular walls. The stiffness is based on the stiffness of the STS connectors.

Springs

Two types of springs are used. Matrix springs are used for connectors between two CLT plates (shear plates and tensile plates). Base spring elements, shown in Figure 67, are used for the connections of the core at foundation level (shear angles and hold-downs). These springs have a nonlinear material model for all directions. They are put in as having no rotational stiffness. For translational stiffness, in the compressive branch, a stiffness close to 0 is applied. In tension, the stiffness of the connectors is applied.

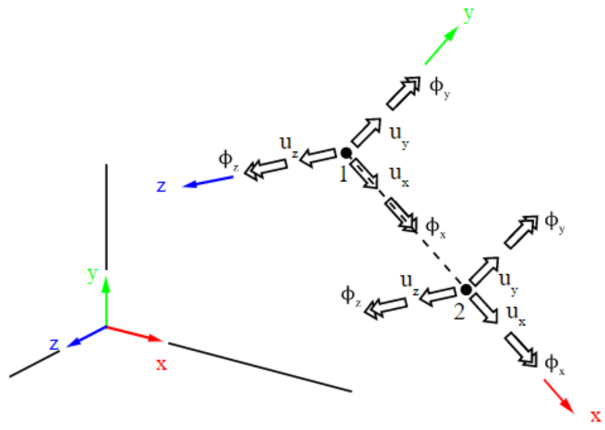

Figure 67 N12SPR Nodal spring element and SP12BA base spring element [56]

9.3.2 Loads and supports

The core is connected to a hinged line support by means of the compression only interface. The base springs are modelled to simulate the connection with shear angles and hold-downs.

For the FEM model made in the case study, the wind load is applied directly on the core. Rigid diaphragms are assumed for the floors, and the wind load is therefore applied as a distributed load at the web. It is not applied on the flanges since this would cause non-realistic out-of-plane bending of the flange. This is also the case for loads from the floors. At each floor level, point loads are placed on the core for simulating the load transfer from beams that carry the floors. The prestress is applied by means of an initial prestress.

9.3.3 Analysis

The analysis applied is non-linear, automatic step size is chosen. In the case the post-tensioning is applied, the analysis is started with a start-step. The second step in the analysis starts with an initial stress from the start step.

9.4 Effective flange width analysis

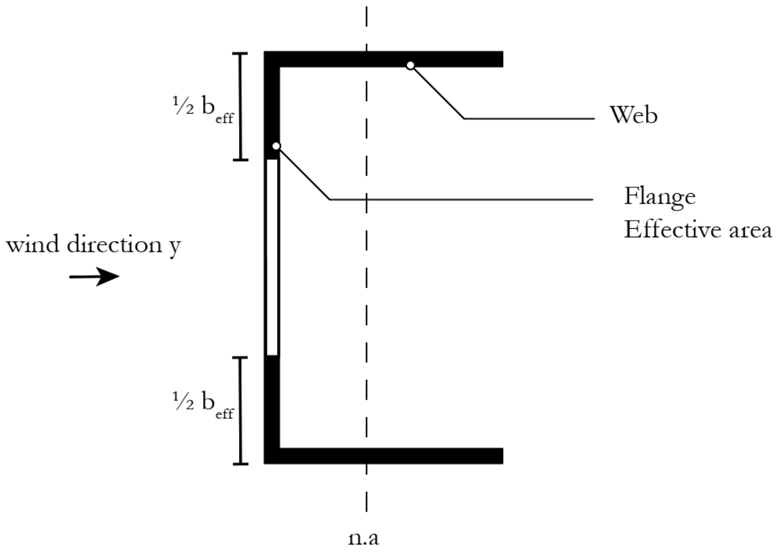

Figure 68 Effective area U-shaped core and position of the neutral axis (n.a.), source: author

In Chapter 5, it has been explained that for determining the bending stiffness of a CLT core, an effective width method can be applied. This implies a reduction of the effective flange width of the core for both shear lag and the connection between perpendicular core walls, as is shown in Figure 68. In this method, the suggested workflow (see 5.1) is tested on the case study core.

In 9.4.1, the shear lag in the core is explored for different core heights. In 9.4.2 addresses the application of the γ- method to the core and shows the influence that the stiffness of the connection between perpendicular walls has on the bending stiffness of the core as a whole.

If an expression is found for the effective width of CLT cores, it would make it possible for the designer to estimate the stresses in the core by hand. In that case bending displacements can be calculated by hand, as well as the needed post-tensioning force to avoid uplift.

The reader should keep in mind that the Effective width analysis in this section solely focusses on wind load in the y-direction.

9.4.1 Shear lag

Eight DIANA models have been made of the U-shaped core, each with a different building height. In these models, the connection between flange and web is modelled as rigid. The lateral displacement from the model is translated to a bending stiffness. From this bending stiffness, the effective flange width can be deducted. The dependencies are shown in Figure 69. The results from the FEM analysis on the shear lag effect of the U-shaped core, see Appendix T.

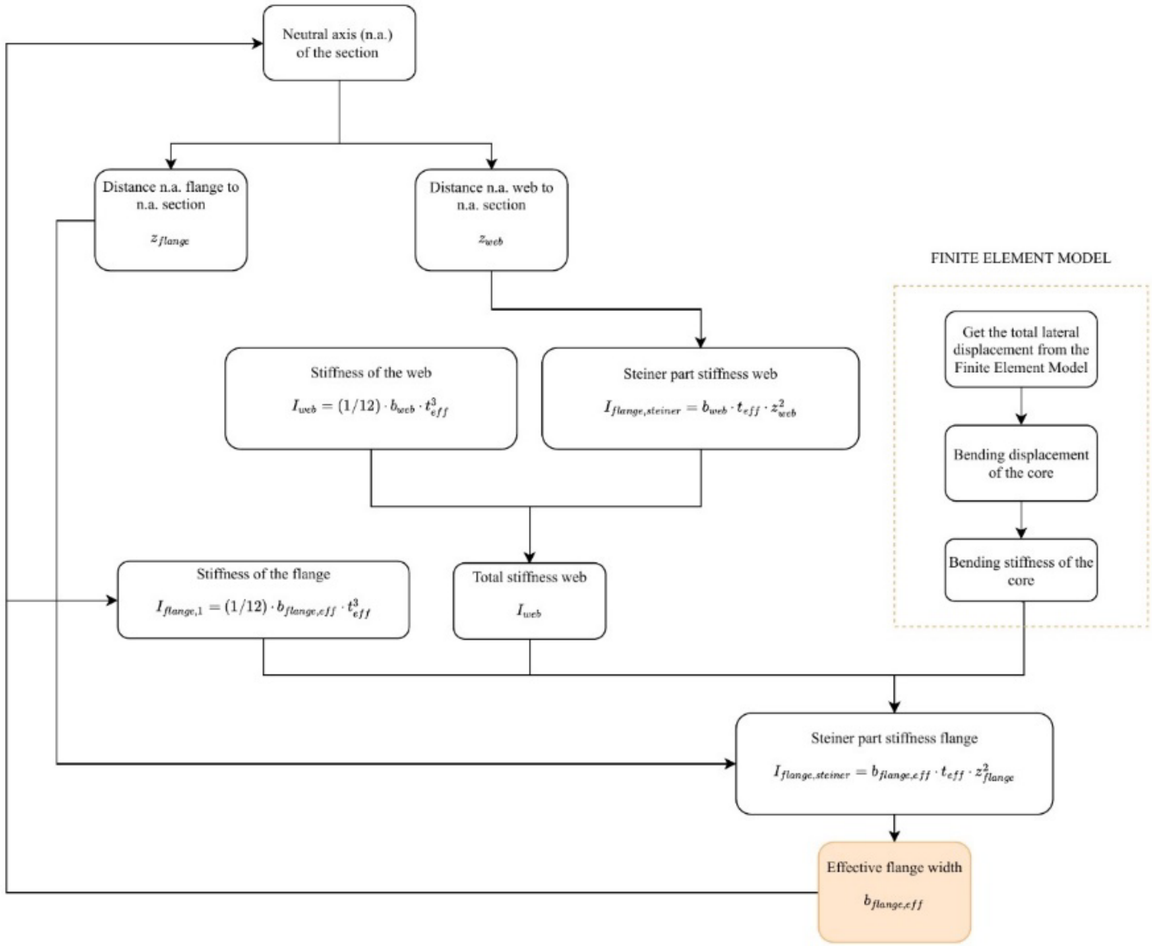

Figure 69 Iteration for finding the effective flange width, source: author

The following conclusions can be made from the results in the DIANA models that have been made:

- Shear lag does play an important role in the bending displacements of the core. A deviation of stresses is observed compared with hand-calculations assuming linear strain.
- The shear lag effect varies over the height of the core. At base of the core, peak stresses are found in the corners of the core. Higher in the core, the reverse effect is visible. This is shown in Figure 70. Plots of the occurring normal stress distribution in both the flange and the web compared to the normal distribution assuming linear strain is shown in Appendix T.
- The effective width of the core is quite accurately described as 0.1 times the reference length (Figure 71). The reference length in this case is equal to twice the core height (the distance between two zero moment points). This is the same as the effective shear lag for plywood as suggested in the Eurocode (See Table 15 on page 37). The results were most accurate in the range of 6 to 8 storeys. For smaller and larger core height, the results were deviating.

- With increase of building height, the effective area of the flange increases, therefore the stiffness increases. Comparing a core of 3 storeys to a core of 10 storeys, the stiffness increased with more than 60% (See Figure 72).

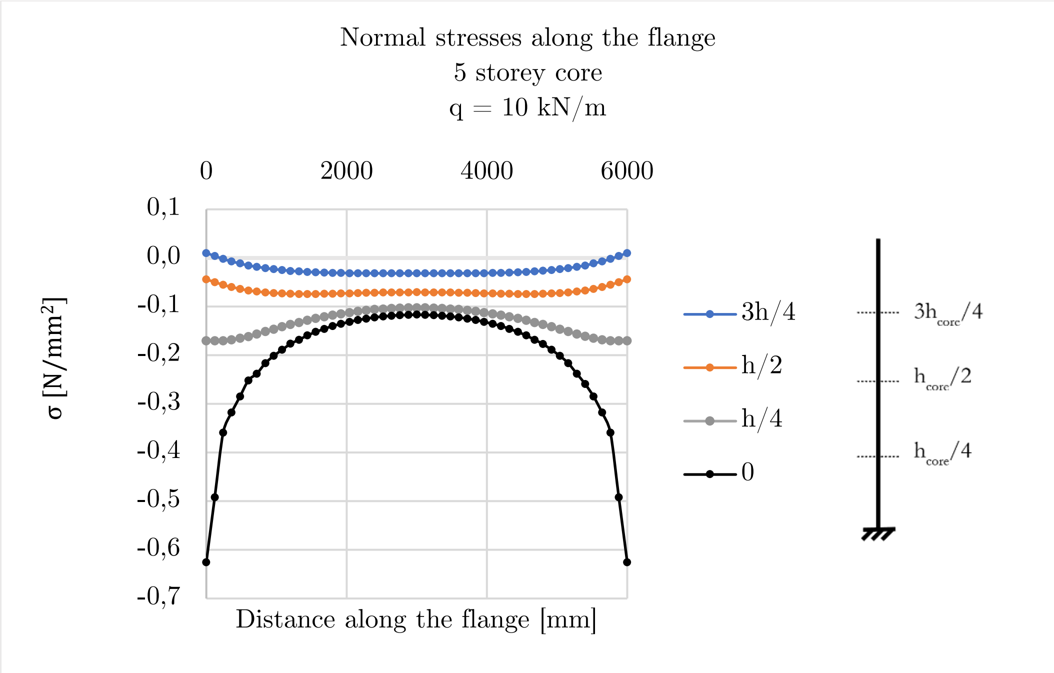

Figure 70 Normal stresses along the flange for different positions, source: author

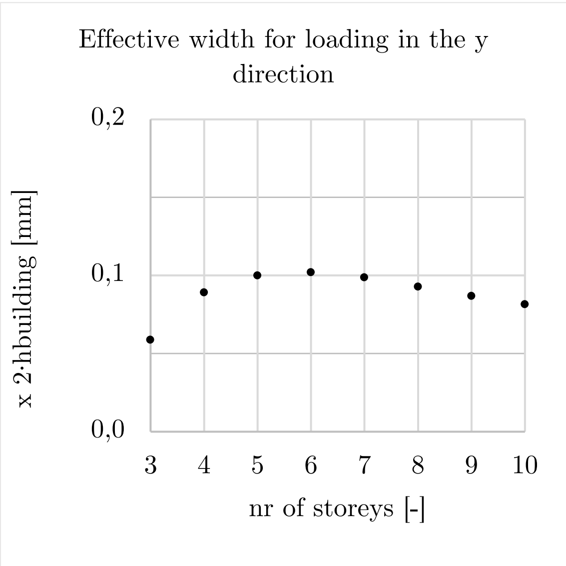

Figure 71 effective width load direction y, source: author

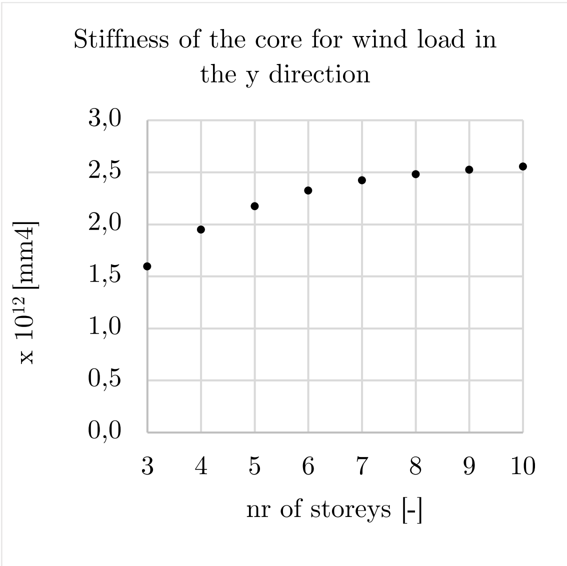

Figure 72 Stiffness of the core for loading y, source: author

$$b_{flange,eff,s-l} = 0.1 \cdot l \tag{45}$$

$$\text{where} \quad l = 2 \cdot h_{building}$$

9.4.2 Semi-rigid connection between flange and web

The cooperation between flange depends on the stiffness of the connection between the perpendicular walls. For the case-study, it is assumed that pairs of STSs are applied, each pair with a distance s of 600 mm to the next (See Figure 73). The stiffness of a pair of angled STSs under lateral loading ($K_{45°,lat}$) was discussed in 4.1.1. Based on the stiffness of the STS, the distributed stiffness of the connection between the flange is assumed:

$$k = \frac{2 \cdot K_{45°,lat}}{s} = 66330 \frac{kN}{m}/m \tag{46}$$

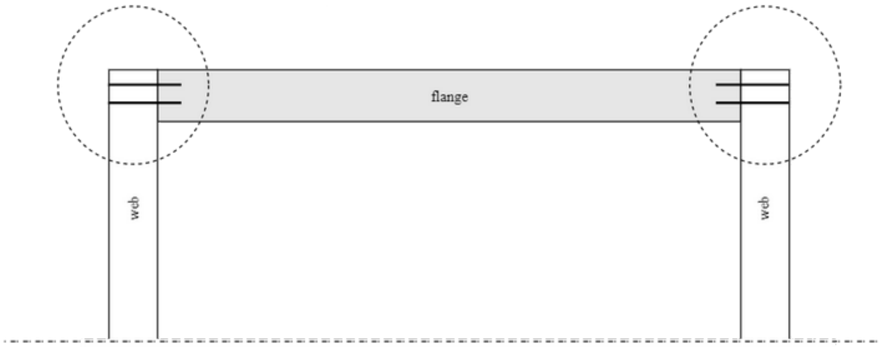

Figure 73 Four STS connections connecting the flange to the web (Schematic) , source: author

9.4.2.1. Hand calculations vs FEMs

A γ-factor was derived from the finite element analysis results of the lateral displacement at the top of the core (see Appendix V). This is compared with the hand-calculated values for gamma based on the γ equation (page 117). Both in the hand calculations for γ and in the translation from FEM displacement results to γ-factor, the effective width for shear lag is assumed to be $0.10 \cdot h_{core}$. In Figure 74, the results from both calculation by the Gamma equation and the FEM model are shown.

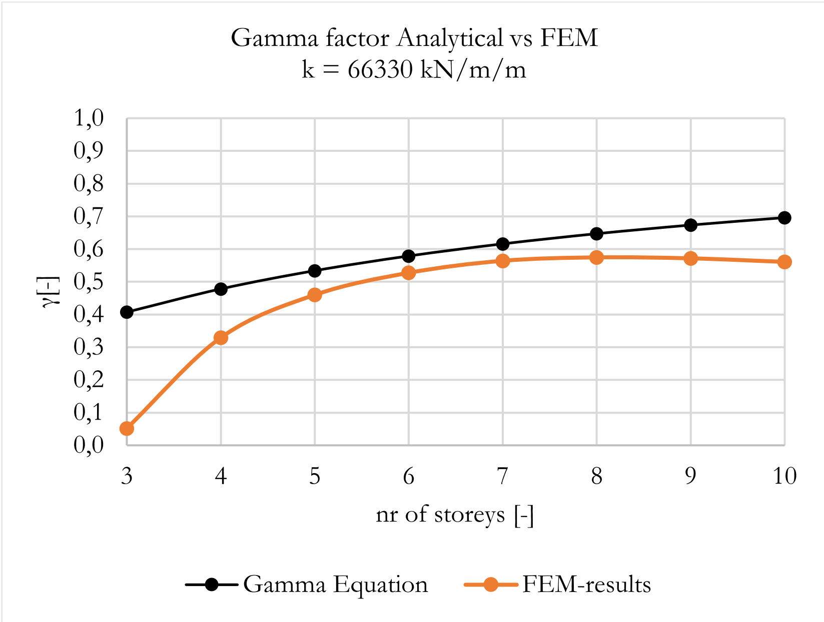

Figure 74 Gamma method, analytical vs FEM result, source: author

The results show that in general, smaller values for γ are found in the finite element model. In the region of 6 7 and 8 stories, prediction by the gamma equation was satisfactory. For the 3-storey model, the analytical method highly overpredicted the cooperation between flange and web.

9.4.2.2. Hand calculations for different values of k

The stiffness of the connection between the flange and the web impacts the stiffness of the core. To show this, the γ-equation is analysed for different stiffness values. Resulting bending stiffness of the core is shown in Figure 75. From this graph, it can be seen that according to the gamma method, the increase in stiffness with stiffness of the connection between flange and web is largest in the region close to k=0. After some point, increasing the stiffness of the corner does not significantly increase the bending stiffness. Designing a stiffer corner than the one in Figure 73, would benefit the bending stiffness of the core.

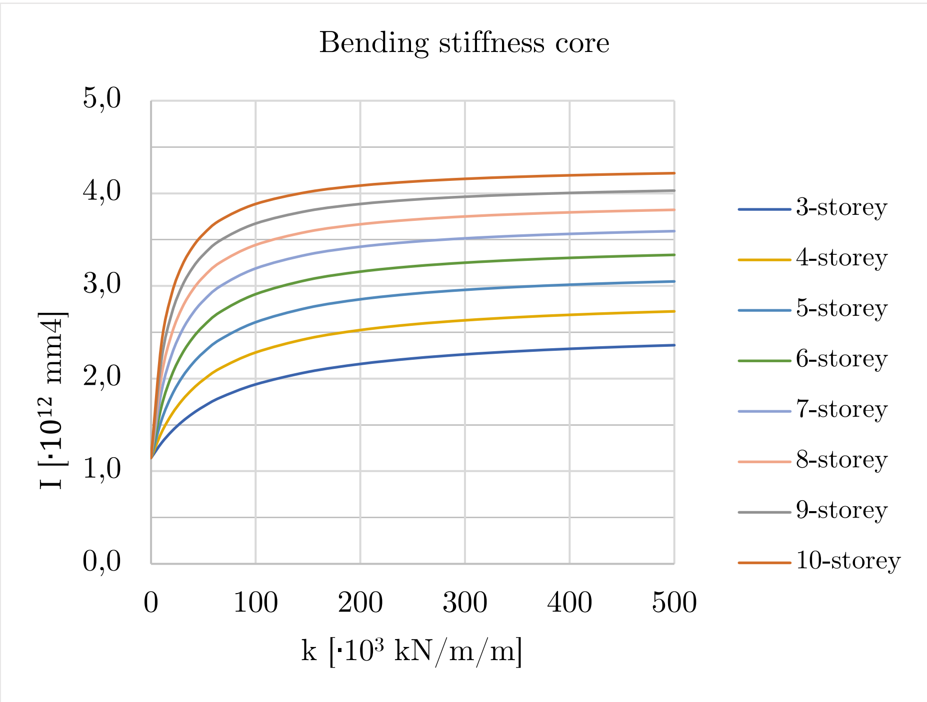

Figure 75 Gamma factor of the flange dependent for different building heights, source: author

9.4.3 Conclusion

From the analysis on the connection between the flange and the web, the following conclusions can be made:

- The finite element analysis has shown that in the core, shear-lag has a large influence on the bending stiffness. The stress distribution in the flange and the core deviates from those assumed in the Bernoulli theory.
- The finite element results indicate that the effective width for shear lag depends on the height of the core. Still, no linear relationship has been found between the height of the core and the effective width for shear lag. More research is needed into this topic.
- The stiffness of the corner connection is a variable that can be adjusted to increase the stiffness of the core. For this core design, based on the γ-equation, it was shown that the benefit of increasing the stiffness depends on the height of the core. In general, the benefit of additional stiffness decreases for higher values of k.
- The gamma method should be used with caution for prediction of the cooperation between the flange and web. A finite element model has been made to compare the γ-equation to modeling results, for a single value of k. It has shown to be a good predictor in certain regions of core height, but in others the analytical formula highly overestimated the cooperation between the flange and web. Further analysis is needed to find the reason for this.

9.5 CLT core without post-tensioning

In this section, the maximum achievable building height when using ordinary connectors in the core is questioned. To limit the number of connectors, and therefore also the displacement due to the connections, it is best to use large CLT panels. The size of the panels is limited by the possibility of transporting and handling large panels on site. For the thesis, the maximum size that is used is a panel size that still fits on a regular trailer with maximum size according to EU regulations (See Appendix P). The largest panels used for the thesis are 12 meters long.

Dependent on the height of the building, the walls in the core can span all storeys, or two CLT walls need to be stacked vertically. The division of the walls for different core heights is shown in Figure 76. The lintels are CLT panels that are assumed to transfer no bending moment. Connections currently available on the market are used in the design of the core. 6 types of connectors can be identified in the design, as shown in Figure 77.

The STS connectors, shear angles and hold-downs assumed are the ones introduced in Chapter 4. Because multiple panels need to be stacked vertically, also tensile plate connectors and shear plates are introduced. More information on these can be found in Appendix Q.

The connection connecting flange and web (connection 6,) is realised with pairs of self-tapping screws. This is shown in Figure 78. Each pair of STS has a distance of $600\ mm$ to the next pair. For the stiffness of this connection, only the stiffness of the screws is included. The interlocking connection makes that the screws alternate direction. It is also likely to facilitate the precise placement of the panels on site. The interlocking effect is not included in the stiffness, as shrinkage of the panel will make guaranteeing the interlocking difficult.

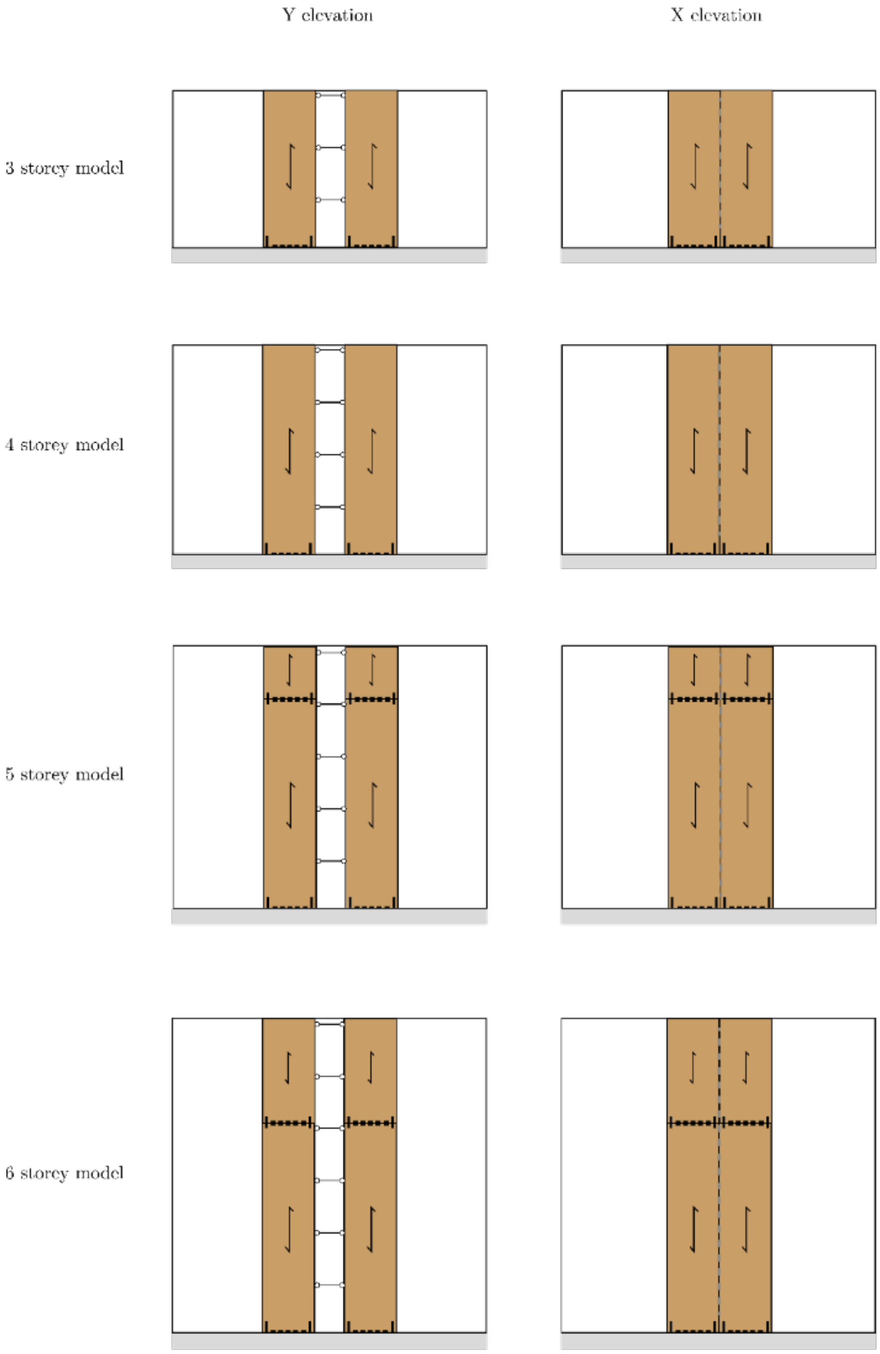

Figure 76 Wall configurations of the un-post-tensioned case study core, source: author

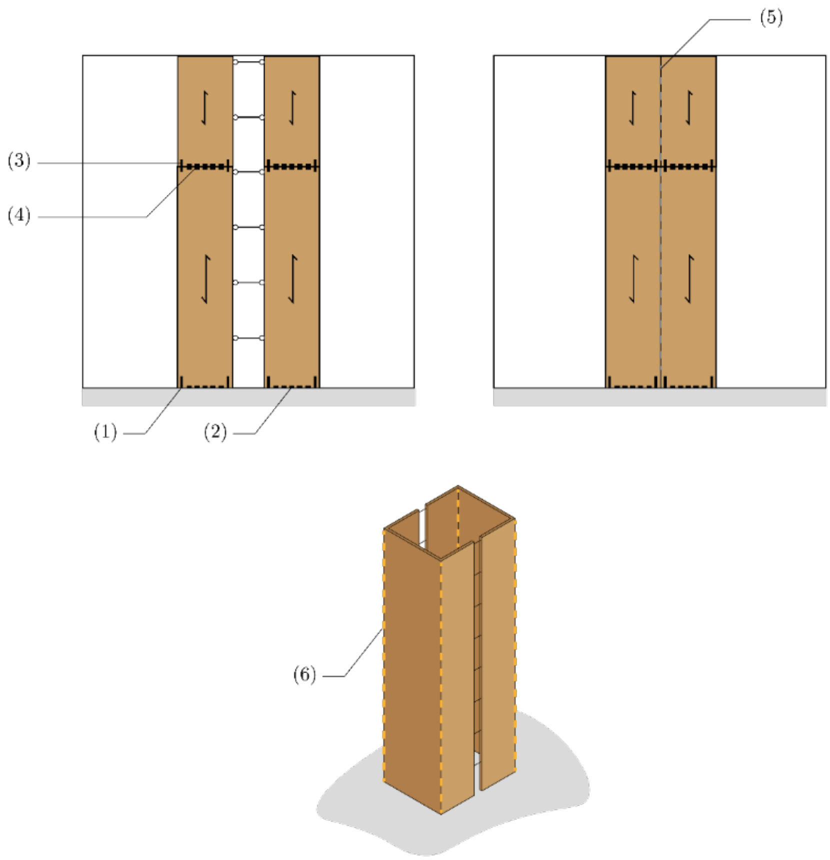

Nr	Type of connector used	Explanation
(1)	Hold-down	resistance against the uplift force
(2)	Shear angles	Resistance against sliding and uplift
(3)	Shear Plate connector	Resistance against sliding and uplift
(4)	Tensile plate connector	Resistance against uplift
(5)	Half lap joint	Transfer of in plane shear between the CLT plates
(6)	Interlocking joint +pairs of angled STS	Connection between the flange and the web for bending

Figure 77 Connections in the CLT core, source: author

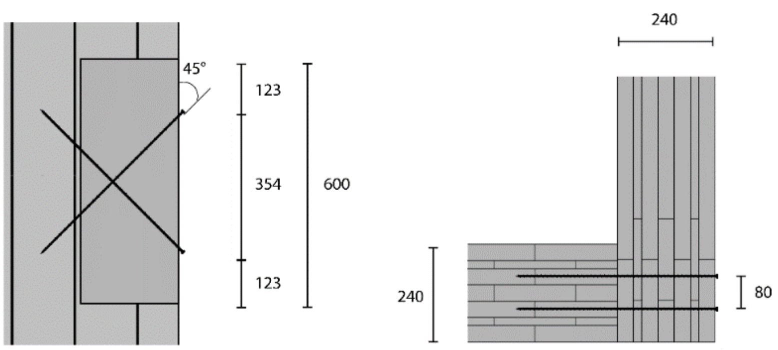

Figure 78 Connection between perpendicular walls(connection nr 6), source: author

9.5.1 *Lateral displacement results*

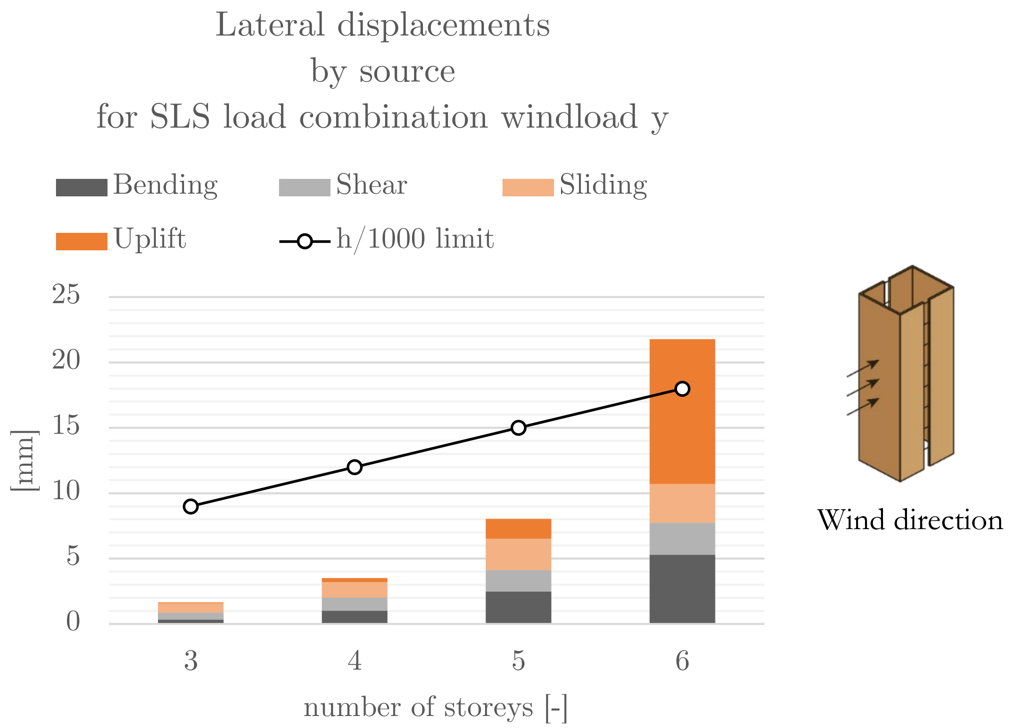

Figure 79 relative contributions to the lateral displacements, source: author

For a building height of 3, 4, 5 and 6 storeys, FEM models have been of the core. From the displacement results in the models, the contribution of the four displacement modes (bending, shear, sliding, rocking) have been isolated. Results are shown in Figure 79. The straight black line depicts the set maximum lateral displacements.

Not all cores models have the same number of hold-downs (contrary to what has been drawn in Figure 76). As the building height goes up, the force in the hold-down increases. When the building is 3, 4 or 5 stories high, a single hold-down at each end of a CLT plate was sufficient for resistance in ULS (UL-2 combination) .For a building height of 6 storeys, an equivalent capacity of three hold-downs was required at each CLT plate end to not exceed the maximum force in the hold-down.

The lateral displacements from the FEM analysis has been depicted in Figure 79. From the results on the lateral displacements in the y-direction, it is clear that the connections are a large contributor to the displacements. Both uplift and sliding are dominant displacement modes. In the five-storey model, the uplift contributed to approximately 20% of the total lateral displacements. Sliding was responsible for approximately 30% of the total lateral displacements. Thus, in total, half of the lateral displacements are due to the connections.

In the six-story model, the uplift increases significantly compared to the five-story model. A reason for this sharp increase is that in the 6-story model, not only uplift displacement from the connection at the ground floor contributes, but also the intermediate joint (at 12-meter height) experiences a resulting uplift force.

9.5.2 Compression toe stress

The 6-story core has been analysed for the maximum compression toe. If in this model, the maximum compression toe stress is not exceeded, surely in the less tall buildings, the compressive stress at the toe will be acceptable.

In Figure 80, the compressive stress at the bottom section of the core is plotted as a diagram along the flanges and the webs. For wind load in the y direction, largest compressive stress is at the location marked (1). The compressive stress marked as (2) is smaller because in that location, the compressive force can also spread along the flange.

The maximum compressive stress is checked for the governing combination (ULS-1) The check is performed on the maximum stress found in the model. The checks are shown in equations 47 to 49.

The verification of a CLT plate under compressive stress should be done for the net-section. Stress results from the FEM are the stresses on the full section. For the verification, the stresses should be multiplied with a factor α.

With a unity check of 0.6 for the maximum compressive stress, there is still a large margin for the maximum compressive stress. If it is decided to post-tension the core, this will increase the maximum compressive stress in the CLT. This should be kept in mind. if the compressive stress is too large, a solution would be to increase the CLT cross-section or to increase α. The last can be done by choosing a CLT of which the section comprises for a large part of lamellas that span in the strong direction (e.g. 80% of the CLT section area is in the stiff direction).

$$\alpha = \frac{t_{CLT}}{t_{CLT}(net)} = \frac{3}{2} \tag{47}$$

$$\sigma_{c,Ed} = \alpha \cdot 6.73 = 10.1\ Mpa \tag{48}$$

$$\frac{\sigma_{c,Rd}}{\sigma_{c,Rd}} = \frac{10.1}{13.40} = 0.75 \leq 1,\ \mathrm{OK} \tag{49}$$

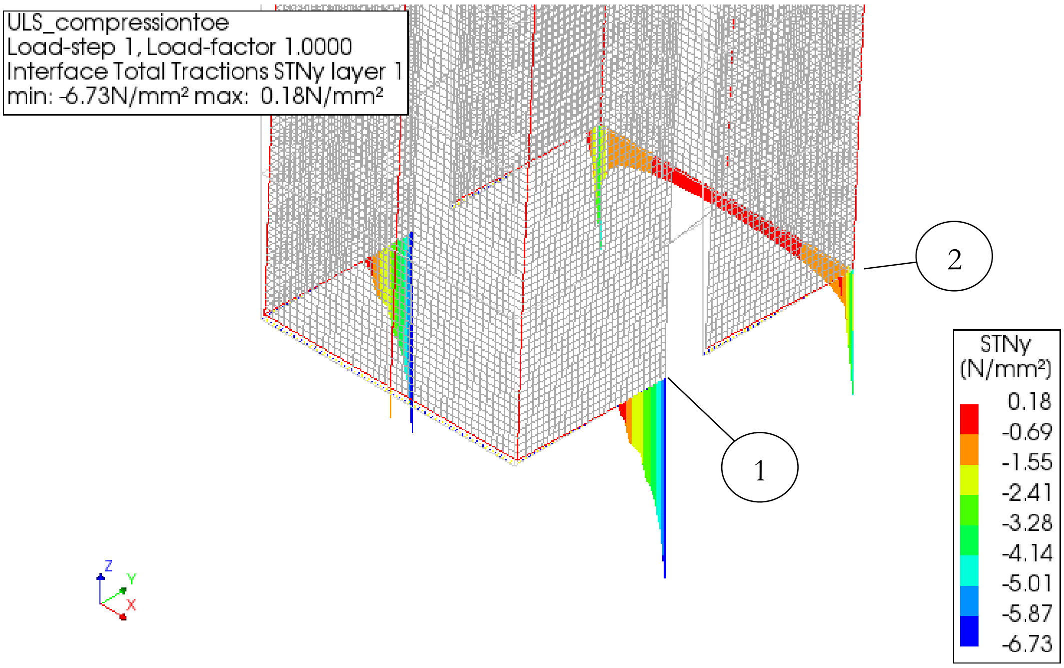

Figure 80 Compression toe stress, source: author

9.5.3 Maximum achievable height

With the current design, the achievable height is limited to five storeys. Uplift proved to be the main contributor to the stiffness of the connections. In the graph on lateral displacements, it is shown that the bending and shear displacements of the core for 6 storeys are much lower than the limit of h/1000. This gives an indication that post-tensioning might be a solution for achieving a higher building with the same core dimension.

In general, if more hold-downs are used, the uplift displacement decreases. With the current core design, to achieve a 6-storey core, an equivalent of 3 hold-downs at each plate end were needed to not exceed the resistance of the hold-downs. This is already a stiff assumption.

Admittingly, this analysis has been performed with a relatively low normal force in the core. The permanent load coming from the floors (9.2.2) was on the lower side. A straightforward way to decrease the uplift would be to increase the normal force in the core. This may be done by including a floor with a higher self-weight. This would also benefit the vibration and acoustic performance of the floors. Another option would be an increase of normal force in the core by increasing the floor span. Furthermore, the CLT plates used in the core walls can be changed by choosing a thicker panel, or a different build-up.

9.6 CLT core with post-tensioning

In Section 9.5, it is visible has shown that most of the displacement of the un-post-tensioned core are due to movement in the connections. In this paragraph, the maximum height of the building will be explored, taking the same core as in 9.5, but applying post-tensioning.

A design of the post-tensioning needs to be made. For this, the workflow presented in chapter 8 has been applied. The structure of the following paragraphs follows the structure of Figure 55 on page 58. With a FE model, the maximum achievable height of the core will be determined. Eventually, the benefit of post-tensioning will be discussed.

9.6.1 Step 1: initial design of the stability system

The design of the CLT core is largely the same compared to the design of the un-post-tensioned core. The size of the core, CLT wall thickness, corner connection design and in-plane shear connection design are the same. Important differences compared to the design of the un-post-tensioned core is that that there are in total 40 post-tension rods placed around the perimeter of the core. The post-tension rods are placed in the central layer of the CLT and are anchored only at top level on the CLT and in the concrete ground floor.

An initial guess of the achievable height can be made by assuming no uplift and sliding takes place. In that case the stiffness of the CLT panels, the corner connection and the in-plane shear connection dictate the stiffness of the core. For simplification it can be assumed that the rods do not contribute to the stiffness of the core. With a hand calculation, it was estimated that an 8-storey building may be achievable with a prestressed core.

An estimation was made of the post-tension force required. This can be related to the expected uplift forces in the core. In this design, it was chosen to apply in total 40 PT rods in the core. In each CLT panel, 5 rods were placed. The rods are embedded in the central layer of the CLT and have an assumed diameter of $d = 32\ mm$.

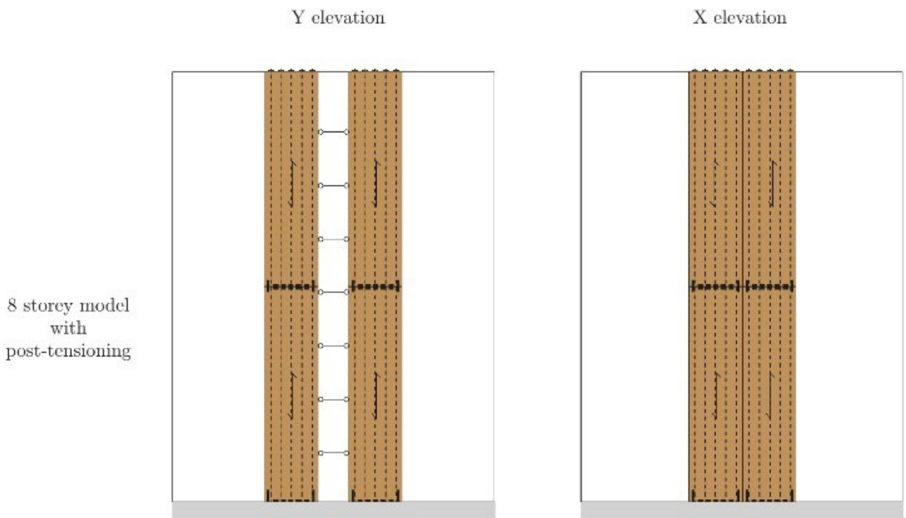

Figure 81 Configuration post-tensioned core, source: author

The applied prestressing force in each rod was increased from $0\ kN$ to $400\ kN$.The effect on the displacement in Y direction at the top of the building is displayed in Figure 82. Two characteristic points in the graph (A,B) are explained.

Point A is the situation in which no post-tension force is applied. When the lateral load is taken by the core, uplift occurs, and the post-tension rods take up this tensile force. Uplift in this case is responsible for 70% of the lateral displacement. **Point B** represents the situation in which the building complies with the lateral displacement restriction of $\frac{h}{1000}$. From this point, an increase of prestressing force does not (significantly) add to the stiffness of the core. This indicates uplift has been avoided.

Based on this graph, it is concluded that a prestress force of $200\ kN$ during the life-time of the building, would be enough to comply with the lateral displacement demand of $\frac{h}{1000}$ at any moment Furthermore, the first $40\ kN$ of prestressing force in each rod were the most effective for decrease of the lateral displacements.

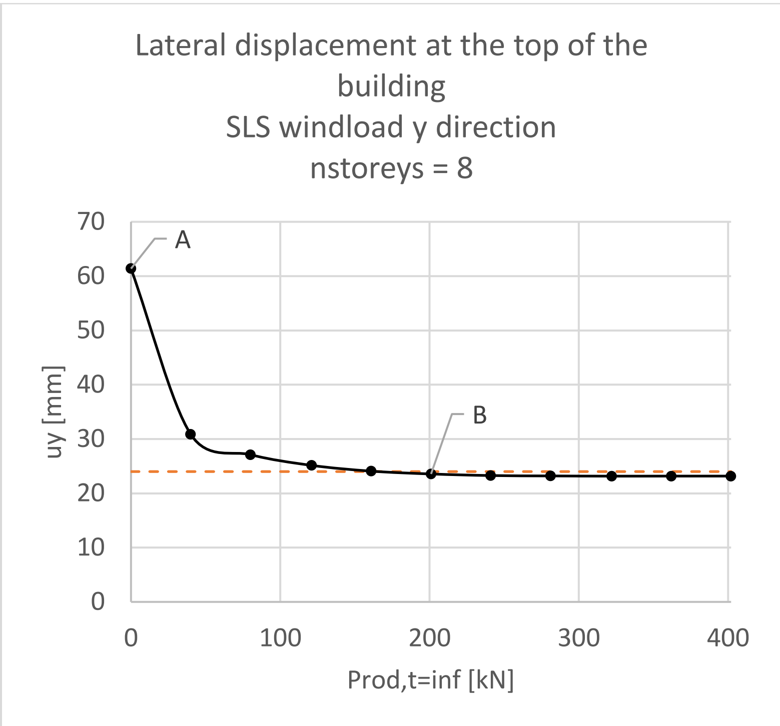

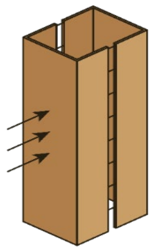

Figure 82 Prestress force vs lateral displacement y direction, source: author

$$P_{t=\infty} \geq 200\ kN \tag{50}$$

$$\emptyset 32\ rods, \qquad \sigma_{p,\infty} = 250 \frac{N}{mm^2} \tag{51}$$

9.6.2 Step 2: Estimation of the long-term losses

For determining the long-term response of the post-tension system, the shrinkage and creep behaviour of the core must be estimated. Assumptions are shown in Table 30. Only an end-creep is included with a k_{def} factor. For the shrinkage, Δ_{MC} takes the maximum moisture change in the structure during the lifetime of the building. This implies no re-tightening is assumed initially.

Table 30 Long-term behaviour assumptions

Creep assumption		
Ultimate creep factor	k_{def}	0.8

Shrinkage assumptions		
Difference in moisture content	Δ_{MC}	4%
Shrinkage coefficient of CLT	$k_{s,CLT}$	0.020
Reduction factor for relaxation	c_{relax}	0.80

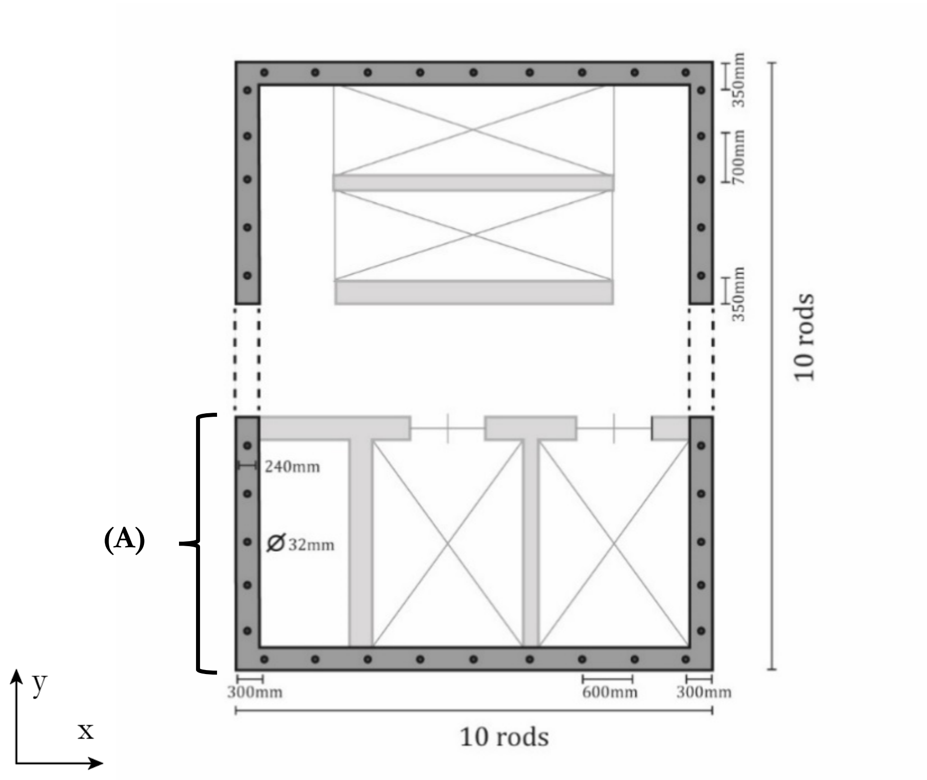

Figure 83 Location of the PT rods and wall (A) for post-tension loss calculations, source: author

The long-term losses are estimated with use of the python code in Appendix M. The prestress force loss calculation in the python code is for a single wall with a single tendon. Therefore an "equivalent prestressed CLT wall" is determined based on the model of the CLT core. The analysis is performed for Wall (A), marked in Figure 83. In this wall, 5 tendons are placed. Thus, the equivalent wall is assumed to be $700\ mm$ wide and $240\ mm$ thick, with a wall height of 24 m (8 storeys).

The prestress loss is dependent on the normal force in the CLT. This normal force should be determined with the quasi-permanent load combination (See 9.2.3). For the case study, it is assumed that all post-tension rods have the same initial prestress force. Though they have the same initial prestress force, the prestress losses will not be equal in all tendons. An important reason for this is the difference in normal force in the wall. The normal force in the wall can be determined with hand calculations or by FEM. In Figure 84, the reaction forces are shown for wall (A) of the core, as this wall experiences the largest axial force. From this the normal force in the equivalent wall is computed.

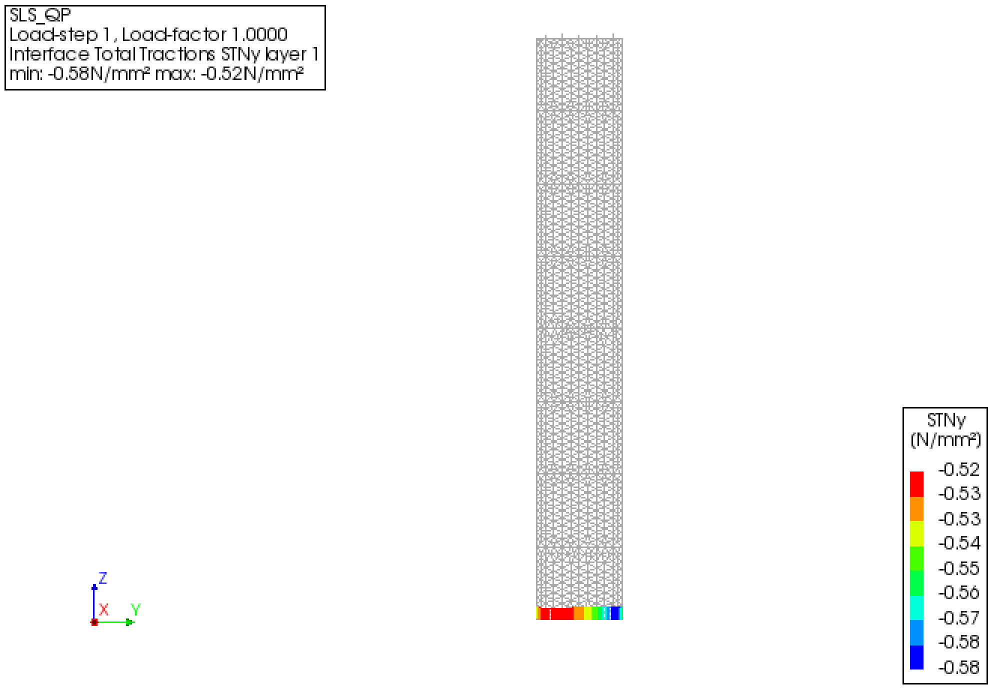

Figure 84 Wall reaction normal stress at the base of the wall for the quasi-permanent load combination (no prestress), source: author

		Force $[kN]$
Normal force in the Equivalent wall (5 tendons in wall A)	N_{eq}	$-92\ kN$

9.6.2.1. Determining the post-tension force loss

Now the normal force in the wall is known, the python code can be run for finding the post-tension loss. The analysis is performed based on an equivalent CLT wall shown in Figure 85. Maintaining a post-tension force of $200\ kN$ in each rod during the lifetime of the building, requires an initial post-tension force of 355 kN.

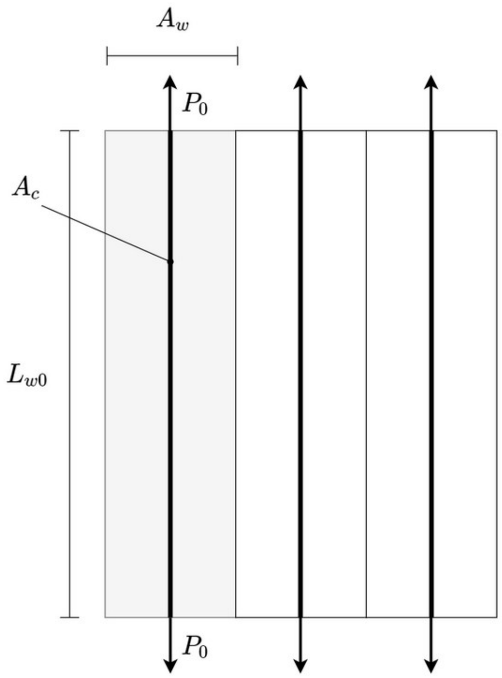

Figure 85 Equivalent prestressed CLT wall, source: author

Table 31 Prestress Losses

	Prestress Force loss [%]
Creep loss only	11%
Shrinkage loss only	33%[2]
Relaxation loss	3%[1]
Creep + shrinkage + relaxation	44%

[1] Because the total loss calculation is made for relaxation combined with creep and shrinkage, only 80% of the relaxation loss calculated on the steel is included here [45]).

[2] $\Delta_{MC} = 4\%$, and shrinkage coefficient of 0.020 is assumed here.

9.6.2.2. Analysis on the influences on the creep and shrinkage loss

Creep and shrinkage are the major contributions to the force loss. The difference in moisture content is a variable that is difficult to determine. In the force loss calculations, a maximum of 4% moisture content in the lifetime of the building was assumed. For the safety of the structure, the sensitivity of the force loss calculation to the moisture level change should be examined.

A creep curve for CLT loaded in-plane is not readily available in literature. In the case-study, the creep is included by adjusting the stiffness of the CLT with a k_{def} factor of 0.8. This is a simplistic approach and does not include all effects on the creep behaviour. For instance, the creep behaviour will also depend on the moisture content of the CLT. Therefore, also an analysis is done on the influence of the creep factor.

> (1) How does the loss depend on the difference in moisture content?
> (2) How does the loss depend on the creep factor k_{def}?

The results from this analysis are presented in Figure 86. From the graph, several conclusions can be drawn:

- Elastic losses and relaxation losses are small compared with creep and shrinkage losses. This can be seen from **point A** in the graph. Total losses from relaxation and elastic losses together are less than 5%.
- A higher creep factor results in more creep loss. For a situation with no shrinkage loss, when doubling the creep (k_{def} from 0.8 to 1.6), the prestress loss increases with 84%.
- The resulting prestress force at $t = \infty$ decreases rapidly with increasing moisture level. For a situation with no creep included, when changing Δ_{MC} from 4% to 8%, the stress loss due to shrinkage is more than doubled. This shows the importance of making a reliable estimation of the moisture content.

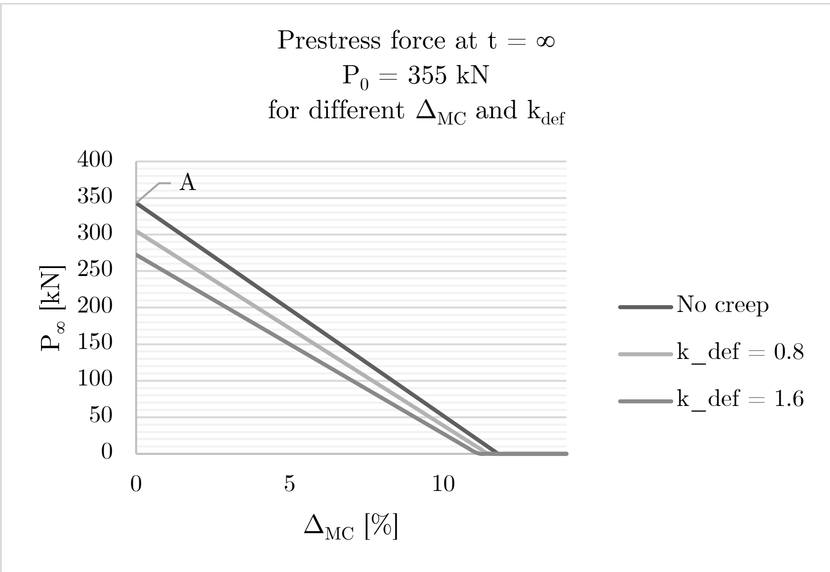

Figure 86 Prestress force loss for different shrinkage and creep, source: author

9.6.3 Step 3: Determine the post-tension force at the reference moment

From the initial post-tension force and the calculated losses, the post-tension force at the reference moment can be derived. In this case the reference moment is the building life, as no retightening is assumed.

Table 32 Estimated total prestress loss

Prestress at t=0	$355\ kN$
Prestress at end-of-life ($k_{def} = 0.8,\ \Delta_{MC} = 4\%$)	$200\ kN\ (-44\%)$

9.6.4 Step 4: Check on SLS requirements

9.6.4.1. Lateral displacement

For this step, the prestress loss at the reference moment ($200\ kN$) was applied to all post-tension bars. Then, the lateral displacement was checked for the relevant load combination (SLS, characteristic). The deformed model is shown in Figure 87. The displacements were checked against the requirement of $\frac{1}{1000} \cdot h_{building}$. The lateral displacements proved to be OK.

$$u_{max} = 23.6\ mm$$
$$u_{req} = \frac{1}{1000} \cdot h_{building} = 24\ mm \qquad (52)$$
$$\frac{23.6}{24} = 0.98 < 1, \qquad OK$$

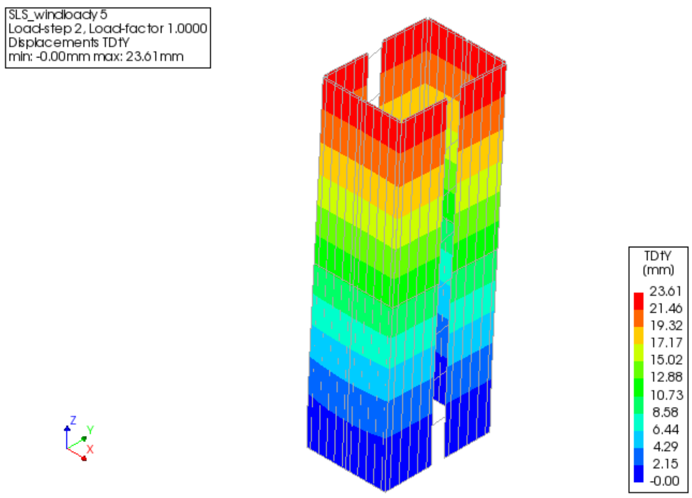

○

○ *Figure 87 SLS, lateral displacements, source: author*

9.6.4.2. *Stress change in the prestressing bars*

Under the wind load, the stress in the rods will change. This is shown in Figure 88. The largest change in steel stress is found in the web, most far away from the neutral axis. The stress change in the flange is lower due to the limited stiffness of the connection between the flange and the web and the occurrence of shear lag.

The steel has been modelled with its full elastic modulus. To show that the steel stress is below the yield-point of the steel and therefore modelling with the full modulus is correct, the stress level in SLS conditions is shown in Figure 89.

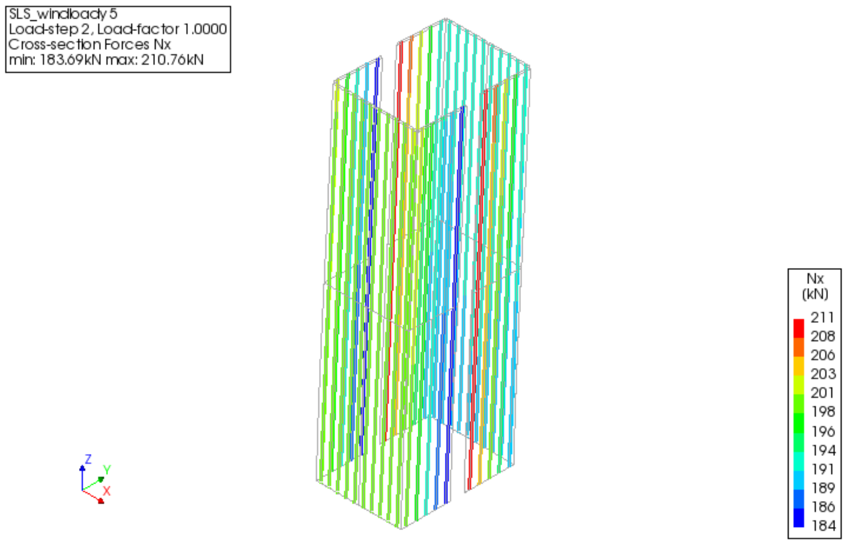

Figure 88 Stress increase in the PT rods under SLS combination with wind loading the y-direction (isometric), source: author

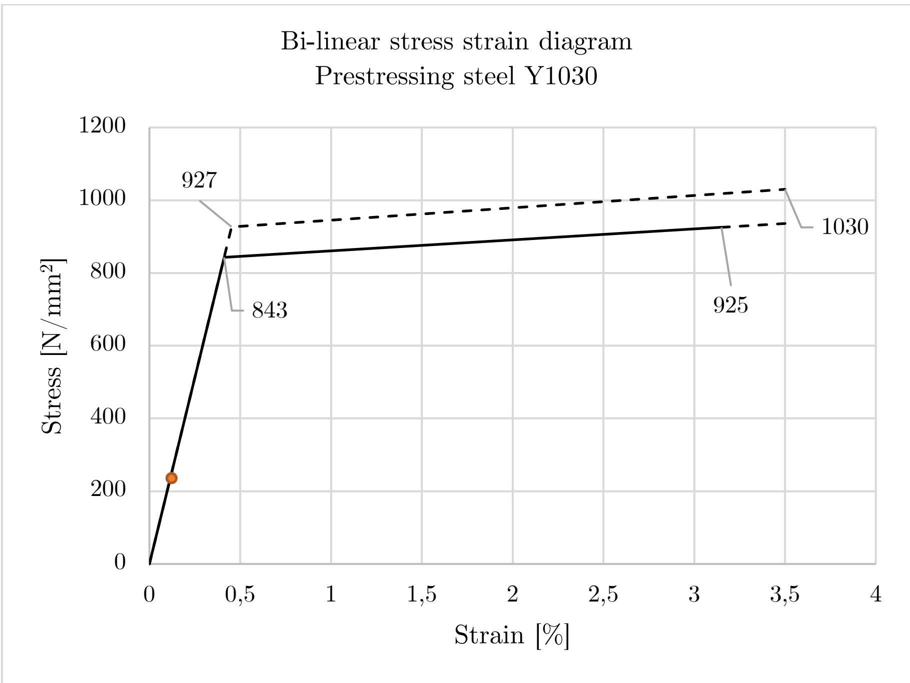

Figure 89 SLS prestressing steel level in the bilinear diagram, source: author

9.6.4.3. *Prevention of sliding by post-tensioning*

To analyse whether there is enough friction on the interfaces to prevent sliding displacement, the base shear force is compared with the compressive stress at ground floor level. The friction coefficients are assumed as in Table 11 on page 26. Because the post-tensioning is beneficial for preventing sliding, the smallest post-tension force should be included. This is the post-tension force after the losses have taken place.

The total compressive force at the base of one of the walls in the web is compared with the lateral force resulting from wind load. The compressive force at the base for ULS has been extracted from the finite element model.

The sliding analysis has been made for the core wall marked (1) in Figure 90. This wall experiences a total compressive force of $1215\ kN$ in SLS. This high compressive force at the interface makes that there is such a high friction that sliding will not occur, as shown in Eq. 53-59.

In the case-study, there is a second horizontal joint at 12-meter height as two CLT panels are stacked vertically (visible in Figure 81). A simplified check is made for this joint. This joint is a joint between two CLT plates, thus μ_F=0.4. It can be assumed that the normal force in the core increases linearly with the height of the core, meaning the normal force at half-way building height (12 m) will be approximately $607\ kN$. Also, the shear force due to wind load will be approximately linearly varying over the height. This means the shear force will be approximately 70 kN for this wall at half-way building height. Result from the friction analysis is that also in this interface, sliding is not likely contributing to lateral displacements (see eq. 53-59).

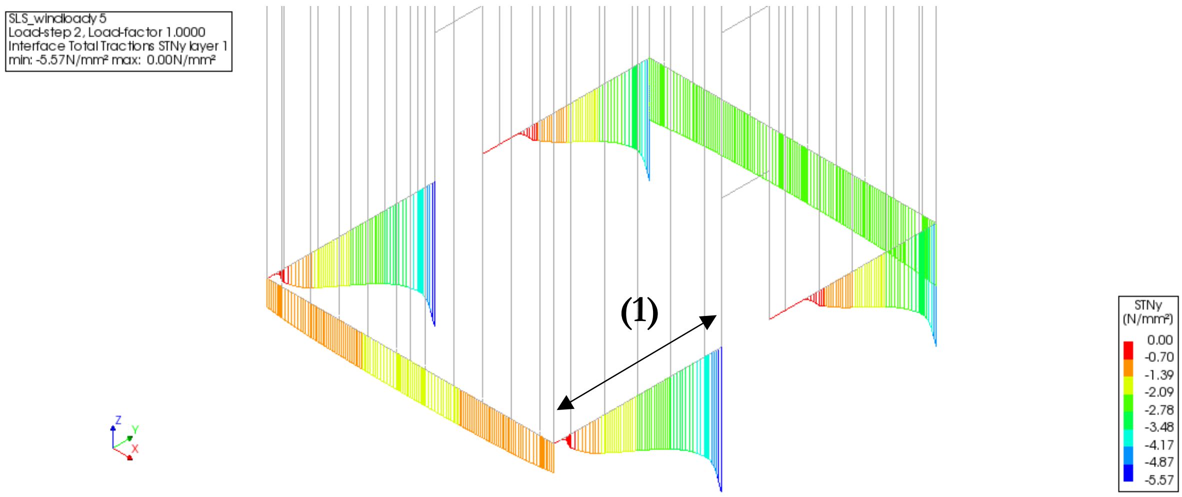

Figure 90 Compressive force at the base in SLS, source: author

$$N_{base} = 1215\ kN \tag{53}$$

$$\mu_F = 0.7\ [-] \quad \text{(CLT on rough concrete)} \tag{54}$$

$$V_{max} = 1215 \cdot 0.7 = 805\ kN \tag{55}$$

$$V_{base,wall} = \frac{561}{4} = 140\ kN \tag{56}$$

(See Appendix N)

$$\frac{V_{base}}{V_{max}} = 0.18 < 1 \tag{57}$$

No sliding occurs

Check on the same wall at half-way building height:

$$V_{max} = 0.4 \cdot 607 = 242\ kN \tag{58}$$

$$\frac{V_{12m}}{V_{max}} = \frac{70}{242} = 0.3 \tag{59}$$

No sliding occurs

9.6.5 Step 5: Check on ULS requirements

9.6.5.1. Compression toe stress

The highest prestressing steel stress occurs before the losses have taken place. Therefore, the ULS check is performed with the prestress force at $t = 0$ $(P_0 = 355\ kN)$ The ULS load combination was applied. The maximum compressive stress is found at the toe (see Figure 91 and Figure 92). This is checked against the compressive resistance of the CLT, correcting for the net-section.

$$\sigma_{c,d,max,FEM} = 8.35\ N/mm^2 \tag{60}$$

$$\frac{\frac{3}{2} \cdot \sigma_{c,d,max,FEM}}{\sigma_{c,Rd}} = \frac{\frac{3}{2} \cdot 8.35}{13.4} = 0.93\ < 1,\ \mathrm{OK} \tag{61}$$

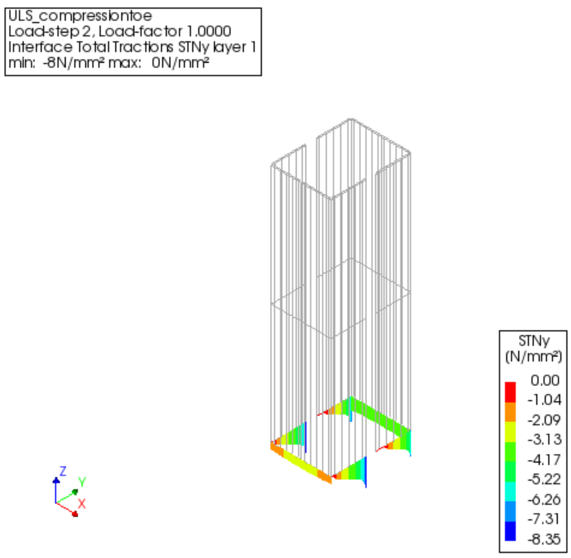

Figure 91 Stress at foundation level, isometric, source: author

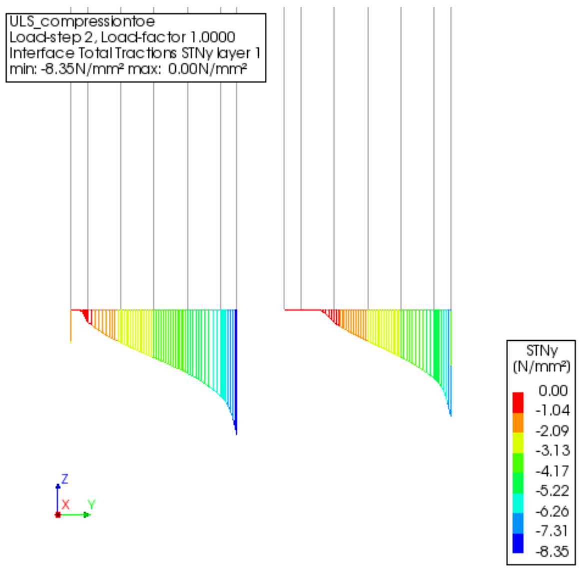

Figure 92 Stress at the foundation level, side-view, source: author

9.6.5.2. *Buckling analysis*

The buckling analysis is performed for a 3.5-meter length wall, in line with paragraph 3.5.3. The stiffness of the CLT panel is extracted from the stiffness matrix generated from CLTdesigner (Appendix R) and shown in Table 33 . Stiffness $E_{0,mean}I_{0,eff}$ corresponds to entry D_{22} in the stiffness matrix. The buckling length is equal to the storey height ($l_{ki} = 3000\ mm$).

The normal stresses in the wall for load combination ULS-3 is shown in Figure 93. The compressive stress in the wall was $3.0 - 3.2\ N/mm^2$, of which approximately $2.2\ N/mm^2$ was due to the prestressing. Adjusting for the net section, the unity check for buckling was 0.74. For the calculation of the buckling factor $k_{c,y}$, reference is made to Appendix S.

$$\frac{\sigma_{c,0,d}}{k_{c,y} \cdot f_{c,0,d}} = \frac{3.2 \cdot \frac{3}{2}}{0.47 \cdot 13.4} = 0.74 < 1,\ \text{OK} \tag{62}$$

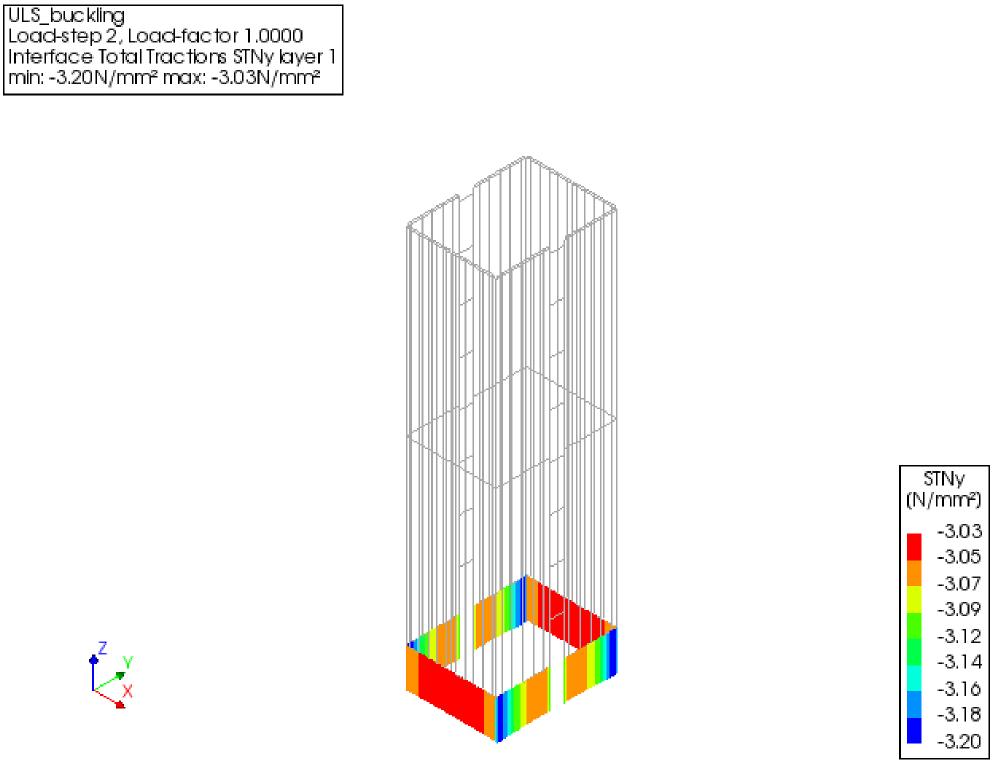

Figure 93 Normal stress at the bottom of the core under combination ULS-3, source: author

Table 33 out of plane stiffness of the L-240/7s panel

Stiffness per m (Appendix R)	$E_{0,mean}I_{0,eff}$	2229.33	$\frac{kNm^2}{m}$
Stiffness per 3.5 m	$E_{0,mean}I_{0,eff}$	6688 $6688 \cdot 10^9$	kNm^2 Nmm^2
Stiffness per 3.5 m	$I_{0,eff}$	$6.08 \cdot 10^8$	mm^4

Table 34 Buckling factor

Net area	$A_{0,net}$	560000	mm^2
Radius of gyration	$i_{0,eff} = \sqrt{\frac{I_{0,eff}}{A_{0,net}}}$	32.95	mm
Slenderness	$\lambda_y = \frac{l_{ki}}{i_{0,eff}}$	91	-
Relative slenderness	$\lambda_{rel,y} = \frac{\lambda_y}{\pi} \cdot \sqrt{\frac{f_{c,0,k}}{E_{0,05}}}$	1.39	-
Buckling coefficient	$k_y = 0.5 \cdot \left(1 + \beta_c \cdot \left(\lambda_{rel,y} - 0.3\right) + \lambda_{rel,y}^2\right)$	1.52	-
Instability factor	$k_{c,y} = \frac{1}{k_{rel,y} + \sqrt{k_y^2 - \lambda_{rel,y}^2}}$	0.467	-

9.6.5.3. *Steel stress*

The steel stress increase under wind load should be checked for the relevant ULS load combination. The steel stress is shown in Figure 94. The stress level in the rods is plotted in Figure 95.

$$P_d = 367\ kN \tag{63}$$

$$\sigma_{p,d} = 456 \frac{N}{mm^2} \tag{64}$$

$$\frac{\sigma_{p,d}}{\sigma_{p,Rd}} = \frac{456}{843} = 0.54\ < 1,\ \text{OK} \tag{65}$$

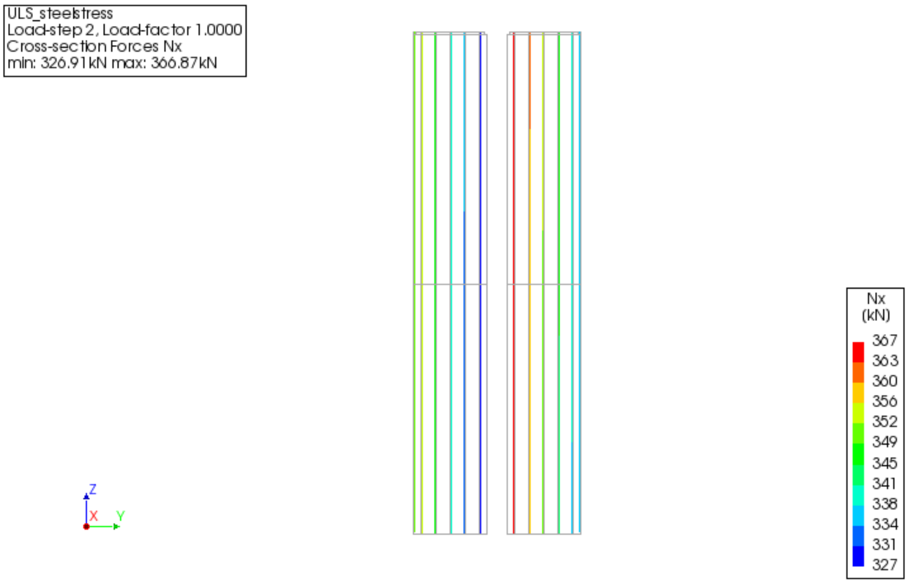

Figure 94 ULS steel stress, source: author

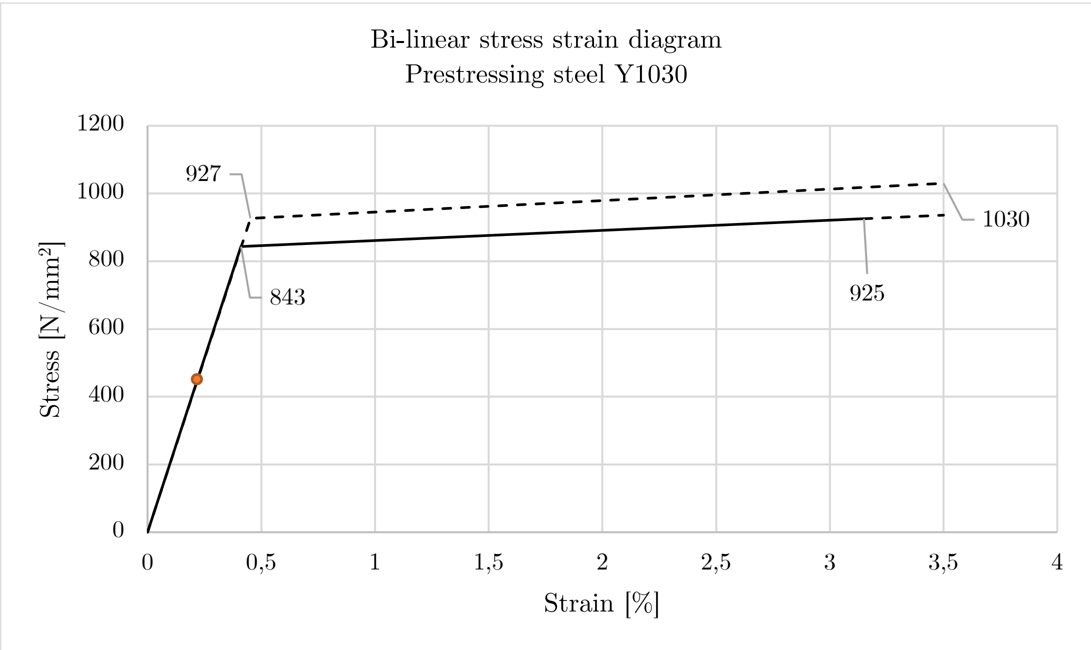

Figure 95 ULS prestressing steel level in the bilinear diagram, source: author

9.6.5.4. Bearing stress check

The stresses under the anchor are checked against the maximum compressive stress in the CLT. This is s a simplified check for the anchor plate. The steel anchor plate assumed is 400 mm long and 160 mm wide. Only the layers of the CLT under the anchor and in the "0" direction are taken into account for the bearing stress (net-section approach, see $\sigma_{bearing}$ in Figure 96).

$$P_{t=0} = 350\ kN \tag{66}$$

$$\sigma_{bearing} = \frac{P_{t=0}}{L_{anchorplate} \cdot d_{0,net,bearing}} = \frac{350E3}{80 \cdot 400} = 10.9\ N/mm^2 \tag{67}$$

$$\frac{\sigma_{bearing}}{f_{c,0,d}} = \frac{10.9}{13.4} = 0.81, \qquad OK \tag{68}$$

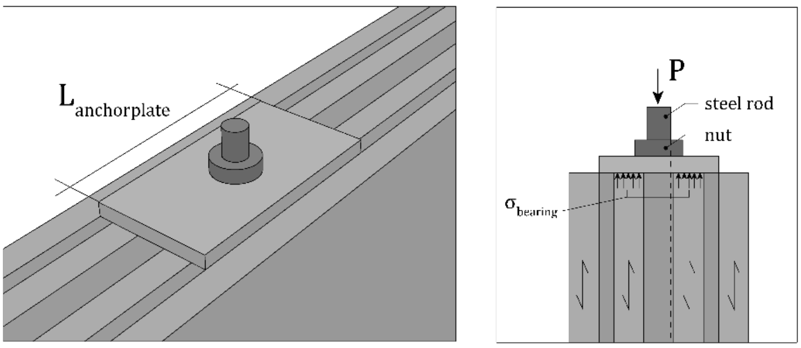

Figure 96 Anchor plate, perspective (left) and side-view (right), source: author

9.6.6 Maximum achievable height

It has been proven that when applying post-tensioning to the core, an 8-storey building is feasible. With a unity check of 0.9 for both the lateral displacements and the maximum compressive stress, we can conclude that this is close to the height limit for this core. It will be explored in this paragraph, how much higher can be built when changing the CLT to a thicker panel.

9.6.6.1. Maximizing the stiffness of the core

Now that it has been proven that post-tensioning can eliminate the displacements related to the connections, the limits of the post-tensioned minimal core can be tested. A thicker CLT panel, with more of its layers oriented parallel to the height of the core, the bending and shear displacement of the panel can be further decreased.

CLT can be produced with large thicknesses, e.g. maximum $500\ mm$ by KLH. For finding the maximum stiffness of the core, 500 mm thick CLT is assumed with 75% of its layers arranged parallel to the building height. Although CLT panels can be produced with this thickness, this is not a standard thickness.

It was found that with this thickness of CLT, 160 kN in each prestressing rod was enough to limit the displacements to below $h/1000$ (see Figure 97). However, with that prestress, the uplift is still significant, causing a small compression area and an exceedance of the maximum compressive force in ULS (Figure 98). Applying a higher prestress limits the uplift therefore provides a larger compressive area and a lower stress for the compression toe stress in ULS. Still, no prestress level is found that causes low enough compression toe stress, even when not accounting for any overstressing to compensate for losses.

$$t_{CLT} = 500\ mm, \qquad \frac{t_{0,CLT}}{t_{CLT}} = 0.75 \tag{69}$$

$$\sigma_P = 210\ N/mm^2 \tag{70}$$

$$P = 169\ kN \tag{71}$$

$$\sigma_{CLT,Ed} = 19.53 \cdot \frac{4}{3} = 26\ Mpa > \ \sigma_{CLT,Rd} \tag{72}$$

The compressive stress is exceeded

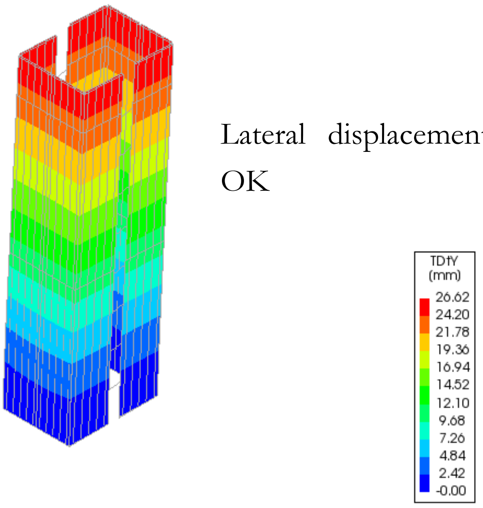

Figure 97 9 storey core SLS displacement, source: author

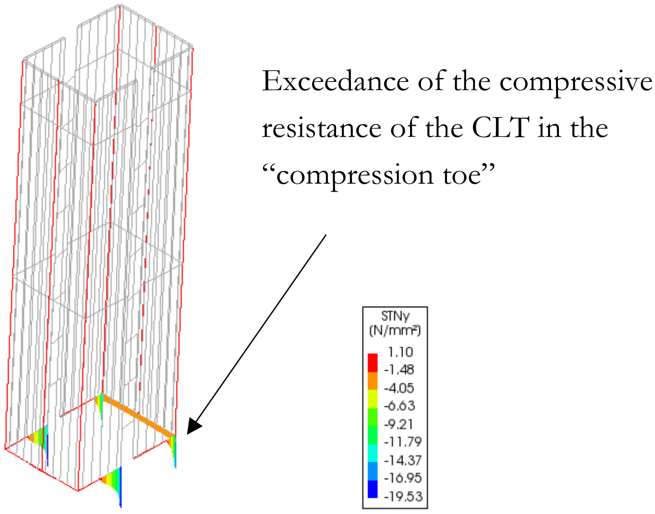

Figure 98 9 storey core, ULS compression toe stress, source: author

9.7 Conclusion

Table 35 shows a comparison between the case-study building stabilized with a non-post-tensioned core versus the case-study building stabilized with a post-tensioned core.

Table 35 Comparison between the un-post-tensioned and post-tensioned core, source: author

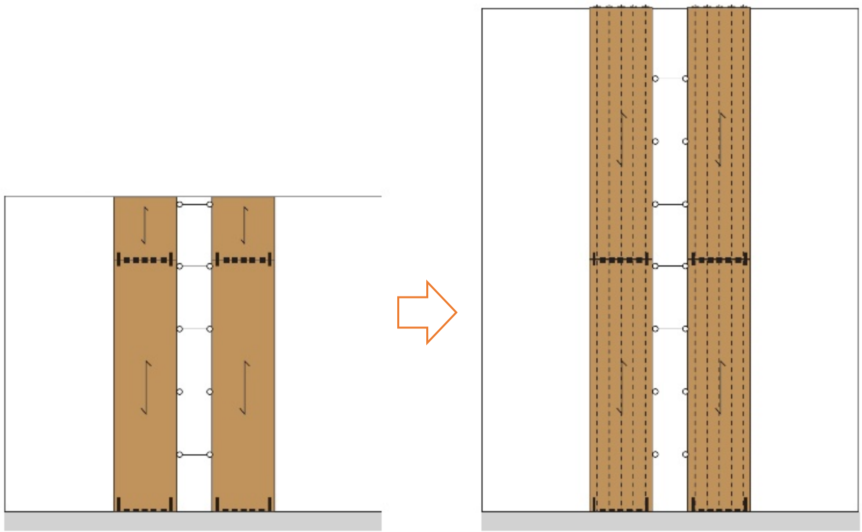

5 storeys Slenderness core = 1.9	8 storeys Slenderness core = 3
No Prestress	Prestress
16 hold-downs 16 tensile plates 40 shear angles 40 shear plates In total 112 connectors	40 prestress rods diameter 32 mm with anchors $P_0 = 355\ kN$

Several things have been learned from the analysis in this chapter:

- Post-tensioning of the core has been proven to be beneficial in this design case. Without post-tensioning and with ordinary connections, a 5-story building was feasible. Half of the displacements in this case was due to the connections. With post-tensioning, this could be almost doubled to 8 storeys.
- The first 40 kN of applied prestress to the bars was most impactful.
- With the applied post-tensioning, ULS compressive stress in the toe is close to the compressive stress in the CLT (unity check of 0.9). The stress check for the compression toe is important in post-tensioned cores.
- Though post-tensioning increases the risk for buckling. Though buckling proved to not be a risk in this design case, when using higher floor to floor height or smaller thickness of CLT, buckling might be a problem.

- Post-tensioning losses are significant, the estimated required overstressing of the rods to account for long-term losses was 44%. Although in the case-study, this overstressing did not result in an exceedance of the compressive resistance, this might be the case in other designs.
- Post-tensioning eliminates the need for the large number of connectors. In the post-tensioned design, any uplift forces are taken by the prestressing steel, which makes hold-downs unnecessary. Also, because of post-tensioning compresses the joint at foundation level and the joint between two stacked CLT walls, sliding will be eliminated. Shear angles and shear plates are not required.

In case the prestress losses require a too high overstressing, there are multiple measures that can be taken by the designer:

(1) Retightening can be applied in the first year after initial stressing of the panels. Creep deformations occur mostly during the first year. Moreover, a large part of the shrinkage by drying of the CLT after completion of the construction will also most likely have taken place in the first year. Therefore, checking and re-tightening of the rods in the first year is sensible.
(2) Controlling the shrinkage loss by controlling the moisture content change of the CLT. The moisture level can be controlled for the moment of post-tensioning by measuring the moisture content across the thickness of the walls before tightening the rods. More strict requirements can be set for the moisture content of the CLT during manufacturing, transportation, storage and placement of the panels. This requires weather precautions on site. One may also use dryers on site for drying the CLT before tightening the rods to lower the MC.

It must be admitted that there is still a large uncertainty in the expected shrinkage of the CLT. The shrinkage is dependent on the changes in moisture content. This again depends on a lot of uncertain factors, such as the climate, the conditions on site and the speed at which CLT adapts to a new relative humidity. All things considered, the assumed change in moisture level (Δ_{MC}) of 4% is likely to be on the high side. A better estimation of the changes of moisture content during the lifetime of a CLT building is therefore added to the suggestions for further study.

Furthermore, a range of values have been found for the shrinkage coefficients of CLT ranging from 0.016-0.040. An arbitrary 0.020 has been assumed in this analysis. The shrinkage coefficient also depends on the arrangement of the layers within the CLT. A better indication of the shrinkage coefficient of CLT panels based on the build-up of the panel is suggested for further study.

Several other topics are interesting for a next design step but have not been included at this point. These include:

- Performance of the core for wind load in the X direction. The lateral displacements proved largest for wind load in the y direction, therefore only the analysis for wind in y direction has been included in this chapter.
- Application of different prestress forces in the different core walls. At this point, prestress forces in all rods have been assumed equal. In the core, depending of load sharing between the flange and the web, each wall experiences a different uplift force, thus requires a different prestress force for prevention of uplift.
- Checks on the lintels were neglected at this point. In a next design step, resistance of the lintels needs to be included. If the CLT plate does not fulfil, a glulam beam may be used as lintel.
- The prestressing relies on the functioning of the anchors. A detailed anchorage design has been neglected at this point but would be necessary in a next design step. This includes the check for "splitting stresses", which are tensile stresses perpendicular to the direction of prestressing, due to spreading of the prestress force.

10 Conclusion

10.1 Introduction

This chapter forms the conclusion of the thesis. In 10.2, the main conclusions of this paper will be formulated by answering the research questions from 1.3.1. A reflection on the goals of the thesis and the research contributions are discussed in 10.3. Several topics suggested for further research can be found in 10.4.

10.2 Answers to the Research Questions

Main Research Question: How effective is post-tensioning a CLT core for reducing lateral displacements of a building?

This thesis has demonstrated that post-tensioning of a CLT core can be beneficial for decreasing the lateral displacements in multiple story buildings. When not post-tensioning, the connections would be responsible for the largest part of the lateral displacements. With adequate post-tensioning, uplift and sliding displacements can be avoided. In addition, the use of many connection can be avoided. In a case study, the achievable height was increased with 60% as a result from post-tensioning.

A Case-Study has been chosen to compare the lateral displacements of a building stabilized with an un-post-tensioned core with a building stabilized with a post-tensioned core. The lateral displacements highly depend on the core design and floorplan. The benefit of post-tensioning could be expressed as a gain in achievable height. In the case-study, it was shown that the achievable height of the building was increased from 5 to 8 stories.

With the case study, it has been shown that the connections are responsible for a large part of the lateral displacement in an un-post-tensioned core. The lateral displacements can be split up in four contributors: Bending, Shear, Sliding and Uplift. The latter two are due to the movement in the connections. With the minimal core dimension, for buildings higher than 3 floors uplift and sliding in the core were responsible for more than 50% of the total lateral displacement. The uplift is related to the moment at foundation level and this moment increases rapidly with the building height. This indicates that with increase of building height, the benefit of post-tensioning becomes higher.

Depending on the level of post-tensioning, uplift can be avoided altogether, or small levels of uplift may be allowed. Hold-downs are not necessary when post-tensioning the core, as the post-tension rods can take up any resulting uplift force that may occur. The rods should be designed to accommodate for this increase in prestressing steel stress under wind loads. Sliding in the interfaces may also be avoided if friction in the interfaces is high enough.

The post-tensioning shows no benefit with regards to reducing shear and bending displacements. This means that it is only beneficial to post-tension the core to the level in which no uplift occurs. Higher post-tension forces do not further decrease the lateral displacements.

The designer must realize that the maximum compressive stress in the CLT limits the maximum post-tension force that can be applied. With increasing building height, the uplift force increases, making a higher post-tension force needed for limiting the lateral displacements. This results in the possibility of exceedance of the maximum compressive stress at the "compression toe". Besides this compression toe stress, due to post-tensioning, also the risk for buckling increases.

Sub Question 1: What is the effective flange width for bending in a CLT core?

Bending displacements of the core depend on the bending stiffness of the core section. With increasing height, the contribution of the bending displacements of the core to the overall lateral displacements of the building increases. Depending on the core section, a bigger or smaller part of the bending stiffness of the core comes from the Steiner Contributions of the core flanges. Next to the geometry of the section, two other important factors can be identified that influence the bending stiffness of the core, namely (1) the shear lag effect and (2) the semi-rigid connection between the core flange and the web.

In the thesis, an approach has been developed for finding the effective width of a CLT core. This approach includes the shear lag effect and the influence of a flexible connection between web and flange by means of an *effective flange width*. In the approach first the maximum effective flange width for shear lag ($b_{fl,eff,s-l}$) is determined which depends on the core height. Second, the influence of the semi-rigid corner is included with a γ-factor. This results in the final effective width for the CLT core: $b_{fl,eff} = b_{fl,eff,s-l} \cdot \gamma$. Using the effective area of the section, the designer can find the stiffness using Bernoulli theory, and estimate the bending deflections of a CLT core.

The effective width method was studied in a Case-Study. Conclusions from this analysis included the following:

- The FEM analysis showed that the effective flange width for shear lag is indeed largely dependent on the core height. Though the results from the model were overall close to the predicted effective width, for certain building heights, the found effective width in the finite element model was smaller (e.g. 3 storeys and 10 storeys). A relationship for the effective flange width for shear lag could not be derived in the timeframe of the thesis.

- For determining the reduction factor γ, which reduces the effective width for the connection between the different core walls, the theory of mechanically connected beams from Eurocode 5 is used. The cooperation factor highly depends on the stiffness of the connection between flange and web with depend on the stiffness of the fasteners and the spacing between the fasteners ($k = \frac{K_{ser}}{s}$). There is a non-linear relationship between the stiffness and the cooperation factor. The cooperation also highly depends on the height of the core. For taller buildings, the cooperation factor is higher.
- The results from comparing the γ-equation calculation to the FEM model were that in some regions, the gamma equation predicts the cooperation quite well. For the Case-Study core this was the case especially for 5, 6, 7 storey height. For smaller and larger building heights, the FEM results were not in agreement with hand calculations. This shows that is important to study the stresses and deformations with a finite element model.
- As an indication: For the connection with angled STS connectors used in the Case-Study (k=66330 kN/m/m), the gamma factor from FEM results was 0,46. It was shown that doubling the stiffness of the connection would result in a significant bending stiffness increase. A stiffer corner design is therefore suggested for further study.

Sub Question 2:How do long-term effects influence the prestress force and how should the prestress losses be quantified?

By performing literature research and analytical calculations, the importance of different long-term losses on the post-tension force were assessed. It was shown that creep, shrinkage and relaxation are important prestress losses. A python code was developed for estimating the prestress loss based on an "equivalent prestressed member". The force loss depends on geometrical parameters, long-term loading and long-term material behaviour, and an iterative procedure is required to find equilibrium between the force in the steel and the force in the CLT. For an indication of the prestress loss, the results of the Case-Study are discussed:

Relaxation of the prestressing steel proved to contribute to the prestress losses the least, with a prestress force loss of 3% over the lifetime of the building. Creep accounted for approximately 11% force loss in the Case-Study with an included creep factor k_{def} of 0.8. The shrinkage loss proved to cause the most force loss, with 33% force loss in the lifetime of the building. In total 43% force loss was found, which is significant, and shows that when prestress losses are not to be neglected in design of post-tensioned structures.

In the Case-Study, the force loss (43%) required significant overstressing of the prestress bars. This did not exceed compressive resistance of the CLT in the compression toe. In other designs the compressive stress might be exceeded. For that case two solutions are suggested in combination with a smaller initial prestress: (1) controlling the moisture content of the CLT panel in construction phase, therefore limiting shrinkage prestress loss and (2) re-tightening in the first year after completion of construction, as then a part of the creep and shrinkage losses will have taken place.

There were large uncertainties in determining the prestress loss. Especially moisture related deformations were hard to predict. It remains uncertain how the MC of the CLT will develop from construction phase to end-of-use. In addition, there is not yet any consensus on the shrinkage coefficient of CLT. A combination of these uncertainties makes it hard to do a reliable estimation of the force loss. It is advisable to measure the MC of the CLT panels on site, during construction. Preferably these measurements are made for different depths in the CLT panel.

10.3 Reflection

10.3.1 Objectives

The objectives of the thesis were outlined in **Error! Reference source not found.**. For each objective it is discussed if the research was successful in reaching it.

1. **Understanding the lateral displacements of un-post-tensioned cores**
   The thesis was successful in *qualitatively* determine four displacement modes that describe the lateral displacement behaviour of a CLT core based on literature research on CLT shear walls. These modes were: bending, shear, sliding and rocking.
   Regarding the bending displacements, the thesis showed that there are two factors that complicate the bending behaviour, namely shear-lag and the semi-rigid connection between flange and web.
   The thesis concluded that due to the many connections in the core, it is advised to perform an FEM analysis to *quantitatively* describe the lateral displacements. This has been successfully done for the case study, for a 3, 4, 5 and 6 story building. By isolating the four different displacement modes, an idea could be given of their relative influence.

2. **Understanding the lateral displacements of post-tensioned cores**
   Qualitatively, from the analysis discussed in objective (1), it was suggested that the post-tensioning could eliminate displacement modes related to the connections (sliding and rocking), if the structure is post-tensioned up to a level where uplift does not occur under wind load. In the case study, the lateral displacements of an 8-storey core were assessed quantitatively. The thesis also successfully showed that the first amount of prestress is most effective in reducing lateral displacements. With a study it was also successfully shown that from the point of no uplift, a further increase of the prestress level does not further reduce the lateral displacements.

3. **Quantifying the effectiveness of post-tensioning of the core**
   The effectiveness of the post-tensioning has been successfully expressed in terms of height gain. The effectiveness is always specific to a design situation. Therefore, this has been done in the case-study through assuming a certain floorplan and minimal core size. The achievable height of this building with an un-post-tensioned core was compared to the achievable height when applying post-tensioning to the core. Admitting, this was only done for a single design situation. With other floorplan, core size different results may be found. Especially, the normal force in the core is of large influence.

4. **Provide an estimation of the effective width of a CLT core**
   From literature study, in the study, two influences on the effective width were identified, being shear lag and the semi-rigid connection between flange and web. With the case-study, the effective width was studied on a U-shaped core. With the case-study it has been shown that clearly the contribution of the flange to the bending stiffness is limited.

   It was successfully shown that the effective width for both shear lag and the semi-rigid connection between flange and web were largely influenced by the height of the core.
   It was attempted to find an expression for the effective width for shear lag. In the Eurocode provides estimations of the effective flange width of timber beams. The Eurocode states that for timber beams, the effective width for shear lag is linearly dependent on the span of the beam. With the case-study core, it has been attempted to find this relationship. Unfortunately, from the finite element results, no expression for the effective width has been found.
   For the influence of the semi-rigid connection on the effective width, the theory of mechanically connected beams was suggested. It was explored if the gamma equation can be used to predict the influence of the connections. The FEM results did not agree with the gamma equation for all building heights.

   The effective width of the core was studied for a single core geometry. To provide a general answer to the effective width of a CLT core, further study with different core geometry is needed. Unfortunately, no conclusive expressions for the effective width have been found.

5. **Identify the most important prestress losses**
   In the thesis, two categories of prestress loss have been identified: immediate losses and long-term losses. With a literature study it has been found the most important prestress losses are the long-term losses. These were creep, shrinkage and relaxation.

6. **Providing a method of quantification of these losses**

In the thesis, a force loss model by Nguyen that includes creep only, has been adjusted to include shrinkage and relaxation. Creep is included through Eurocode approach, by including a creep factor. No creep curve for CLT is researched.

A python model has been developed that can calculate the prestress force loss based on an "equivalent stressed member". For a certain initial prestress loss, geometrical input, material input and force loss input, the model can calculate long-term force loss. This python model returns a single force loss value for a moment when all creep, shrinkage and relaxation has occurred.

7. **Providing a way of including the prestress losses in the design process of an un-post-tensioned core**

   A design scheme has been introduced for the design of a post-tensioned CLT core. This design scheme shows how the prestress losses should be included in design. Two important guidelines are: For checking the displacements (SLS), the prestress level after the losses have taken place should be assumed. For checking stresses (ULS), the prestress level just after tightening should be assumed (no losses). The design scheme can be a helpful tool for the designer to understand the design steps needed.

10.3.2 Research Contributions

Though more and more cross-laminated timber buildings are being built around the world, there are still unknowns in the design of CLT structures. Besides, as far as the author knowns, no prestressed cross-laminated timber cores have been built. There was a clear opportunity for the study to add to the body of knowledge. The research contributions include the following.

- No studies on post-tensioned CLT cores are known to the author. However, there are studies and experiments on post-tensioned CLT shear walls. Most of these studies focus on seismic design and therefore on energy dissipation. The current thesis can provide insight into serviceability limit state governed design.
- The different displacement modes of CLT shear walls have been studied before. The current study is the first known to the author that shows the contribution of the different displacement modes to the total lateral displacement. It is also the first study that shows the decrease of lateral displacement due to post-tensioning. This is valuable information for the designer.
- Since no previous studies on the effective width of a CLT core have been found by the author, also no information on the effective flange width of a CLT core was available in literature. This thesis provides information on the cooperation of different CLT shear walls when they are combined to form a core.
- Estimation of the prestress force loss is important when designing prestressed structures. It is even more important for timber structures because timber experiences large shrinkage

and creep deformations. The thesis is the first known to the author to provide insight in how the estimation of the prestress losses relate to the design process of a CLT core.

- Nguyen has provided a valuable model for calculation of prestress loss based on an "equivalent stressed member". His work included creep elaborately but did not include relaxation and shrinkage prestress losses. The current work has included shrinkage and relaxation in the analytical model. Furthermore, the work provides the reader with a python model that can be used for calculation of the losses.

10.4 Suggestions for further study

In the timeframe of the thesis, some topics had to be approached in a simplified manner or be left out of the analysis. These topics would be interesting for further research, as for most of the topics (almost) no literature is available.

- **Shrinkage coefficient of CLT panels.**
  In the study, shrinkage proved to be an important cause of prestress loss during the lifetime of the building. Large range of shrinkage coefficients for CLT can be found in literature. A choice between these available shrinkage coefficients has been made in the case-study in the thesis. The shrinkage coefficient is likely to depend a lot on the internal geometry of the CLT, as wood shrinks differently along different directions. More research into the shrinkage coefficient of CLT based on the internal geometry would be beneficial for better estimating shrinkage behaviour of the CLT plates. With that, better estimations of prestress force loss can be made.
- **Creep curve of CLT panels under compressive loading.**
  In the thesis, creep of CLT has been included with a creep factor (k_{def}). Creep of CLT is a complicated subject and calculating creep with a single creep factor is an oversimplification of the actual creep behaviour. If a creep model could be found that more accurately describes the creep behaviour, prestress creep losses could be better estimated. Also, when the creep behaviour versus time is known, a better strategy for re-tightening may be formulated.
- **Estimation of moisture content change of CLT panels in construction phase.**
  Shrinkage has a large influence on the prestress force loss. The largest change in moisture content is expected to be reached during construction phase. This depends on weather conditions and precautions on site. In the thesis, an informed estimation has been included in the case-study by referencing moisture content measurements in the Limnologen project. It is likely an overestimation of the moisture content. A topic for further study would be the moisture content change in CLT panels in construction phase.
- **Anchorage design on CLT panels.**

Information on the anchorage design of prestressed timber structure is not available in literature. The introduction of the prestressing forces in post-tensioned structures with no bond depends fully on the anchors. Local stresses should not exceed the resistance of the CLT. Furthermore, spreading of the prestressing force should be studied. With the spreading of the force, “splitting forces” may arise. These are tensile stresses perpendicular to the direction of prestressing, close to the anchor. These stresses should be resisted by the CLT. There might also be prestress losses related to the type of anchorage.

- **Design for a stiff connection between two perpendicular CLT walls**.
  The cooperation between flange and web of a CLT core is influenced by the connection between flange and web. The stiffer the connection is, the higher the bending stiffness of the core. In the thesis, the connection assumed was pairs of angled STS connectors. Further study is recommended for a stiffer connection.
- **Diaphragm action in CLT floors and the transfer of wind load to the cores.**
  In the thesis, the floors are assumed perfectly rigid. They are not included in the analysis. It is expected that the wind force transfer from floor to core is dependent on the stiffness of the floors. Therefore, a study into the transfer of wind-load from floor to core would be beneficial.
- **Fire safety design of a CLT core.**
  CLT is sensitive to fire. In the Eurocode, only guidelines with respect to solid wood are available. The behaviour of CLT plates under fire load is a subject of study. Fire design for the CLT core is extra important as the core may be a critical space for fleeing the building in the event of fire. Multiple precautions are available, like protective sheeting or impregnating. The fire behaviour of CLT and an appropriate fire design for the CLT core is recommended for further study.

11 References

[1] M. Yehehis, K. Hewage, C. Alam, C. Eskicioglu and R. Sadiq, “An overvieuw of construction and demolition waste management in Canada: a lifecycle analysis approach to sustainability.,” *Clean Technol. Environ. Policy,* pp. 81-91, 2012.

[2] “Klimaatakkoord,” 2019. [Online]. Available: https://www.klimaatakkoord.nl/klimaatakkoord/documenten/publicaties/2019/06/28/klimaatakkoord.

[3] CE Delft, “Meten is Weten in de Nederlandse Bouw, Milieu-impacts van Nederlandse bouw- en sloopactiviteiten in 2010,” 2015.

[4] M. Zubizaretta, J. Cuadrado, A. Orbe and H. Garcia, “Modeling the environmental sustainability of timber structures: A case study,” *Environmental Impact Assessment Review,* 2019.

[5] A. T. Balasbaneh and A. K. B. Marsono, “Strategies for reducing greenhouse gas emissions from residentialsector by proposing new building structures in hot and humid climaticconditions,” *Building and Environment,* 2017.

[6] H. Darby, A. Elmaulim and F. Kelly, “A case study to investigate the life cycle carbon emissions and carbon storage capacity of a cross laminated timber, multi-story residential building.,” 2013.

[7] The European Cooperation of Science and Technology, “Action FP1402,” [Online]. Available: https://www.cost.eu/actions/FP1402/#tabs|Name:overview.

[8] T. Hodsdon, “Structural Design of CLT Stability Systems,” Arup, 2019.

[9] I. Lukacs, C. Pradel, A. Björnfot and R. Tomasi, “State-of-the-art: Timber floor diaphragms”.

[10] United Nations, Economic commission for Europe, committee on forests and forest industry, “Draft Forest Production Market Statement,” Geneva, 2019.

[11] OIB Aurstrian institute of Construction Engineering, “European Technical Assessment ETA-14/0349,” 2020.

[12] O. Espinoza, V. R. Trujillo, M. F. L. Mallo and U. Buehlmann, “Cross-Laminated Timber: Status and Research Needs in Europe,” 2015.

[13] DERIX, “X-Lam - Cross-laminated timber: large-format construction components for roofs, ceilings and walls”.

[14] ProHolz, “Cross-Laminated TImber Structural Design: Basic engineering principles according to Eurocode,” 2014.

[15] "Mass_timber -CLT," 2020. [Online]. Available: https://processing-wood.com/processes/mass_timber/#CLT.

[16] Ledinek, "Ledinek X press cross laminated timber press Brettsperrholzpresse," 2020.

[17] Construction.com, [Online]. Available: https://www.construction.com/CE/articles/2010/Apr_ARedit_slideshow/slide.asp?slide=14. [Accessed 30 08 2020].

[18] T. E. C. o. S. a. Technology, "action FP1402 - COST," [Online]. Available: https://www.cost.eu/actions/FP1402/#tabs|Name:overview.

[19] "NEN-EN 338:2016," 2016.

[20] M. Pereira and C. Calil, "Strength and Stiffness of Cross Laminated Timber (CLT) panels produced with Pinus and Eucalyptus: experimental and analytical comparisons," Rio de Janiero, 2019.

[21] I. P. Christovasilis, M. Brunetti, F. Maurizio, M. Nocetti and D. Vassallo, "Evaluation of the Mechanical Properties of," *Construction and Building Materials,* 2016.

[22] CLT Designer, [Online]. Available: https://www.cltdesigner.at/.

[23] T. Bogensberger, T. Moosbrugger and G. Silly, "Verification of CLT-plates under loads in plane," *WCTE 2010,* 2010.

[24] G. SchickHofer, "CLT - European Expean Experience - Properties & Design - Research & Testing," Tokyo, 2013.

[25] "NEN-EN 1995-1-1+C1+A1," 2011.

[26] EN, "EN1995-1-1 (2004): Eurocode 5: Design of Timber structures - Part 1-1: General rules and rules for buildings," Brussels, 2004.

[27] O. Perret, C. Douthe, A. Lebee and K. Sab, "A shear strength vristerion for the buckling analysis of CLT walls," 2020.

[28] I. K. Abeysekera, A. J. Smith and A. C. Lawrence, "Safe design of indeterminate systems in a brittle material.," Arup, 2018.

[29] COST, "Properties, Testing and Design of Cross Laminated Timber: A state-of-the-art report by COST Action FP1402 / WG2," 2018.

[30] M. Shahnewaz, "Performance of cross-laminated timber shear walls for platform construction under lateral loading.," Vancouver, 2018.

[31] V. Awad, L. Giresini, M. Koshihara, M. L. Puppio and M. Sassu, "Experimental Analysis and Numerical Models of CLT Shear Walls under Cyclic Loading," 2017.

[32] A. Hossain, M. Popovski and T. Tannert, "Group Effect for Shear Connecitons with Self-tapping-tapping Screws in CLT," 2019.

[33] G. Flatscher, K. Bratulic and G. Schickhofer, "Screwed joints in cross-laminated timber structures," Quebec: World conference of timber engineering, 2014.

[34] Rothoblaas , “WHT Angle bracket for tensile load”.

[35] M. Piazza and T. Sartori, “Seismic-Rev: Experimental campaign on rothoblaas products. Mechanical property investigation by monotonic and cyclic loading.,” University of Trento, departement of Environmental and Mechanical Engineering.

[36] Rothoblaas, “TITAN N Angle bracket for shear loads in solid walls”.

[37] J. Leonard, “Investigation of Shear Lag Effect in High-rise Buildings with Diagrid.,” Master’s thesis of Engineering, 2007.

[38] “Lecture 14.10: Simple Braced Non-Sway Multi-Storey Buildings,” [Online]. Available: http://fgg-web.fgg.uni-lj.si/~/pmoze/ESDEP/master/wg14/l1000.htm. [Accessed 31 08 2020].

[39] S. Ray, “Reinforced concrete: Analysis and Design,” Blackwell Science, 1995.

[40] British Standard Institution, “BS5400: Steel, concrete and composite bridges, Part 5, Code of practice for the design of composite bridges,” British Standard Institution, 1979.

[41] R. D. Hoult, “Shear Lag Effects in Reinforced Concrete C-shaped walls,” Melbourne, 2019.

[42] T. Holden, C. Devereux, S. Haydon, A. Buchanan and S. Pampanin, “NMIT Arts & Media Building - Innovative structural design of a three storey post-tensioned timber building,” 2016.

[43] A. Rosenkilde, K. Jarnerö and M. Axelson, “Flervåningshus med trästomme – Uppföljning av Kv Limnologen och Kv Rya, Rydebäck [Multi-storey house with wooden frame - Follow-up of Kv Limnologen and Kv Rya, Rydebäck],” 2008.

[44] Å. Frantz, “Limnologen – Inblick i svenskt träbyggande [Limnologen - An insight into Swedish timber construction],” Växjö Universitet, 2008.

[45] T. Akbas, R. Sause, J. M. Ricles and R. Ganey, “Analytical and Experimental lateral-load response of Self-Centering Post-tensioned CLT walls,” 2017.

[46] Z. Xia and J. W. van de Kuilen, “Lateral behavior of post-tensioned cross laminated timber walls using finite element analysis,” WCTE , 2014.

[47] T. T. Nguyen, “Modeling of Creep Behavior of Real-Time Hybrid Simulation of a CLT-LIFS Building,” The University of Alabama, Sucaloosa, Alabama, 2017.

[48] J. Walraven and C. Braam, “Lecture notes Prestressed Concrete,” TU Delft, 2019.

[49] Dywidag-systems international, “GEWI Threadbar Systems”.

[50] “EN 1992-1-1 Eurocode 2: Design of concrete structures - Part 1-1: General rules and rules for buildings,” 2011.

[51] K. Jarnerö, “Tekniska data för byggprojekt - Kv Limnologen i Växjö,” SP Trätek, 2008.

[52] H. J. Blas and C. Sandhaas, Timber Engineering: Principles for design, Karlsruhe: KIT Scientific Publishing, 2017.

[53] Swedish Wood , "The CLT handbook," 2019.

[54] E. Serrano, "Overview and Summaries of Sub Projects Results," Växjö University, Växjö, 2009.

[55] dataholz.eu, "dataholz.eu," 05 07 2020. [Online]. Available: https://www.dataholz.eu/en/components/intermediate-floor/version/kz/tdmnxs01/nr/1/con/nuDataholz/act/bauteilVarianteDatenblatt/la/en/doc.pdf.

[56] DIANA FEA bv., "User's Manual -- Release 10.4," 2020.

[57] E. Serrano, "Limnologen – Experiences from an 8- storey timber building," 2009.

[58] "tendon loss (tendon group)," [Online]. Available: http://manual.midasuser.com/en_tw/civil/830/Start/07_Results/12_Result_Tables/09_Tendon/Tendon_Loss_(Tendon_Group).htm.

[59] J. Walraven and C. Braam, Prestressed Concrete, TU Delft, 2019.

[60] H. Blaß and C. Sandhaas, Timber Engineering - Principles for Design, KIT Scientific Publishing, 2017.

[61] A. Polastri, C. Loss, L. Pozza and I. Smith, "CLT buildings laterally braced with core and perimeter walls," in *WCTE world conference on Timber Engineering*, Vienna, Austria, 2016.

[63] Weinig, "cross-laminated-timber-CLT," 2020. [Online]. Available: https://www.weinig.com/en/system-solutions/examples-of-applications-uses/cross-laminated-timber-clt.html.

[64] The European Cooperation for Science and Technology, "Costfp1402," [Online]. Available: https://webarchiv.typo3.tum.de/TUM/costfp1402/home/index.html.

[65] F. Colling, "Creep Behavior of cross laminated timber in service class 2," Institut für Holzbau (IfH) - HS-Augsburg.

[66] F. Sarti, A. Palermo and S. Pampanin, "Simplified Design Procedures for Post-Tensioned Seismic Resistant Timber Walls," 15 WCEE, Lisboa, 2012.

[67] C. Dolan and H. H.R., "Design recommendations for concrete structures prestressed with FRP tendons," 2001.

[68] RDW, "Overzicht maten en gewichten in Nederland," 2012.

[69] L. Franzoni, A. Lebée, F. Lyon and G. Foret, "Advanced modeling of Cross Laminated Timber (CLT) Panels in Bending," 2015.

[70] *NEN-EN 1991-1-1,* 2019.

[71] holz.bau forschungs gmbh, [Online]. Available: cltdesigner.at.

Appendix A. In-plane shear stiffness of CLT plates

The primary factors influencing the in-plane shear stiffness of the CLT are the following:

- The factor $\frac{a}{t}$. a denotes the width of an individual board in the CLT and t denotes the thickness of the board. This parameter characterizes the internal geometry of the CLT.
- The mean shear modulus of the boards $G_{0,mean}$.

The in-plane shear stiffness of the CLT plate for in plane shear loading is different for the two situations: (1) Narrow faces of the boards are glued (2) Narrow faces of the boards are not glued.

For situation (1), the in-plane shear stiffness of the CLT panel is equal to the corresponding shear stiffness of the timber boards. In the case of unglued interfaces (situation (2)), two mechanisms contribute to the shear stiffness. Because cracks occur due to changes in the building climate, it is recommended to always regard the narrow faces unglued.

Table 36 Mechanisms for in-plane shear

Mechanism	Explanation
1 "Pure shear" 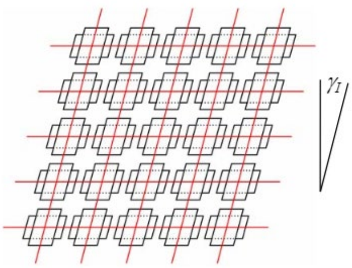 	This is due to the in-plane shear stiffness of the boards.
2 "Torsional" 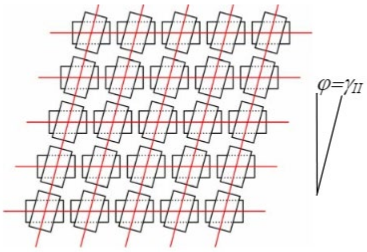 	Mechanism to is a result of the redistribution of stresses to be able to have the shear stresses on the narrow sides equal to zero. This mechanism is the rotation caused by the torsional moment acting on both sides of the glued interface.

The shear deformation due to the two mechanisms can be determined with the equations below. The total shear deformation of the panel is the addition of the two mechanisms. This stiffness is approximately $3/4$ times the shear stiffness of the base material.

$$\gamma_I = \frac{\tau_0}{G_{0,mean}} \tag{73}$$

$$\gamma_{II} = \frac{t}{2} \cdot \frac{\tau_0 \cdot t \cdot a^2}{\frac{G_{0,mean}}{2} \cdot \frac{a^4}{6}} = \frac{6 \cdot \tau_0}{G_{0,mean}} \cdot \left(\frac{t}{a}\right)^2 \tag{74}$$

Where:

γ_I	The shear deformation due to mechanism I
γ_{II}	The shear deformation due to mechanism II
$G_{0,mean}$	The shear deformation due to mechanism I
t	Average board thickness in the cross-section
a	Average board width (150 mm is recommended)

$$\gamma = \gamma_I + \gamma_{II}$$

$$\frac{\gamma_I}{\gamma_I + \gamma_2} = \frac{G^*}{G_{0,mean}} = \frac{1}{1 + 6 \cdot \alpha_{FE-FIT,ortho} \cdot \left(\frac{t}{a}\right)^2} \tag{75}$$

$$\alpha_{FE-FIT,ortho} = 0.32 \cdot \left(\frac{t}{a}\right)^{-0.77}$$

Where:

G^*	The shear modulus of the CLT element
$\alpha_{FE-FIT,ortho}$	The correction factors (From fitting results from several FE models)

$$G^* \approx 0.75 \cdot G_{0,mean} \tag{76}$$

Appendix B. Extended Gamma Method

The extended gamma method can be used for finding the effective bending stiffness of a CLT plate that is loaded out of plane [14]. An advantage of the extended gamma method over the regular gamma method is that it is also valid for CLT with more than three layers, and for CLT with layers of different thickness and elastic modulus.

For CLT with more than 3 layers, the following linear system must be solved to find the gamma values [14]:

$$[V] \cdot \gamma = s \tag{77}$$

$$\begin{bmatrix} v_{1,1} & v_{1,2} & 0 & 0 & 0 \\ v_{2,1} & v_{2,2} & v_{2,3} & 0 & 0 \\ 0 & v_{3,2} & v_{3,3} & v_{3,4} & 0 \\ 0 & 0 & \cdots & \cdots & \cdots \\ 0 & 0 & 0 & v_{m,m-1} & v_{m,m} \end{bmatrix} \cdot \begin{bmatrix} \gamma_1 \\ \gamma_2 \\ \gamma_3 \\ \vdots \\ \gamma_m \end{bmatrix} = \begin{bmatrix} s_1 \\ s_2 \\ s_3 \\ \vdots \\ s_m \end{bmatrix} \tag{78}$$

$$C_{j,k} = \frac{b \cdot G_{R,jk}}{d_{j,k}} \tag{79}$$

$$D_i = \frac{\pi^2 \cdot E_i \cdot b \cdot d_i}{l_{ref}^2} \tag{80}$$

$$v_{i,i-1} = -C_{i-1,i} \cdot a_{i-1} \tag{81}$$

$$v_{i,i} = \left(C_{i-1,i} + C_{i,i+1} + D_i\right) \cdot a_i \tag{82}$$

$$v_{i,i+1} = C_{i,i+1} \cdot a_{i+1} \tag{83}$$

$$\gamma = [\mathrm{V}]^{-1} \cdot s \tag{84}$$

The parameter D depends on the dimensions of the layer (b, d), the shear modulus $(G_{v,R})$ and the effective length $\left(L_{eff}\right)$. This effective length is the distance between the zero moments in the beam. Distance a is the distance etween the gravity center of a layer and the gravity center of the complete cross section.

Appendix C. Stiffness of CLT shear walls

No consensus exists on how to calculate the stiffness, and several methods exist for calculation of the lateral displacements. Two methods by Hummel et al. and Casagrande et al are discussed here. These methods assume some or all the four displacement modes of CLT shear walls as stated below:

- Bending
- In-plane shear
- Rocking
- Sliding

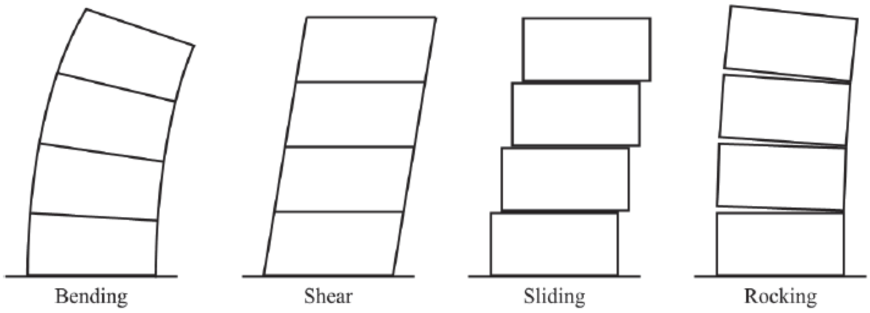

Method 1 – Casagrande et al.

Three deformations are included in the analysis by Casagrande et al. : in-plane shear deformation, rigid-body translation and rigid-body rotation. The effect of the vertical load is also considered. No bending is considered.

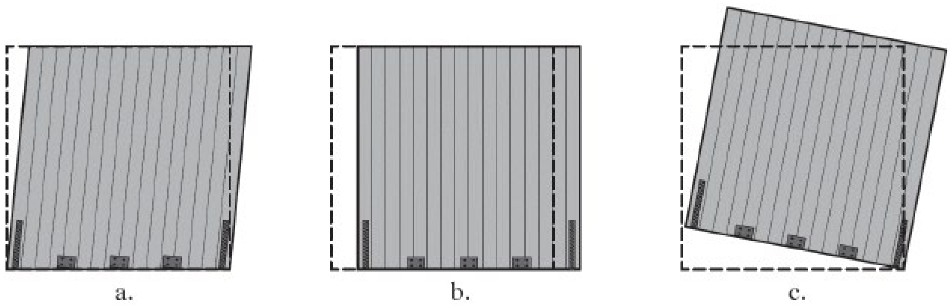

$\Delta = \Delta_h + \Delta_a + \Delta_p$

Contribution from rocking (c.):

$$\Delta_h = \gamma \cdot h = \left(\frac{F \cdot h}{\tau \cdot l} - \frac{q \cdot l}{2}\right) \cdot \frac{h}{k_h \cdot \tau \cdot l}$$

where:

γ is the rigid rotation angle

$\tau \cdot l$ is the inernal lever arm (τ should be assumed 0.9)

q is the distributed load at the top of the wall

k_h is the stiffness of the hold down

Contribution from rigid body translation

$$\Delta_a = \frac{F \cdot i_a}{k_a \cdot l}$$

Where

i_a is the spacing between the angle brackets

k_a is the stiffness of the angle brackets

Contribution from in-plane shear deformation

$$\Delta_p = \zeta \cdot h = \frac{F \cdot h}{G_{CLT} \cdot t_{CLT} \cdot l}$$

Where

t_{CLT} is the thickness of the CLT panel

G_{CLT} is the shear modulus of the panel

Method II – Hummel et al.

This method is a lot like method I but includes all four displacement modes of a CLT shear wall. For the bending. For rocking both elastic foundation and rigid foundation are considered.

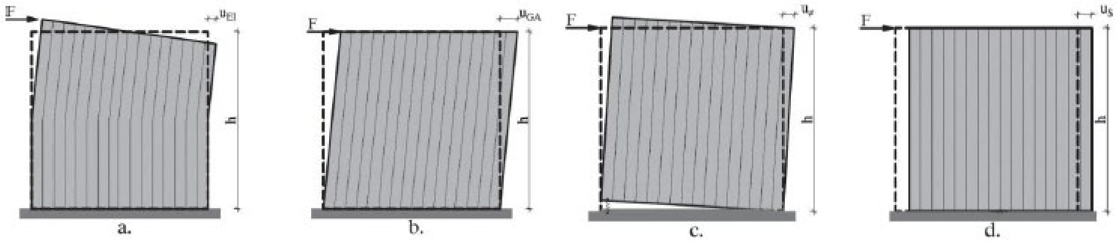

For the bending displacements (a):

$$u_{EI} = \frac{F \cdot h^3}{3 \cdot EI_{ef}}$$

With:

$EI_{ef} = E_0 \cdot \left\{\sum d_i \cdot \frac{l^3}{12}\right\}$ is the effective bending

For the shear displacements (b):

$$u_{GA} = \frac{F \cdot h}{GA_{ef}}$$

With:

$$GA_{ef} = G_{eff} \cdot A = \frac{G}{1 + 6 \cdot \left[0.32 \cdot \left(\frac{t}{a}\right)^{-0.77}\right] \cdot \left(\frac{t}{a}\right)^2} \cdot A$$

For the rocking displacements (c):

$$u_{\phi} = \begin{cases} \frac{h}{e} \cdot \frac{Z}{K_z}, Z = \max\left\{F \cdot \frac{h}{e} - \frac{(p \cdot l)}{2}; 0\right\} - Rigid\ foundation \\ \frac{h^2}{l^* - \frac{l_c}{3}} \cdot \frac{2 \cdot F}{k_D \cdot l_c^2}, k_d = \frac{E_s \cdot b_s}{t_s} - Elastic\ foundation \end{cases}$$

For the sliding displacements (d):

$$u_s = \frac{F}{K_s}$$

Appendix D. Rothoblaas tests on stiffness of hold-downs

Find below the Rothoblaas test results from their Seismic-Rev report that are used in the thesis for the stiffness of the hold-downs. The test result for the stiffest hold-down (WHT620, full fastening) is used in the thesis.

EVALUTATION OF SLIP MODULUS K_{ser}

- $K_{1,ser}$ experimental average value for WHT joints on GL24h Glulam and on CLT

WHT type	configuration	fastening type	n_v	$K_{1,ser}$ [N/mm]	
		Ø x L [mm]	[pcs]	GL24h	CLT
WHT340	• total fastening • without washer	LBA nails Ø4,0 x 60	20	-	**3440**
	• total fastening • with washer	LBA nails Ø4,0 x 60	20	**5705**	**7160**
	• partial fastening • with washer	LBA nails Ø4,0 x 60	12	-	**5260**
WHT440	• total fastening • with washer	LBA nails Ø4,0 x 60	30	**6609**	**10190**
	• partial fastening • with washer	LBA nails Ø4,0 x 60	20	-	**8060**
WHT540	• total fastening • with washer	LBA nails Ø4,0 x 60	45	-	**11470**
	• partial fastening • with washer	LBA nails Ø4,0 x 60	29	-	**9700**
WHT620	• total fastening • with washer	LBA nails Ø4,0 x 60	52/55	**13247**	**13540**
	• partial fastening • with washer	LBA nails Ø4,0 x 60	30/35	**9967**	**10310**

Figure 99 Test results by Rothoblaas for stiffness of WHT hold-downs

Appendix E. Hold-down resistance

The assumed hold-down is:

- WHT620 with WHT70L washer
- M24 anchor
- Screws, $\emptyset 5.0\ x\ 50\ mm$
- Fully Fastened

The design resistance for this hold-down is $68.2\ kN$ based on the resistance in the steel section.

$$R_d = \min \begin{cases} \dfrac{R_{k,timber} \cdot k_{mod}}{\gamma_m} \\ \dfrac{R_k}{\gamma_{steel}} \\ R_{d,concrete} \end{cases} = 68.2\ kN \tag{85}$$

Resistance of the hold-down in:		[kN]
Timber	$\dfrac{R_{k,timber} \cdot k_{mod}}{\gamma_m} = \dfrac{106.2 \cdot 0.9}{1.25}$	76.5
Steel	$\dfrac{R_k}{\gamma_{M2}} = \dfrac{85.2}{1.25}$	68.2
Concrete	$R_{d,concrete}$	73.5

configuration	$R_{1,K}$ TIMBER: holes fastening Ø5 type	Ø x L [mm]	n_v [pcs]	$R_{1,k\ timber}$ [kN]	$R_{1,K}$ STEEL: $R_{1,k\ steel}$ [kN]	γ_{steel}	$R_{1,d}$ CONCRETE: $R_{1,d\ uncracked}$ VIN-FIX PRO Ø x L [mm]	[kN]	$R_{1,d\ cracked}$ EPO-FIX PLUS Ø x L [mm]	[kN]
• total fastening • washer WHTW70L • M24 anchor	LBA nails	Ø4,0 x 40	55	**86.4**	**85,2**	γ_{M2}	M24 x 270	**73,50**	M24 x 270 M24 x 323	**60,6** **75,6**
		Ø4,0 x 60	55	**106,2**						
	LBS screws	Ø5,0 x 40	55	**86,4**						
		Ø5,0 x 50	55	**106,2**						
• partial fastening • washer WHTW70L • M24 anchor	LBA nails	Ø4,0 x 40	35	**55,0**	**85,2**	γ_{M2}	M24 x 270	**73,50**	M24 x 270 M24 x 323	**60,6** **75,6**
		Ø4,0 x 60	35	**67,6**						
	LBS screws	Ø5,0 x 40	35	**55,0**						
		Ø5,0 x 50	35	**67,6**						

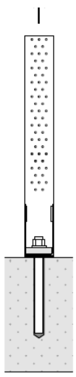

Figure 100 Test results by Rothoblaas for resistance of WHT 620 hold-downs

Appendix F. Effective width by Hoult

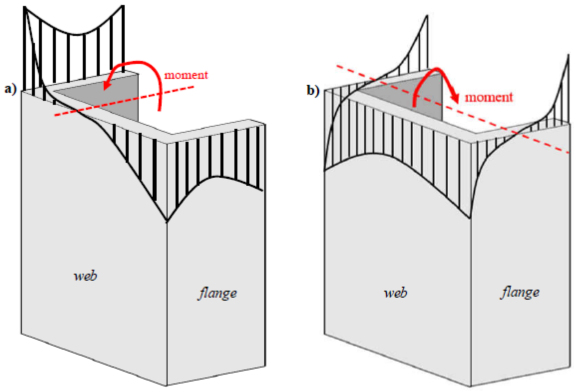

Figure 101 C-shaped core with expected strain distributions for bending about the (a) major axis and (b) minor axis (with web in tension) [41]

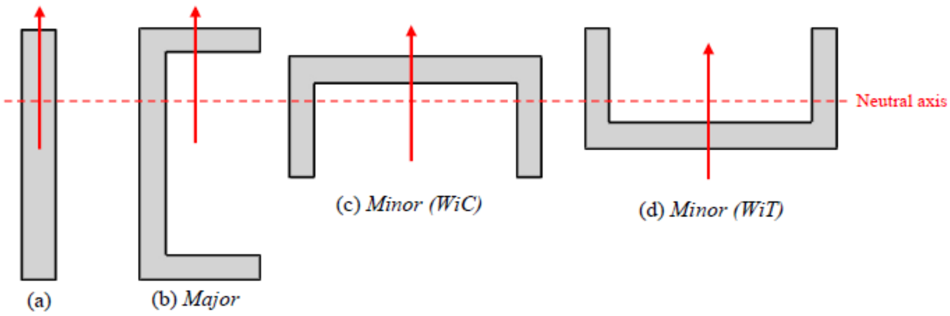

Figure 102 Modes of bending for concrete cores [41]

Mode of Bending	LS	Reinforcement	α	β
Major (FiT)	Yield/ULS	concentrated	0.72	0.0
		distributed	0.81	-1.0
Major (FiC)	Yield	concentrated/distributed	0.64	0.8
	ULS	concentrated/distributed	0.80	-3.6
Minor (WiC)	Yield/ULS	concentrated/distributed	0.87	0.0
Minor (WiT)	Yield	concentrated	0.73	1.0
		distributed	0.84	0.0
	ULS	concentrated/distributed	0.88	0.0

Figure 103 values for α and β according by Hoult [41]

Appendix G. Upper and lower limit of the core stiffness

To illustrate how the corner connection affects the stiffness of the core, two limits can be distinguished. In that case the stiffness of the corner connection for shear force is equal to zero. This limit will provide a lower limit for the stiffness of the core. The second limit is one in which all four sides of the core fully cooperate. The corner connection is in this case considered rigid. This is the upper limit for the stiffness. With a semi-rigid corner connection, the actual stiffness of the core will be somewhere in between upper and lower limit for the stiffness.

For a square core with thickness of the walls much smaller than the width of the core ($t \ll a$) (Figure 104), the ratio between the upper limit stiffness and the lower limit stiffness is approximately 4 (Eq. 86- 90). The same ratio holds for the displacements. When the core walls fully cooperate, the lateral displacements will be four times smaller compared to when they do not cooperate. In this analysis shear lag is not included.

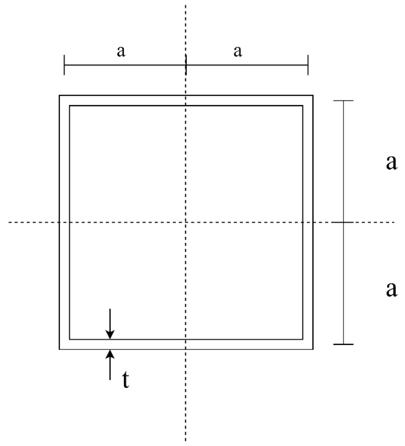

Figure 104 Square core, t<<a

$$I_{core,min} = 2 \cdot \left(\frac{t \cdot (2a)^3}{12} + \frac{2a \cdot t^3}{12} \right) \tag{86}$$

$$I_{core,max} = 2 \cdot \left(\frac{t \cdot (2a)^3}{12} + \frac{2a \cdot t^3}{12} + 2a \cdot t \cdot a^2 \right) \tag{87}$$

$$t \ll a, \text{therefore } t^3 \ll a^3$$

$$I_{core,min} \approx \frac{4}{3} t a^3 \tag{88}$$

$$I_{core,max} \approx \frac{4ta^3}{3} + 4ta^3 \tag{89}$$

$$\frac{I_{core,\max}}{I_{core,min}} \approx 4 \tag{90}$$

Appendix H. Reference project: Limnologen

The limnologen project shows that building multiple story buildings with post-tensioned CLT is feasible. The project serves as an inspiration and reference for the current thesis.

The limnologen project is a set of four buildings in Växjö, Sweden. The project is part of a local strategy “Mer trä i byggandet” [More timber in construction] [51]. The buildings all consist of eight floors. Seven floors with a CLT structure sit on top of a floor with a concrete structure. [51]

Multiple research projects have been done for post-tensioning structures. Even full-scale testing has been performed in the past. However, these projects often focus on ULS design under earthquake load. The focus is often on damping, energy dissipation and self-cantering for mitigating damage after an earthquake event. In the Limnologen building however, the post-tensioning system has been used for limiting uplift, thus for serviceability load conditions. Because the Limnologen project was topic of multiple research projects, measurement data on for example the long-term deformation, long-term prestress force and relative humidity are available.

Figure 105 South Façade Limnologen

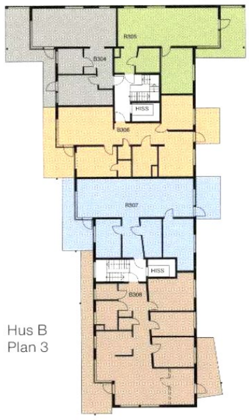

Figure 106 Typical floorplan Limnologen

Stability system of the Limnologen building

The floor and walls of the ground floor are executed in concrete. For the other floors, the stability is provided by CLT shear walls and timber framed walls. Both interior and Exterior walls are used for stabilizing. This includes 18 interior walls with total length of 63,8 meters, and 10 outer walls with a total of 49.6 m [51].The floors act as rigid diaphragms. [51] 48 post-tensioning rods are imbedded in the walls for taking up the uplift forces. [51] In this way the hold-down connections at the walls can be avoided. The rods are anchored in the concrete floor slab on the ground floor and extend to the top of the building. [44].

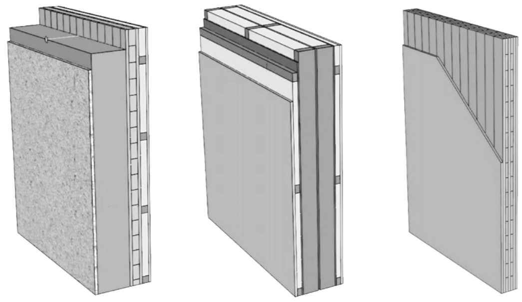

Figure 107 Left = exterior wall, middle = apartment separating timber framed wall, right = partition wall within an apartment (Serrano, Limnologen – Experiences from an 8- story timber building , 2009).

The building plan is far from regular, which is not ideal for design of this stability system. Most of the exterior walls, and also some interior walls are part of the stability system [44] In the floorplan of floor level 3 is shown, with black dots at the location of the tension rods. The tension rods must be re-tightened after some time due to relaxation in the steel, creep deformations in the wood and due to shrinking. [57]. Also, settlements may influence the force of the steel, and the force in the cable must be checked during use stage to verify that the system is still working.

Figure 108 Walls contributing to the stability [51]

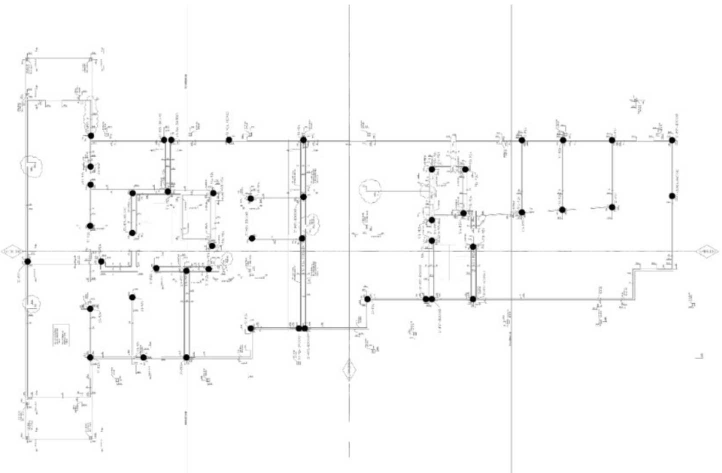

Figure 109 Floor plan level 3, post-tension rods marked with black dots

Design of the post-tensioning system

The post-tensioning is executed with bars, that extend from the foundation of the building all the way to the roof. At the foundation level, bars are cast in the concrete floor to serve as anchors for the post-tension rods. The bars are coupled at intermediate points using a simple coupler and isolated in the walls with foam. At the top floor, the post-tension rods are anchored by simple steel bars. For some images of the construction (reference), see Figure 16 - Figure 17.

Figure 110 Concrete bottom floor for enhancing the stability

Figure 111 Tie-rods cast in the concrete floor at ground-level

Figure 112 Isolating the post-tension rods in the timber framed walls

Figure 113 coupling two tie-rods at intermediate height

Figure 114 Anchorage of the PT bars at highest point

Stress and displacement measurements

Because the Limnologen project was part of a research project, both the stress and deformation of the building were measured.

The post-tension rods are M24 rods. When the walls were installed, the rods were post-tensioned with a hydraulic jack or torque wrench up to half the maximum tensile stress of the bars. [51]. Applying post-tension with a jack is more reliable than using a torque wrench, and to have accurate results, not only the force but also the elongation of the bars needs to be specified. [43]. Without reducing the lift force or considering misalignment, the maximum compressive force is 369 kN in a 7.1 m long outer wall. The maximum lift force was 133 kN in a 3.7 m long inner wall. Considering a change of the lift force and misalignment changed these values to 335 kN and 165 kN respectively [51].

The development of the deformations over time were measured in the Limnologen Project. After one year the rate of deformation diminished considerably. [54] In addition to the deformation, also the relative humidity (HD) and temperature were measured.

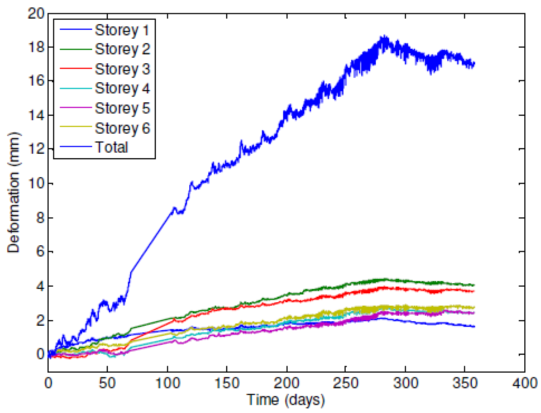

Figure 115 Vertical deformation vs time in the limnologen project [54]

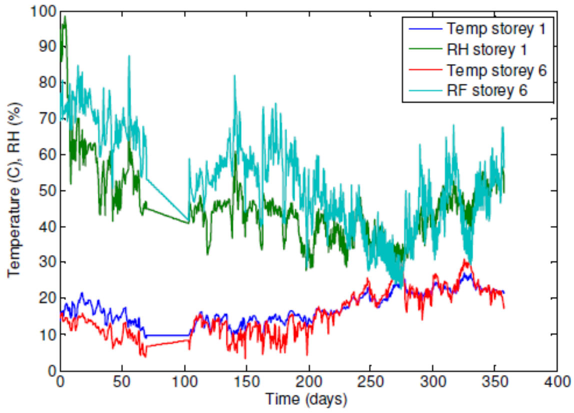

Figure 116 Temperature and RH vs time in the Limnologen project [54]

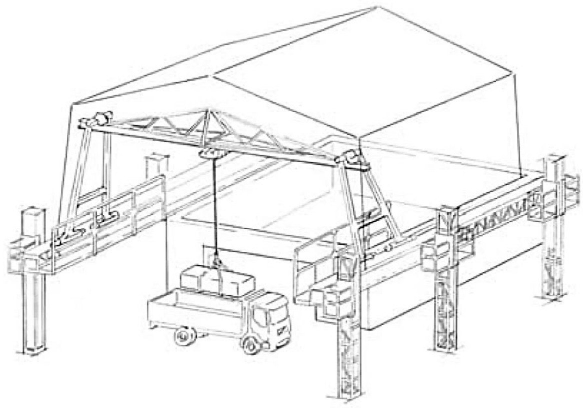

Figure 117 Tent used in construction of Limnologen

Appendix I. Derivation of the effective cable length

Displacement of the CLT panel is caused by the post-tension force and permanent loads and variable loads on the wall. Let's denote the post-tension force (at t=0) as P_0 and all other vertical loads combined N. The shortening of the CLT plate under the post-tension force and normal force is denoted Δw. From Equations 91-99 the effective cable length can be found. Equations below are from Nguyen's dissertation paper [47].

$$\Delta_w = \frac{P + N}{K_w} \tag{91}$$

$$L_{c0} = L_{ci} - \Delta_c \tag{92}$$

$$L_{c0} = L_{ci} - \frac{P_{0,cable} \cdot L_{c0}}{E_c \cdot A_c} \tag{93}$$

$$L_{c0} = L_{w0} - \Delta_w - \frac{P_{0,cable} \cdot L_{c0}}{E_c \cdot A_c} \tag{94}$$

$$L_{c0}(E_c \cdot A_c) = (L_{w0} - \Delta_w) \cdot (E_c \cdot A_c) - P_{0,cable} \cdot L_{c0} \tag{95}$$

$$L_{c0}(E_c \cdot A_c) + P_{0,cable} \cdot L_{c0} = (L_{w0} - \Delta_w) \cdot (E_c \cdot A_c) \tag{96}$$

$$L_{c0} = \frac{(L_{w0} - \Delta_w) \cdot (E_c \cdot A_c)}{(E_c A_c + P_0)} \tag{97}$$

$$L_{c0} = \frac{L_{w0} - \Delta_w}{1 + \frac{P_0}{E_c A_c}} \tag{98}$$

$$L_{c0} = \frac{L_{ci}}{1 + \epsilon_{c0}} \tag{99}$$

Appendix J. Immediate prestress losses

Friction loss

Frictional forces may exist between the prestressing rod and the surrounding material. This friction may be studied using Coulomb Friction. The Coulomb friction coefficient is the ratio between the force along the axis of the tendon and the force normal to the axis of the tendon. The force in the tendon, at any location along the tendon, may be expressed as in Eq. .

The equation shows that the prestress force decreases along the element due to friction and wobble. Assumptions have been made regarding friction loss in the scope of the thesis. The prestressing in the thesis has is assumed to be designed with bars. These have no curvature ($\kappa = 0$), therefore no force loss due to curvature is included.

Wobble is the unintended angular rotation of the prestressing rod due to a duct that are inevitably not straight, and cause deformations in the prestressing rod/bar. Since the thesis concerns post-tensioning of CLT, ducts are not strictly needed. In the Limnologen project, no ducts have been applied (6.8.2). If there is a large enough tolerance for the prestress bar it could be avoided that the bar comes in contact with the CLT. Wobble should then not be included.

$$P = P_0 \cdot e^{-\mu(\kappa+\phi_1)\Delta r} \tag{100}$$

[48]

Where:

P	Force in the tendon at a given point
P_0	Force at the reference point
μ	The Coulomb Friction coefficient
κ	Curvature at a given point in the tendon
ϕ_1	The Wobble parameter (extra curvature to account for local irregularities)
Δr	The distance from the reference point

Anchorage loss

Depending on the type of anchor used, there might be slip in the anchor after releasing the jack. This can reduce the post-tension force. This effect is called wedge set or anchorage loss. The manufacturer of the anchorage device should provide the amount of slippage that can be expected, if any.

Losses due to subsequent tensioning of bars in one element

When a CLT panel is post-tensioned with multiple tendons, the post-tensioning of a tendon influences the stress level of previously tensioned tendons. In Figure 118, this is shown for a panel with two tendons. When the first tendon is tensioned, the CLT bar deforms elastically, and when the right prestress level in the tendon is reached, the tendon is anchored. Next, the right tendon is tensioned. Under the prestress in this tendon, the CLT panel again shortens elastically. The left tendon follows the deformation and therefore this tendon shortens, which equates a decrease of prestress force. Derivations for the stress loss due to subsequent tensioning of multiple tendons can be found in

A solution for this is to not try to bring all tendons to their final prestress subsequently, but to first apply some tension to all tendons. After, the different prestress rods can be tensioned alternatingly until all tendons have reached the required prestress level. In the case study in this thesis, it is assumed that stress loss due to subsequent post-tensioning is avoided.

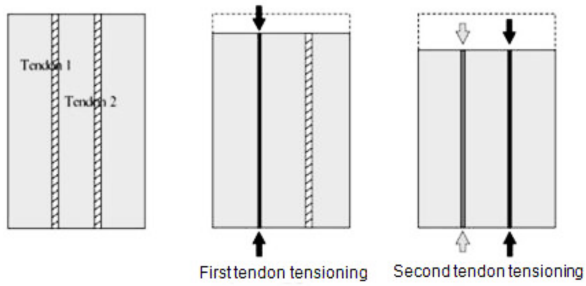

Figure 118 Subsequent tensioning of bars in the same element from [58]

Appendix K. Subsequent post-tensioning of multiple bars

All following equations for the estimation of the stress loss due to subsequent post-tensioning are extracted from the Lecture notes on prestressed concrete [59].

When post-tensioning the first bar, the shortening of the CLT is:

$$\Delta l_{CLT} = \frac{-P_m \cdot l_{clt}}{E_c A_c}$$

The shortening of the first prestressing tendon caused by the prestressing of the following (n-1) tendons is:

$$\Delta l_{pel} = -\frac{(n-1) P_m l_{CLT}}{E_{CLT} A_{CLT}}$$

The loss of prestressing force in the first tendon is:

$$\Delta P_{el} = (n-1) P_m \frac{E_p A_p}{E_{CLT} A_{CLT}}$$

Calculating the sum of all tendons:

$$\sum \Delta \mathrm{P_{el}} = \frac{n(n-1)}{2} P_m \frac{E_p A_p}{E_c A_c}$$

The average loss per tendon:

$$\Delta_{P_{el}} = \frac{(n-1)}{2} P_m \frac{E_p A_p}{E_c A_c}$$

Appendix L. Prestress loss due to relaxation of the prestressing steel

When the prestress tendon or bar is stretched and maintained at a constant strain, the prestress force in the element does not stay constant in time. The steel stress will decrease. This decrease of stress with time at a constant strain is called relaxation.

The relaxation of the prestressing steel depends on the initial steel stress (factor μ), the temperature (t_{eq}) and the relaxation level of the steel. Equation 101 for prediction of relaxation losses is from on prestressed concrete structures. According to EN1992-1-1, steel bars are in class 3 and have a stress loss after 1000h of about 4.0%. The final stress loss due to relaxation is calculated using t=500 000 h. [48]

For reference, for steel Y1030H, the final stress loss due to post tensioning is expected to be maximum 11%. When shrinkage and creep are included in the analysis, a reduction may be applied to the relaxation loss. The reduction factor may be assumed to be 0.8 in line with EN1992-1-1-2004. This reduction is appropriate because shrinkage and creep reduce the steel stress, which in turn reduce the relaxation losses in the steel [48].

$$\frac{\Delta\sigma_{pr}}{\sigma_{pi}} = 1.98 \cdot \rho_{1000} \cdot e^{8.0\mu} \cdot \left(\frac{t}{1000}\right)^{0.75(1-\mu)} \cdot 10^{-5}$$
$$\mu = \frac{\sigma_{pi}}{f_{pk}}, \qquad \sigma_{pi} = |\sigma_{pm0}| \tag{101}$$

$$\mu = \frac{773}{1030} = 0.75 \tag{102}$$

$$\frac{\Delta\sigma_{pr}}{\sigma_{pi}} = 1.98 \cdot 4 \cdot e^{8.0 \cdot 0.75} \cdot \left(\frac{500000}{1000}\right)^{0.75(1-0.75)} \cdot 10^{-5} \approx 11\% \tag{103}$$

Appendix M. Python code for prestress loss

```python
# -*- coding: utf-8 -*-
"""
Created on Fri May 15 16:43:58 2020

@author: Tigist.Znabei
"""
import scipy.optimize
import numpy as np
import pandas as pd
# input arguments

def prestress_after_losses(P_0, A_c= 804, E_c=205000, A_w=240.*700, L_w0=27000, E_w0=7333, F_N=92000, k_def=0.8, del_MC=4, phi_s=0.020, fpk=1030, c=0.8):

    tol=0.1

    def effective_length():
        K_w = E_w0*A_w/L_w0
        del_w_initial = (P_0+F_N)/K_w
        L_ci = L_w0-del_w_initial
        eps_c= P_0/(E_c*A_c)
        L_c0=L_ci/(1+eps_c)
        K_c = E_c*A_c/L_c0
        # check the prestressing force
        P_new = (L_ci-L_c0)*K_c
        diff = P_0-P_new
        if diff<tol:
            return(L_c0)
        else:
            print( "diff not ok")

    # presress loss uses the found effective length

    def prestress_loss_cs(P_start):
        L_eff = effective_length()
        K_w= E_w0*(1/(1+k_def))*A_w/L_w0
        del_w_1 = ((P_start+ F_N)/K_w) + phi_s/100 * del_MC * L_w0
        L_ci= L_w0-del_w_1
        del_c= L_ci-L_eff
        K_c = E_c*A_c/L_eff
        P_1y= del_c*K_c
        del_w_2= ((P_1y+ F_N)/K_w) + phi_s/100 * del_MC * L_w0
        diff = del_w_1 - del_w_2
        return(abs(diff))

    def relaxloss(fpk, A_c, P_0, rho_1000 = 4., t=500000.):
        s_pi=P_0/A_c
        mu= s_pi/fpk
        del_s_relax = 1.98*rho_1000*np.exp(8.0*mu)*((t/1000.)**(0.75*(1-mu))*10**-5*s_pi)
        del_P_relax = del_s_relax *A_c
        return(del_P_relax)
        "when combining with creep/shrinkage a reduction on the relaxation loss is appropriate"

    # find the Prestressing force after losses

    def P_after_losses():
        P_after_cs=scipy.optimize.minimize(prestress_loss_cs, P_0, method="Powell").x
        r_loss= relaxloss(fpk, A_c, P_0)
        P_after_loss = np.round(P_after_cs - c*r_loss)
        percentage_cs_loss = np.round((((P_0-P_after_cs)/P_0)*100))
        percentage_relax_loss = np.round(100*(c*r_loss/P_0))
        return(P_after_loss, percentage_cs_loss, percentage_relax_loss)
    if P_after_losses()[0]>0:
        return(P_after_losses())
    else:
        return(0,P_after_losses()[1], P_after_losses()[2])

# find a prestressing force that pairs with the target after the losses

def prestress_before_losses(P_target):
    def find_initial_prestress(P):
        diff= abs(prestress_after_losses(P)[0]-P_target)
        return(diff)
    a = scipy.optimize.minimize(find_initial_prestress, P_target, method="Powell").x
    return(np.round(a))
```

Appendix N. Wind force calculation

Table 37 dimensions of the case-study-building

Dimension		$[m]$
Building width	b	18
Building depth	d	18
Building height	h	variable

$$F_w = c_s c_d \cdot \sum c_f \cdot q_p(z_e) \cdot A_{ref} \tag{104}$$

Where:

$c_s c_d$	Structural factor
c_f	Force coefficient
$q_p(z_e)$	Peak velocity wind pressure for height z_e
A_{ref}	Reference area on the structure

For the peak velocity wind pressure, it is assumed that the building will be in the Netherlands (Wind Zone II). The wind pressure is determined in line with NEN-EN 1991-1-4. The distribution of the wind force along the height depends in the dimensions of the building. For a building with the height smaller of equal to the width of the building, the wind pressure that is applied is uniform along the height of the building. When the height of the building is between one and two times the building width, the wind pressure will be applied in two blocks. In , it is shown what the reference height (z_e) should be. For buildings taller than $2b$, reference is made to EN-199-1-4. The terrain category assumed is

The structural factor $c_S c_d$ considers the effect of the interaction between the occurrence of the peak wind pressure on the surface and the effect of vibrations of the structure due to turbulence. For buildings smaller than $15\ m$ height, the structural factor can be taken to be 1.0. For taller buildings, EN 1991-1-4 provides an elaborate calculation method. As a simplification, in the thesis, the factor. $c_s c_d$ is taken to be equal to 1.0.

Constants for calculation of the wind pressure		
Wind Area		II (Amsterdam)
Basic value of the basic wind speed	$v_{b,0}$	$27.0\ m/s$
Wind density	ρ	$1.25\ kg/m^3$
Terrain category		II (rural)

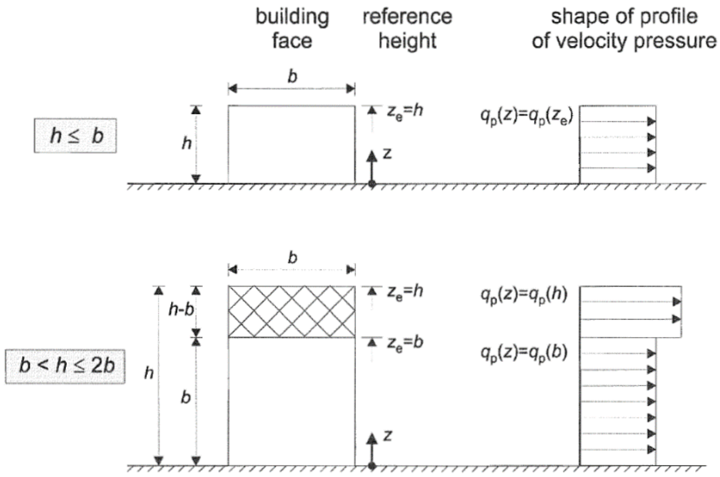

Figure 119 Reference height z_e depending of the building dimensions (EN-1994-1-1)

Table 38 Wind pressure at reference height

Number of stories $[-]$	Building height $[m]$	z_{e1} $[m]$	z_{e2} $[m]$	$q_p(z_{e1})$ $[\frac{kN}{m2}]$	$q_p(z_{e2})$ $[\frac{kN}{m2}]$
1	3	3		0.75	
2	6	6		0.93	
3	9	9		1.04	
4	12	12		1.13	
5	15	15		1.19	
6	18	18		1.25	
7	21	18	21	1.25	1.3
8	24	18	24	1.25	1.34
9	27	18	27	1.25	1.38
10	30	18	30	1.25	1.41
11	33	18	33	1.25	1.44
12	36	18	36	1.25	1.47

For calculation of the wind force, the relevant force coefficients should be applied. This is done for suction (leeward side) and pressure (windward side) combined. When the wind is applied to the leeward and windward side as the same time, a reduction factor of 0.85 may be applied to the applied wind force.

From the distributed wind loads, the base moment and base shear can be computed.

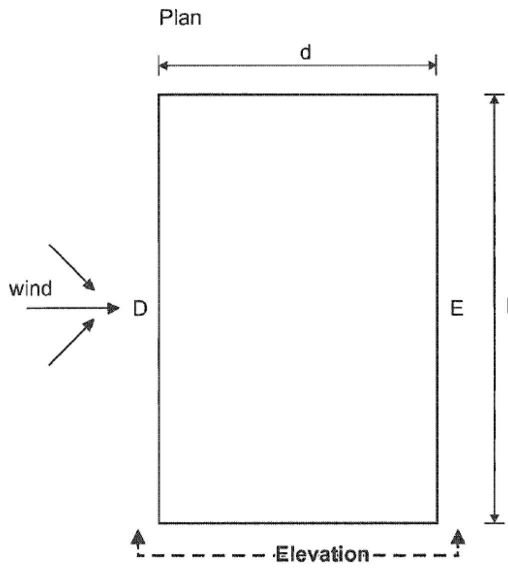

Figure 120 Suction and Pressure facades, plan view

h/d	$c_{f,A}$	$c_{f,B}$	$c_{f,C}$	$c_{f,D}$	$c_{f,E}$
5	-1.2	-0.8	-0.5	0.8	-0.7
≤ 1	-1.2	-0.8	-0.5	0.8	-0.5

$$q_{wind,k} = c_s c_D \cdot \left(\left|c_{f,D}\right| + \left|c_{f,E}\right|\right) \cdot q_p(z_e) \cdot 0.85 \tag{105}$$

Number of stories $[-]$	Building height $[m]$	$\frac{h}{d}$ $[m]$	$c_{f,D}$ $[-]$	$c_{f,E}$ $[-]$	$\left(\left|c_{f,D}\right| + \left|c_{f,E}\right|\right)$ $[-]$	$q_{wind,k,1}$ $[\frac{kN}{m2}]$	$q_{wind,k,2}$ $[\frac{kN}{m2}]$
1	3	0.17	0.8	-0.50	1.30	0.83	
2	6	0.33	0.8	-0.50	1.30	1.03	
3	9	0.50	0.8	-0.50	1.30	1.15	
4	12	0.67	0.8	-0.50	1.30	1.25	
5	15	0.83	0.8	-0.50	1.30	1.31	
6	18	1.00	0.8	-0.50	1.30	1.38	
7	21	1.17	0.8	-0.51	1.31	1.39	1.45
8	24	1.33	0.8	-0.52	1.32	1.40	1.50
9	27	1.50	0.8	-0.53	1.33	1.41	1.55
10	30	1.67	0.8	-0.53	1.33	1.42	1.60
11	33	1.83	0.8	-0.54	1.34	1.43	1.64
12	36	2.00	0.8	-0.55	1.35	1.43	1.69

Table 39 Base shear force and Base moment for wind load

Number of stories $[-]$	Building height $[m]$	Base shear $[kN]$	Base moment $[kNm]$
1	3	22	67
2	6	83	333
3	9	155	838
4	12	236	1618
5	15	320	2663
6	18	410	4028
7	21	485	5549
8	24	561	7402
9	27	638	9639
10	30	715	12237
11	33	794	15238
12	36	874	18666

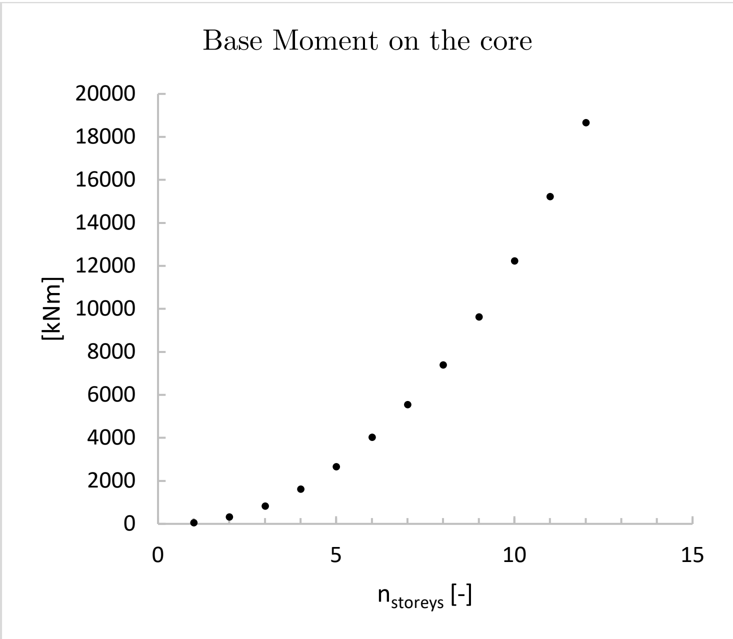

Figure 121 Base moment due to wind

Appendix O. Example build-up CLT floor by dataholz

dataholz.eu

Designation:	gdmtxn01-00
Last updated:	5/7/20
Source:	Holzforschung Austria
Editor:	HFA, SP

Intermediate floor - gdmtxn01-00

intermediate floor, solid wood construction, without lining, dry, with filling, wooden surface

Performance rating

Fire protection performance	**REI**	60

maximum span = 5 m; maximum load $E_{d,fi}$ = 5 kN/m²
Classified by HFA

Germany

REI60

Load $E_{d,fi}$ according to the German certification document

Corresponding proof: manufacturer-specific

Thermal performance	**U**	
	Diffusion	suitable
Acoustic performance	**R_w (C;C_{tr})**	62(-5;-13) dB
	$L_{n,w}$ (C_I)	50(-1)

Assessed by Müller-BBM

Mass per unit area	**m**	202.50 kg/m^2

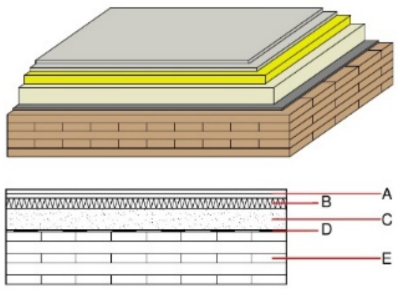

Register of building materials used for this application, cross-section (from outside to inside, dimensions in mm)

	Thickness	Building material	Thermal performance				Reaction to fire
			λ	μ min – max	ρ	c	EN
A	25.0	dry screed	0.210	8	900	1.050	A1
B	30.0	impact sound absorbing subflooring MW-T [s' = 40MN/m³]	0.040	1	160	0.840	A2
C	60.0	elastic bonded fill (m' aprrox. 90 kg/m²) elastic bonded, m' = 90 kg/m²	0.700	1	1500	1.000	A1
D	0.2	trickling protection					E
E	140.0	cross laminated timber	0.130	50	500	1.600	D

Sustainability rating (per m^2)

Database ecoinvent

$OI3_{Kon}$	44.5

Calculated by HFA

Database GaBi (ÖKOBAUDAT)

Built-in renewable materials	**kg**	68.520
Biogenic carbon in kg CO_2-e.	**kg CO_2**	98.630
Energy use of Primary Energy	**MJ**	967.990
Share of renewable PE	**%**	31.210

Calculated by TUM

dataholz.eu – Catalogue of timber building materials, components and component connections reviewed to consider thermal, acoustic, fire performance requirements and ecological drivers for timber construction released by accredited testing institutes.
These datasheets will generally be accepted as proofs of compliance by building authorities.

Page 1

dataholz.eu

Designation: gdmtxn01-00
Last updated: 5/7/20
Source: Holzforschung Austria
Editor: HFA, SP

Details of sustainability rating

Database ecoinvent

Lifecycle (Phases)	GWP [kg CO_2-e.]	AP [kg SO_2-e.]	EP [kg PO_4-e.]	ODP [kg R11-e.]	POCP [kg Ethen-e.]	
A1 - A3	-58.980	0.229	0.082	3,52E-6	0.028	

Lifecycle (Phases)	PERE [MJ]	PERM [MJ]	PERT [MJ]	PENRE [MJ]	PENRM [MJ]	PENRT [MJ]
A1 - A3	67.796	957.600	1025.396	683.583	27.875	711.458

Database GaBi (ÖKOBAUDAT)

Lifecycle (Phases)	GWP [kg CO_2-e.]	AP [kg SO_2-e.]	EP [kg PO_4-e.]	ODP [kg R11-e.]	POCP [kg Ethen-e.]	
A1 - A3	-71.715	0.127	0.023	3,67E-6	0.020	
C1 - C4	113.766	0.016	0.004	1,68E-7	0.001	
A1 - C4	42.385	0.143	0.026	3,83E-6	0.021	

Lifecycle (Phases)	PERE [MJ]	PERM [MJ]	PERT [MJ]	PENRE [MJ]	PENRM [MJ]	PENRT [MJ]
A1 - A3	297.825	1161.286	1456.312	618.702	42.774	660.692
C1 - C4	4.314	-1160.600	-1156.286	46.970	0.000	46.970
A1 - C4	302.141	0.686	300.027	665.844	42.774	707.835

Appendix P. Maximum size CLT panel for transport

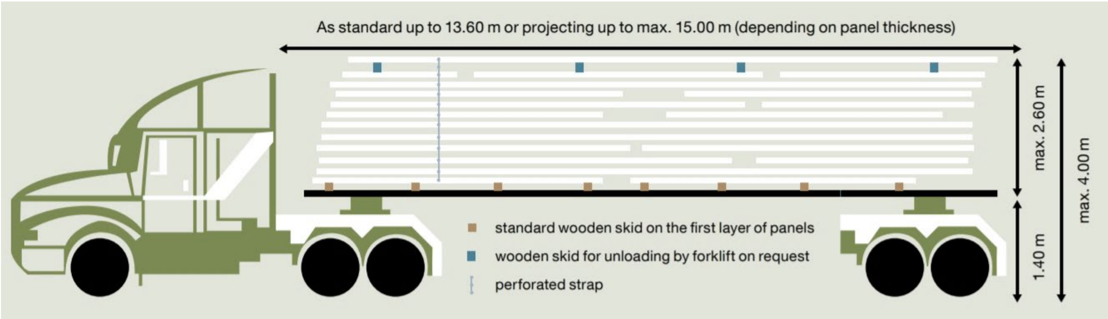

Figure 122 Horizontal transport of CLT panels with a trailer

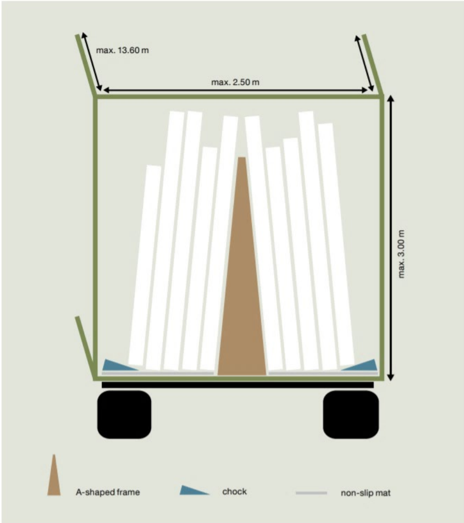

Figure 123 Vertical transport of CLT panels with a trailer

Appendix Q. Tensile and shear plates

It may be needed to make horizontal joints in the CLT core. In that case tensile forces need to be transferred between stacked CLT panels. For this, steel plates may be used. An example is the relatively new Rothoblaas plate connectors (Rothoblaas WHTPT820 for tensile force). In this hold-down is shown in a platform type of construction. However, these connectors can also be used in balloon construction.

Since the ETA of this connector does not supply a value for K_{ser}, an assumption is made relating the stiffness of this connection to that of the tested hold-down. In the hold-down, 52 nails were used, having together a stiffness of 13540 N/mm (260 N/mm/nail). Assuming the WHTPT820 is fully nailed, and seeing the two groups of nails as working in series, the stiffness may be assumed as in Eq. 108.

For the transfer of shear forces between stacked CLT panels, shear plate connectors may be used. Rothoblaas TTP300 connector is an example of such connector.

For this connector, the ETA also does not provide a value for K_{ser}, therefore an estimation is made based on the test results of the Rothoblaas shear angles. It is assumed, the connection is connected with 14 screws/nails under the contact line of the CLT plates, and 14 screws/nails above.

The tensile stiffness can be related to that of the TCN shear angle. For the stiffness in 2/3 direction, test result for another shear angle with 28 screws is taken from the ETA. In the ETA, the stiffness of a TTS240 connection, with 2×14 screws were tested. This resulted in a stiffness of 5600 N/mm. The same value can be assumed for the TTP300 plate.

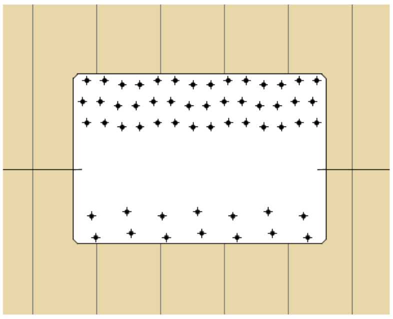

Figure 124 Rothoblaas shear plate in balloon type construction

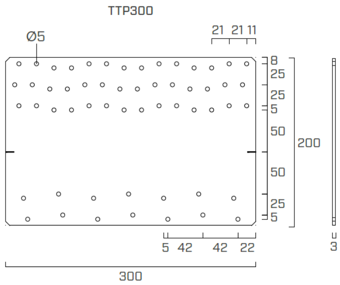

Figure 125 Geometry of the TTP300 shear plate connector

$$K_{1,ser} = \frac{5500}{2} = 2750\ N/mm \tag{106}$$

$$K_{2/3,ser} = 5600\ N/mm \tag{107}$$

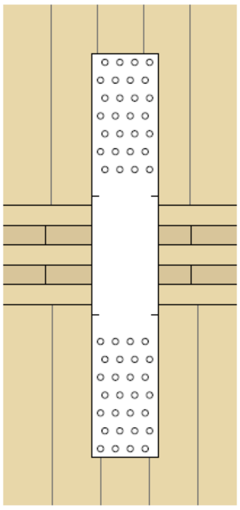

Figure 126 Rothoblaas tensile plate WHTPT820 in platform type construction

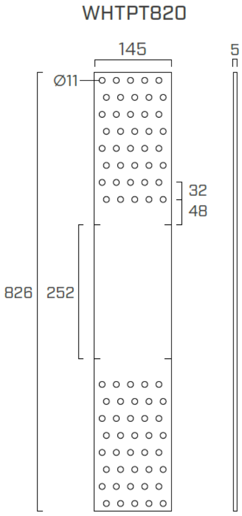

Figure 127 Geometry of the WHTPT820 connector

$$K_{1,ser} = 260 \cdot \frac{40}{2} = 5200\frac{N}{mm} \tag{108}$$

Appendix R. Stiffness matrix from CLTdesigner

Properties of CLT panel Derix exported from CLTdesigner.at

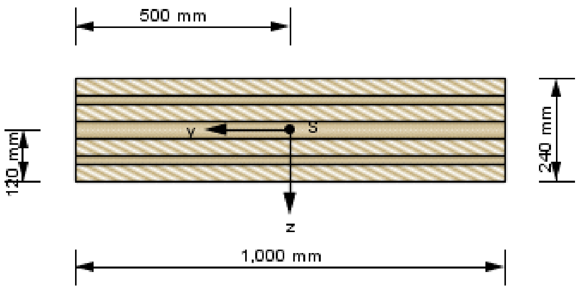

Derix CLT panel L-240/7s

Stiffness Matrix Elements (Bending and Torsion)		
D11	10,442.67	kNm
D12	0	kNm
D13	0	kNm
D22	2,229.33	kNm
D23	0	kNm
D33	496.873	kNm
Stiffness Matrix Elements (Shear)		
D44	21,759.72	kN/m
D45	0	kN/m
D55	12,397.21	kN/m
Stiffness Matrix Elements (Membrane)		
D66	1,760,000	kN/m
D67	0	kN/m
D68	0	kN/m
D77	880,000	kN/m
D78	0	kN/m
D88	111,734.19	kN/m

Translating stiffness matrix entries to I_{eff}:

$$D_{11} = EI_{eff} = 10442.67\ kNm = 10442.67E6\ Nmm$$

$$I_{eff,stiff} = \frac{10442.67\text{E6 Nmm}}{11000 \dfrac{\text{N}}{\text{mm}^2}} = 949334\ mm^3$$

$$D_{22} = EI_{eff} = 2{,}229.33\ \text{kNm} = 2229.33E6\ Nmm$$

$$I_{eff,lessstiff} = \frac{2229.33E6 \text{ Nmm}}{11000 \frac{\text{N}}{\text{mm}^2}} = 202666\, mm^3$$

Appendix S. Calculation of the instability factor (Maple)

Maple Code for calculation of the Instability fator $k_{c,y}$

> $f\_c0k := 21 \# \frac{N}{mm2}$:

$$f\_c0k := 21 \tag{1}$$

> $E\_05 := 9160 \# \frac{N}{mm2}$:

$$E\_05 := 9160 \tag{2}$$

> $I\_eff := 6.08E8 \# mm^3$:

$$I\_eff := 6.08\ 10^8 \tag{3}$$

> $l\_ki := 3000$ #mm:

$$l\_ki := 3000 \tag{4}$$

> $A\_0\_net := 3500 \cdot 160$ #mm:

$$A\_0\_net := 560000 \tag{5}$$

> $i\_0\_eff := \mathrm{sqrt}\left(\frac{I\_eff}{A\_0\_net}\right)$

$$i\_0\_eff := 32.95017885 \tag{6}$$

> $\lambda\_y := \frac{l\_ki}{i\_0\_eff}$

$$\lambda\_y := 91.04654678 \tag{7}$$

> $\lambda\_y\_rel := evalf\left(\frac{\lambda\_y}{\mathrm{Pi}} \cdot \mathrm{sqrt}\left(\frac{f\_c0k}{E\_05}\right)\right)$

$$\lambda\_y\_rel := 1.387635866 \tag{8}$$

> $\beta\_c := 0.1$: # *for CLT, value from the Proholz guide:*

> $k\_y := evalf\left(0.5 \cdot \left(1 + \beta\_c \cdot (\lambda\_y\_rel - 0.3) + \lambda\_y\_rel^2\right)\right)$

$$k\_y := 1.517148442 \tag{9}$$

> $k\_c\_y := evalf\left(\frac{1}{k\_y + \mathrm{sqrt}\left(k\_y^2 - \lambda\_y\_rel^2\right)}, 3\right)$

$$k\_c\_y := 0.467 \tag{10}$$

Appendix T. Normal stress distribution in the U-shaped core

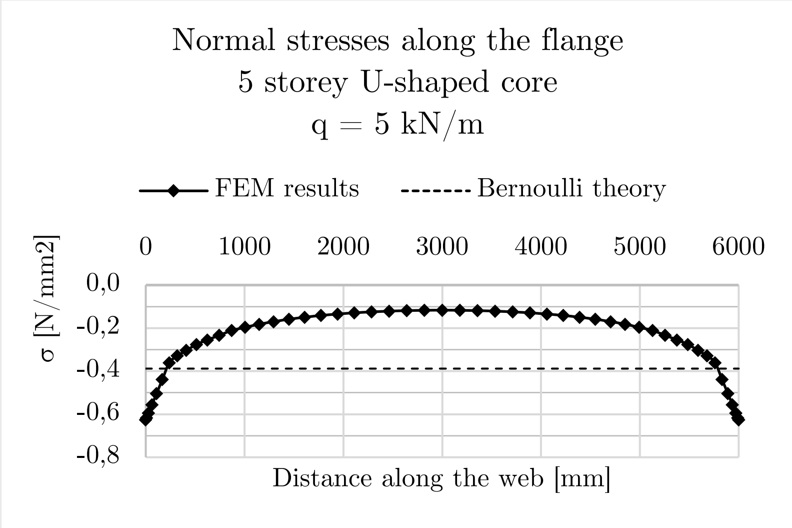

Figure 128 Normal stresses along the flange of a 5-storey core

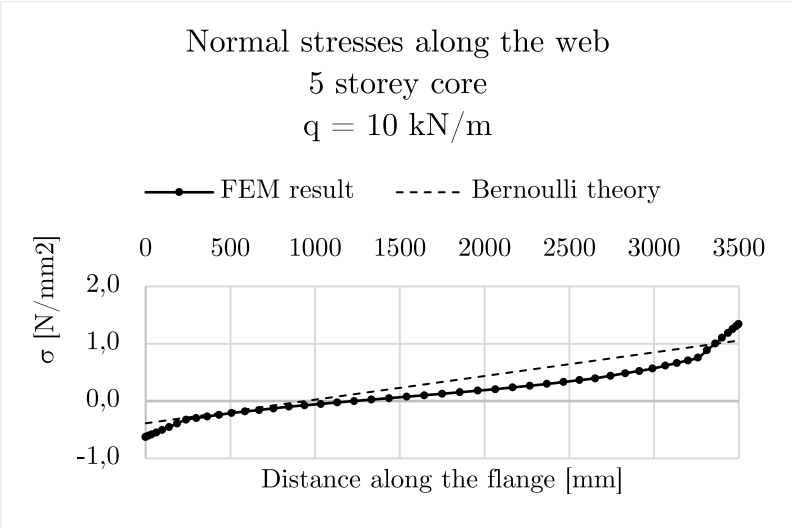

Figure 129 Normal stresses along the web of a 5-storey core

Appendix U. Shear Lag Analysis U-shaped core

Table 40 Input variables of the finite element model

Storey height	h_{storey}	$3000\ mm$
Wall thickness	t_{CLT}	$240\ mm$
Effective thickness	$t_{CLT,eff}$	$160\ mm$
Distributed force	q	$10\ kN/m$

Table 41 Stiffness of the U-shaped core derived from FEA

Stiffness of the U-shaped core for uniform load in the y-direction 10 kN/m					
Storey nr	building height	Lateral displacement FE result	Lateral displacement FE result	Lateral displacement FE result	Stiffness
		wind y	shear	bending	I
[-]	mm	[mm]	[mm]	[mm]	[x10^12 mm^4]
3	9000	0.94	0.473	0.47	1.60
4	12000	2.05	0.840	1.21	1.95
5	15000	3.96	1.313	2.65	2.17
6	18000	7.02	1.891	5.13	2.33
7	21000	11.70	2.574	9.13	2.42
8	24000	18.56	3.361	15.20	2.48
9	27000	28.19	4.254	23.94	2.52
10	30000	41.26	5.252	36.01	2.56

Table 42 Stiffness contributions of the flange and the web

Storey nr	**Stiffness**					
	z	$I_{web,steiner}$	$I_{web,total}$	$I_{flange,total}$	$I_{flange,steiner}$	$\frac{I_{flange}}{I_{total}}$
[-]	mm	[x10^{11} mm^4]	[x10^{12} mm^4]	[x10^{11} mm^4]	[x10^{11} mm^4]	
3	1520	0.30	1.20	3.93	3.92	49%
4	1340	0.94	1.33	6.16	6.15	63%
5	1225	1.54	1.45	7.21	7.20	66%
6	1147	2.03	1.55	7.76	7.74	67%
7	1099	2.38	1.62	8.03	8.02	66%
8	1069	2.60	1.66	8.17	8.16	66%
9	1047	2.77	1.70	8.26	8.24	65%
10	1030	2.90	1.72	8.32	8.31	65%

Table 43 Effective width of the U-shaped core

Storey nr	**Effective width of the flange**				
[-]					
3	1061.78	mm	=	0.06	x $2h_{building}$
4	2142.78	mm	=	0.09	x $2h_{building}$
5	3000.03	mm	=	0.10	x $2h_{building}$
6	3676.39	mm	=	0.10	x $2h_{building}$
7	4150.79	mm	=	0.10	x $2h_{building}$
8	4464.70	mm	=	0.09	x $2h_{building}$
9	4701.37	mm	=	0.09	x $2h_{building}$
10	4893.52	mm	=	0.08	x $2h_{building}$

Appendix V. Gamma factor analysis U-shaped core

Table 44 Gamma calculation flange of the U-shaped core

nr storeys	h_{core}	z	b_{flange}	$A_{net,flange}$	γ_{flange}
[-]	[mm]	[mm]	[mm]	[mm²]	[-]
3	9000	1520	1062	169884	0.54
4	12000	1340	2143	342845	0.51
5	15000	1225	3000	480005	0.53
6	18000	1147	3676	588223	0.57
7	21000	1099	4151	664127	0.62
8	24000	1068	4465	714352	0.66
9	27000	1047	4701	752220	0.70
10	30000	1030	4894	782963	0.74

Table 45 New neutral axis of the core

nr storeys	$b_{flange,\gamma}$		$A_{eff,flange,\gamma}$	$A_{total,\gamma}$	z_{new}
[-]	[mm]		[mm²]	[mm²]	[mm]
3	571	10%	91426	1211426	1618
4	1085	18%	173665	1293665	1515
5	1602	27%	256290	1376290	1424
6	2109	35%	337508	1457508	1345
7	2568	43%	410922	1530922	1280
8	2962	49%	473882	1593882	1230
9	3306	55%	528913	1648913	1189
10	3609	60%	577424	1697424	1155

Table 46 Total stiffness U shaped core

nr storeys	$I_{flange,self}$	$I_{flange,steiner}$	I_{flange}	z_{web}	$I_{webs,steiner}$	I_{web}	I_{total}
[-]	[mm^4]	[mm^4]	[mm^4]	[mm]	[mm^4]	[mm^4]	[mm^4]
3	2.0E+08	2.4E+11	2.4E+11	132	2.0E+10	5.9E+11	8.3E+11
4	3.7E+08	4.0E+11	4.0E+11	235	6.2E+10	6.3E+11	1.0E+12
5	5.5E+08	5.2E+11	5.2E+11	326	1.2E+11	6.9E+11	1.2E+12
6	7.2E+08	6.1E+11	6.1E+11	405	1.8E+11	7.6E+11	1.4E+12
7	8.8E+08	6.7E+11	6.7E+11	470	2.5E+11	8.2E+11	1.5E+12
8	1.0E+09	7.2E+11	7.2E+11	520	3.0E+11	8.7E+11	1.6E+12
9	1.1E+09	7.5E+11	7.5E+11	561	3.5E+11	9.2E+11	1.7E+12
10	1.2E+09	7.7E+11	7.7E+11	595	4.0E+11	9.7E+11	1.7E+12